"This is an Accepted Manuscript of an article published by Taylor & Francis in Journal of Macromolecular Science, Part A on April 27, 2017, available online: http://dx.doi.org/10.1080/10601325.2017.1312678"

Case studies with mathematical modeling of free-radical multi-component bulk/solution polymerizations: Part 2

David Dorschner, Woosung Jung, Marzieh Riahinezhad, Thomas A Duever, and Alexander Penlidis*

Institute for Polymer Research (IPR), DePartment of Chemical Engineering, University of Waterloo, Waterloo, Ontario, N2L 3G1, Canada

Received, Revised and Accepted December 2016

Abstract

In Part 2 of this series of two extensive overviews of multi-component polymerization case studies, we again present mathematical modeling results with experimental confirmations. Part 2 represents a refinement and expansion of the detailed and extensive

mathematical model presented in Part 1 for free-radical, bulk and/or solution multi-component polymerizations. The expansion is mainly with respect to depropagation, thus making the model more fluent at elevated polymerization temperatures and, in parallel, with additional features as backbiting (with systems involving butyl acrylaye). The model considers up to six monomers (unique in the literature), for either batch or semi-batch reactor modes. As the simulator database contains several monomers, initiators, solvents, chain transfer agents and inhibitors, all tested over a wide range of polymerization conditions, from data in both academic and industrial laboratories, several hundred combinations of ingredients can be modeled. The many outputs generated by the model include conversion, molecular weight, polymer composition, branching indicators, sequence length, as well as many other polymerization characteristics related to both production rate and polymer quality. Although the only literature data found to date contain a maximum of four monomers, model predictions for homo-, co-, ter- and tetra-polymerizations show reasonable agreement against the data at both regular and elevated temperatures. With these expansions, this model is directed towards becoming a complete free-radical polymerization tool for training and educational uses both in industry and academia.

Keywords: Bulk polymerization; solution polymerization; free-radical polymerization; mathematical modeling; copolymerization; terpolymerization; depropagation; backbiting

*__Correspondence to:__ Alexander Penlidis, Institute for Polymer Research (IPR), Department of Chemical Engineering, University of Waterloo, Waterloo, Ontario, N2L 3G1, Canada. Tel.: (519) 8884567, ext: 36634; E-mail: penlidis@uwaterloo.ca

1. Introduction

This paper (Part 2 of a series of two articles) is complementary to the modeling case studies of Jung et al. (1). The equations for the full mathematical model will not be repeated herein again, for the sake of brevity, since details can be found in (1). Symbols have been kept the same as in Part 1. Some additional equations will be shown in the appropriate sections below (and new symbols only will be defined upon first use) related to depropagation and backbiting cases. The objectives are to contribute to the enhancement of the hexa-polymerization model database of Part 1 (1) and to increase the versatility of the simulator by creating several extensions. The original model (1, 2) with the current extensions (3) can predict with great accuracy any of the rates of reaction or polymer quality outputs in a typical polymerization scenario (conversion, molecular weights, branching indicators, polymer composition, sequence length, etc.). The model has the ability to simulate batch and semi-batch, bulk or solution, isothermal or nonisothermal, ideal or diffusion-limited kinetics, and depropagation/backbiting charactersitics. More than 10 complex case studies are tackled in the current paper from

research or industrial pilot-plant situations. Finally, numerous explicit tables appear in the appendices, summarizing useful database items for initiators, monomers, and other polymerization recipe ingredients. All these features increase the range of the model's applicability as well as the user's confidence in the model's reliability for describing multicomponent polymerization scenarios.

2. Experimental

2.1. Preamble

As mentioned in Part 1 of the series (1), this paper also contains extensive mathematical modelling results and experimental data. The experimental data come from many sources and they represent a mix of research laboratory and pilot-plant data. As such, actual experimental details can be found under the 'Results and Discussion' section, when different data sources (and their corresponding literature references) and data behavior are discussed and compared to model predictions. Due to this extensive mathematical modeling and before we start the discussion of the obtained results, a brief background on multi-component polymerizations along with their mathematical modelling is in order, with emphasis on depropagation and backbiting. Tables of sources of information from the literature, relevant to the simulation results or containing useful data sets, are also cited in this section.

2.2. Background information (polymerization model/data sources)

Useful reference lists for tetra-, ter- and co-polymerizations are cited in Tables 1 and 2. These references contain either mathematical model development aspects or data sets relevant to the case studies and simulation results of the current paper.

Table 1. Reference list for tetra- and ter-polymerizations

Monomer system	**Reference**	**Focus**
Tetra-	Sahloul (4)	Data
Ter-	Alfrey and Goldfinger (5, 6)	Polymer composition
	Walling and Briggs (7)	Polymer composition
	Valvassori and Sartori (8)	Polymer composition
	Galbraith *et al.* (9)	Reactivity ratios
	Hamielec *et al.* (10, 11)	Model equations
	Dubé and Penlidis (12, 13)	Model testing
	Hocking and Klimchuk (14)	Polymer composition
	Dubé and Penlidis (15)	Data
	Dubé *et al.* (16)	Model equations
	McManus *et al.* (17)	Model testing
	Gao and Penlidis (18)	Model testing

	Keramopoulos and Kiparissides (19)	Model testing
	McManus *et al.* (20)	Data /Depropagation
	Leamen *et al.* (21)	Depropagation
	Li and Hutchinson (22)	Kinetics
	Wang (23)	Depropagation/Backbiting

Table 2. Reference list for co-polymerizations

Reference	**Focus**
Branson and Simha (24)	Modeling
Alfrey and Goldfinger (5)	Polymer composition
Mayo and Lewis (25)	Polymer composition
Simha and Branson (26)	Modeling
Wall (27)	Polymer composition
Stockmayer (28)	Composition distribution
Merz *et al.* (29)	Polymer composition
Skeist (30)	Polymer composition
Walling (31)	Modeling
Mayo and Walling (32)	Reaction kinetics
Bradbury and Melville (33)	Reactivity ratios
Lowry (34)	Depropagation

Harwood and Ritchey (35)	Sequence length
Meyer and Lowry (36)	Polymer composition
Otsu *et al.* (37, 38)	Reactivity ratios
Cameron and Kerr (39)	Reactivity ratios
Chan and Meyer (40)	Polymer composition
Harwood (41)	Sequence length
Howell *et al.* (42)	Depropagation
Izu and O'Driscoll (43)	Depropagation
Wittmer (44)	Depropagation
Fischer (45)	Depropagation
Johnston (46)	Modeling
Chow (47)	Reactivity ratios
Gaddam *et al.* (48)	Reactivity ratios
Johnson *et al.* (49)	Modeling
Dionisio and O'Driscoll (50)	Modeling
Patino-Leal *et al.* (51)	Reactivity ratios
Reilly and Patino-Leal (52)	Reactivity ratios
Borchardt (53)	Reactivity ratios
Hill *et al.* (54)	Sequence length
Duever *et al.* (55)	Reactivity ratios

Lord (56)	Model testing
Teramachi *et al.* (57)	Composition distribution
Borchardt (58)	Reactivity ratios
Garcia-Rubio *et al.* (59)	Reactivity ratios/Model testing
Balaraman *et al.* (60)	Composition/Sequence length distribution
Catala *et al.* (61)	Reactivity ratios
Krüger *et al.* (62)	Depropagation
Tacx *et al.* (63)	Composition distribution
Dubé (64)	Reactivity ratios/Model testing
O'Driscoll and Huang (65, 66)	Modeling
Davis *et al.* (67)	Kinetics
Dubé *et al.* (68, 69)	Reactivity ratios/Model testing
Dubé *et al.* (70, 71)	Reactivity ratios
Kapur and Brar (72)	Modeling
Engelmann & Schmidt-Naake (73)	Composition distribution
Reilly *et al.* (74)	Reactivity ratios
Switata-Zeliazkow (75)	Modeling
Xie and Hamielec (76)	Modeling
Kim (77)	Reactivity ratios/Model testing
Vivaldo-Lima *et al.* (78)	Modeling

Dubé and Penlidis (12, 13)	Reactivity ratios/Model testing
Liu *et al.* (79)	Reactivity ratios
Rossignoli and Duever (80)	Reactivity ratios
McManus and Penlidis (81)	Reactivity ratios/Model testing
Brar and Dutta (82)	Reactivity ratios
Gao and Penlidis (83)	Model testing
Polic *et al.* (84)	Reactivity ratios
Brandrup *et al.* (85)	Kinetics and reactivity ratios
Chambard *et al.* (86)	Reactivity ratios
Martinet and Guillot (87)	Depropagation
McManus *et al.* (88)	Reactivity ratios
Hakim *et al.* (89)	Reactivity ratios
Palmer *et al.* (90, 91)	Depropagation
Buback *et al.* (92)	Reactivity ratios
Scholtens *et al.* (93)	Composition distribution
Dubé *et al.* (94)	Depropagation
Grady *et al.* (95)	Depropagation
Kim and Harwood (96)	Sequence length
Wolf *et al.* (97)	Reactivity ratios
Fernandez-Garcia *et al.* (98)	Modeling

Cheong and Penlidis (99)	Depropagation
Sahloul and Penlidis (100, 101)	Reactivity ratios
Sahloul *et al.* (102)	Reactivity ratios
Leamen *et al.* (21)	Depropagation
Li *et al.* (103)	Depropagation
Jianying *et al.* (104)	Reactivity ratios
Li *et al.* (105)	Depropagation
Abdollahi *et al.* (106)	Reactivity ratios
Mun *et al.* (107)	Reactivity ratios
Fujisawa and Penlidis (108)	Modeling
Wang and Hutchinson (109, 110)	Depropagation
Popescu *et al.* (111)	Modeling
Wang (23)	Depropagation/Backbiting

Table 3 is the reference list for all the homo-polymerization papers used as additional model confirmation studies further to the cases of Part 1 (1).

Table 3. Reference list for homo-polymerizations

Reference	Focus
Bywater (112)	Depropagation
McCormick (113)	Depropagation
Nair and Muthana (114)	Kinetics
Carlsson *et al.* (115)	Kinetics
Raghuram and Nandi (116, 117)	Kinetics
Hui and Hamielec (118)	Kinetics/Modeling
Friis and Nyhagen (119)	Kinetics
Arai and Saito (120)	Modeling
Husain and Hamielec (121)	Modeling
Garcia-Rubio *et al.* (122)	Modeling
Marten and Hamielec (123)	Modeling
Stickler (124)	Modeling
Stickler *et al.* (125)	Modeling
Buback *et al.* (126)	Kinetics
Buback (127)	Kinetics/Modeling

Dubé *et al.* (70, 71)	Kinetics/Modeling
Kumar and Gupta (128)	Kinetics
Kuindersma (129)	Model testing
Gao (130)	Model testing
Buback *et al.* (131)	Kinetics
Hutchinson *et al.* (132)	Kinetics
Beuermann *et al.* (133)	Kinetics
Gao and Penlidis (134)	Model testing
Lyons *et al.* (135)	Reaction kinetics
Gao *et al.* (136)	Model testing
Beuermann *et al.* (137)	Kinetics
Hutchinson *et al.* (138)	Kinetics
Buback *et al.* (139)	Kinetics
Maeder and Gilbert (140)	Kinetics
Beuermann *et al.* (141)	Kinetics
Buback *et al.* (142)	Kinetics
Dhib *et al.* (143)	Model testing
Asua *et al.* (144)	Kinetics
Nising and Meyer (145)	Kinetics
Peck and Hutchinson (146)	Kinetics/Modeling

Gao *et al.* (147)	Modeling
Quan *et al.* (148)	Kinetics
Vargun and Usanmaz (149)	Kinetics
Willemse *et al.* (150)	Backbiting
Buback and Junkers (151)	Kinetics
Rantow *et al.* (152)	Modeling
Matthews *et al.* (153)	Molecular weights
Nikitin *et al.* (154)	Backbiting
Chen *et al.* (155)	Kinetics
Ahmad *et al.* (156)	Modeling
Barth *et al.* (157)	Backbiting
Castignolles (158)	Modeling
Nikitin and Hutchinson (159)	Backbiting
Van Herk (160)	Modeling
Wang *et al.* (161)	Depropagation
Wang *et al.* (162)	Backbiting
Zorn *et al.* (163)	Kinetics

2.3. Additional Model Features/Options

2.3.1. Depropagation

Depropagation is the reverse propagation reaction. It depends on the system ceiling temperature, it usually only occurs in significant amounts at elevated temperatures and is considered negligible elsewhere. This can be depicted by considering the Gibbs free energy during polymerization:

$$\Delta G_p = \Delta H_p - T\Delta S_p \quad (1)$$

where ΔH_p and ΔS_p are the change in enthalpy and entropy, respectively.

Propagation occurs when ΔG_p is negative. This is generally easy enough to obtain as a polymerization (propagation) reaction is highly exothermic and therefore, has a large negative enthalpy. The change in entropy is also negative as each propagation reaction removes degrees of freedom. With both enthalpy and entropy negative, the reaction is only spontaneous depending on the temperature of the system. At equilibrium where ΔG_p = 0, the ceiling temperature is reached.

For reversible propagation (see also section 2.2.3.3 of Part 1 of the series (1)):

$$R_r^{\cdot} + M \leftrightarrow R_{r+1}^{\cdot} \tag{2}$$

$$R_p = k_p[R^{\cdot}][M] - \overline{k_p}[R^{\cdot}] = k_p^{eff}[R^{\cdot}][M] \tag{3}$$

$$k_p^{eff} = k_p - \frac{\overline{k_p}}{[M]} \tag{4}$$

where $\overline{k_p}$ and k_p^{eff} are the depropagation rate constant and the effective propagation rate constant, respectively. The two-pointed arrow in Equation 2 represents both steps (forward and reverse (propagation and depropagation, respectively).

As can be seen, at high monomer concentrations k_p^{eff} will approach k_p. This is intuitive as an increase in the amount of monomer(s) would shift the balance to the right side of the reaction, acting as a driving force for propagation. Equilibrium (denoted by

subscript eq) occurs at a specific monomer concentration forcing $k_p^{eff} = 0$ or close to zero.

$$K_{eq} = \frac{k_p}{k_p} = \frac{1}{[M]_{eq}} \quad (5)$$

The fact that equilibrium occurs at a finite monomer concentration implies that a system where depropagation is present in every monomer never reaches full conversion. The method used to model this phenomenon is Krüger's probabilistic approach (62, 164). Through material balances and reaction probabilities, it can describe depropagation of any or all monomers in the system. In a six-monomer system, 72 reactions now take place: the original 36 propagation reactions as well as the 36 depropagation reactions (see Equations 21 to 27 of Part 1 (1)).

Although for the terminal model one only considers the final monomer unit on the chain, now we need to consider the penultimate unit as well. Krüger's method uses reaction probabilities to determine information about the penultimate unit.

Matrix algebra is used again to solve for the radical fractions (see Equation 20 of Part 1 (1)). With the radical fractions and penultimate unit probabilities thus determined, the monomer balances as well as output calculations (conversion, polymer composition, etc.) can be solved as before. The cross-depropagation rate constants used above are estimated from co-polymerization data or are taken from the literature quite similarly to the method of obtaining propagation rate constants (2).

2.3.2. Backbiting and β-scission of butyl acrylate

Backbiting (bb) occurs when a propagating secondary radical extracts a hydrogen atom from the pen-penultimate position. This is depicted in Figure 1. A tertiary or midchain radical (Q_r) remains to continue propagating at a slower rate.

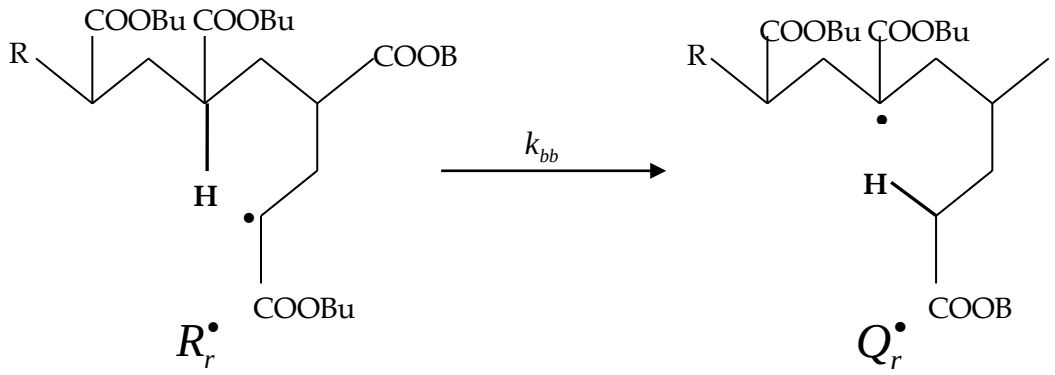

Figure 1. Backbiting of butyl acrylate

$$R_{bb} = k_{bb}[R\cdot] \quad (6)$$

The driving force for backbiting is that the tertiary radical formed is more stable even at ambient temperatures (150, 154). The midchain radical formed via backbiting can combine with a monomer, beta-fragment or terminate; chain transfer is assumed negligible.

Propagation of the tertiary radical creates a new backbone leaving the existing chain portion as a short-chain branch (SCB). The propagating radical after reacting with a monomer is now assumed to exhibit secondary radical kinetics, hence using $R^{\bullet}$ instead of $Q^{\bullet}$.

$$Q_{\dot{r}} + M \xrightarrow{k_p^{tert}} R_{\dot{r}+1} \quad (7)$$

$$R_p^{tert} = k_p^{tert}[Q\cdot][M] \quad (8)$$

Beta-scission usually occurs at 140°C and above (152). This is when the tertiary radical splits at the beta position leaving a dead polymer chain with a terminal double bond and a radical of length two. This phenomenon significantly affects the molecular weight of the polymer. The reverse scenario, where a dead trimer and a long chain radical is formed, is deemed nonexistant due to lack of short-chained species detected by Electrospray Interface-Fourier Transform Mass Spectrometer (ESI-FTMS) spectral analysis (95).

$$Q_r^{\cdot} \xrightarrow{k_\beta} P_{r-2} + R_2^{\cdot} \tag{9}$$

$$R_{beta} = k_{beta}[Q^{\cdot}] \tag{10}$$

The tertiary radical might also undergo termination, either with a fellow tertiary radical or with the more common secondary radical. Disproportionation and combination are both possible but unlike secondary radicals, tertiary radicals are more likely to terminate via disproportionation (165). The termination by combination ratios (to overall termination) for secondary-secondary, secondary-tertiary, and tertiary-tertiary radicals are assumed as 0.9, 0.3, and 0.1, respectively, following suggestions by (146).

$$Q_r^{\cdot} + R_s^{\cdot} \xrightarrow{k_{tc}^{tert-sec}} P_{r+s} \textbf{ or } \xrightarrow{k_{td}^{tert-sec}} P_r + P_s \quad (11)$$

$$Q_r^{\cdot} + Q_s^{\cdot} \xrightarrow{k_{tc}^{tert-tert}} P_{r+s} \textbf{ or } \xrightarrow{k_{td}^{tert-tert}} P_r + P_s \quad (12)$$

$$R_t^{tert} = k_t^{tert-sec}[Q\cdot][R\cdot] + k_t^{tert-tert}[Q\cdot]^2 \quad (13)$$

Explanations for several new symbols pertinent to this Part (and not appearing in Part 1 (1) of this series) are now in order:

$[R_0^{\cdot}]$ molar concentration of radicals of chain length zero (initiator decomposition)

$[R_1^{\cdot}]$ molar concentration of radicals of chain length one

$[R_1^{\cdot}]^{TDB}$ molar concentration of radicals of chain length one with a terminal double bond

$[R_2^{\cdot}]$ molar concentration of radicals of chain length two

[TDB] molar concentration of molecules with terminal double bonds

[SCB] molar concentration of molecules with short chain branches

Using the moment equations and monomer and radical balances (as per Part 1 (1) of the series), the number of (short) chain branches per chain, CBC, and the number of terminal double bonds per chain, TDBC, can be calculated:

$$CBC = \frac{[SCB]}{\mu_1} \tag{14}$$

$$TDBC = \frac{[TDB]}{\mu_1} \tag{15}$$

2.4. Model Features/Options

The complete model (1-3) can now handle the following configurations/conditions: (a) Homo- up to a hexa-polymerization systems, (b) Bulk and solution polymerizations, (c) Batch and semi-batch operation modes, (d) Isothermal and non-isothermal scenarios (where a temperature profile is present), (e) Ideal and diffusion-controlled kinetics, (f) Self/thermal initiation of styrenics and/or butyl acrylate, (g) Branching and cross-linking reactions, (h) Depropagation, (i) Copolymer composition control, (j) Single and multiple initiators, and (k) Backbiting of butyl acrylate.

The following outputs can be generated as instantaneous or cumulative properties (as appropriate): Overall and Partial conversion; Overall and individual rate of polymerization; Total reacting mixture volume; Monomer and radical species concentrations; Other species concentrations (initiator(s), solvent, CTA, inhibitor, etc.); Residual monomer fraction and radical fractions; Instantaneous/accumulated polymer composition; Instantaneous/ accumulated polymer composition distribution; Instantaneous/accumulated number- and weight-average molecular weights; Instantaneous/accumulated polydispersity index (PDI); Instantaneous/accumulated molecular weight distribution (linear chains only); Instantaneous/accumulated number- and weight-average sequence lengths; Sequence length distribution; Instantaneous/accumulated triad fractions; Number-average tri/tetra-functional branches per molecule; Polymer glass-transition temperature and free volume characteristics; Pseudo termination/propagation/transfer reaction rate constants and initiator efficiency profiles.

2.4.1. Database characteristics

Within the model database, there are thousands of different combinations of ingredients available. This is due to the large number of monomers accessible within the database. The simulation results are obtained without changing the ingredient database items. The monomers available for simulation are: Acrylic acid (AA); Acrylontrile (AN); Alpha-

methyl styrene (AMS); n-Butyl acrylate (BA); n-Butyl methacrylate (BMA); Ethyl acrylate (EA); Glycidyl methacrylate (GMA); Hydroxyethyl acrylate (HEA); Hydroxyethyl methacrylate (HEMA); Methacrylic acid (MAA); Methyl methacrylate (MMA); Styrene; Vinyl acetate (VAc).

The available initiators are: Azobisisobutyronitrile (AIBN); Butyl peroxide (BPO); Di-tert-butyl peroxide (dTBPO or Trigonox B); Tert-butyl peroxybenzoate (TBPB or Trigonox C); Tert-butyl peroxyacetate (TBPA or Lupersol 70).

Finally, other ingredients include: Chain transfer agents (CTAs) with carbon tetrachloride, octanethiol and dodecanethiol; Solvents with toluene, xylene, benzene and ethyl acetate; Inhibitors, if present, with oxygen and benzoquinone. Several more initiators, solvents, chain transfer agents and inhibitors are accessible and easily adaptable from the original polymerization modeling software WATPOLY (18). The most important elements of this extensive and comprehensive database for monomers, solvents, initiators and chain transfer agents have been included in the appendices of the current paper.

2.4.2. Model testing/troubleshooting

Several examples used to test and refine the model are shown in the following sections based on information from references 1-3. Systems already simulated earlier (1-2) are cited in Table 4. The multicomponent polymerization systems discussed in section 3 of the current paper are either complementary to Part 1 (1) or new simulation scenarios, including laboratory and/or pilot plant data. With performance under so many different conditions, the model can definitely be considered diverse and effective.

Table 4. Previous model simulations from references 1, 2

Homo-polymerization	AN, BA, BMA, EA, HEA, MMA, Sty, VAc
Co-polymerization	BA/MMA, BA/VAc, MMA/VAc, Sty/AN, Sty/BA, Sty/EA, Sty/HEA
Ter-polymerization	BA/MMA/VAc, EA/HEA/MAA, EA/HEA/Sty, EA/MAA/Sty
Tetra-polymerization	EA/HEA/MAA/Sty

3. Results and Discussion

3.1. Co-Polymerization of Styrene and Ethyl Acrylate

Abdollahi *et al.* (106) conducted experiments for the co-polymerization of styrene (Sty) and ethyl acrylate at 70°C in benzene-d_6 solution. Conversion and polymer composition were recorded for five different initial monomer mole fractions, f_{Sty0} = 0.1668, 0.271, 0.548, 0.715, and 0.894, as well as Partial conversion for the f_{sty0} = 0.1668 and 0.548 experiments. The reactivity ratios used, $r_{Sty\text{-}EA}$ = 0.717 and $r_{EA\text{-}Sty}$ = 0.128, were previously tested against data reported by (81) and (4).

Figure 2 shows the polymer composition of styrene for each of the runs; and Figures 3 and 4 show the partial monomer conversions for the first and third experiment. All the trends are captured well regardless of the initial monomer mole fraction.

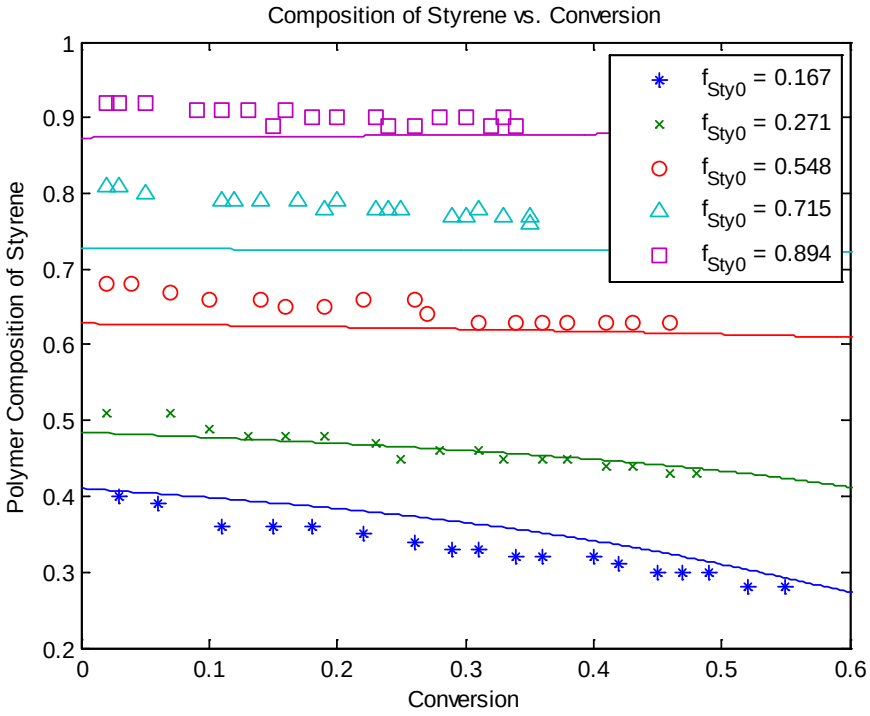

Figure 2. Simulation of the co-polymerization of Sty/EA, T = 70°C, $[BPO]_0$ = 0.045M.

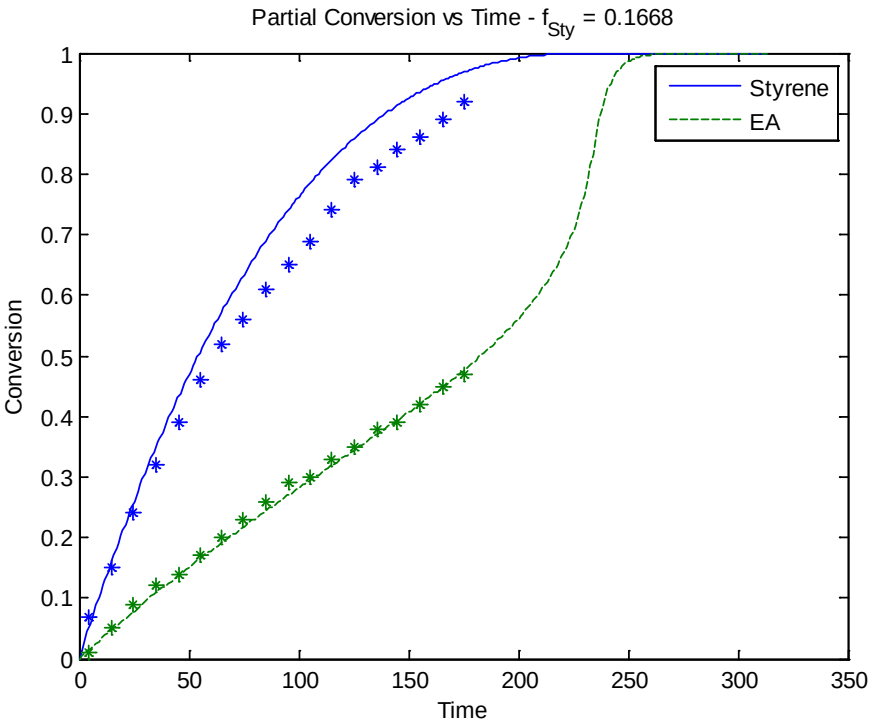

Figure 3. Simulation of the co-polymerization of Sty/EA, T = 70°C, $[BPO]_0$ = 0.045M, f_{Sty0} = 0.1668.

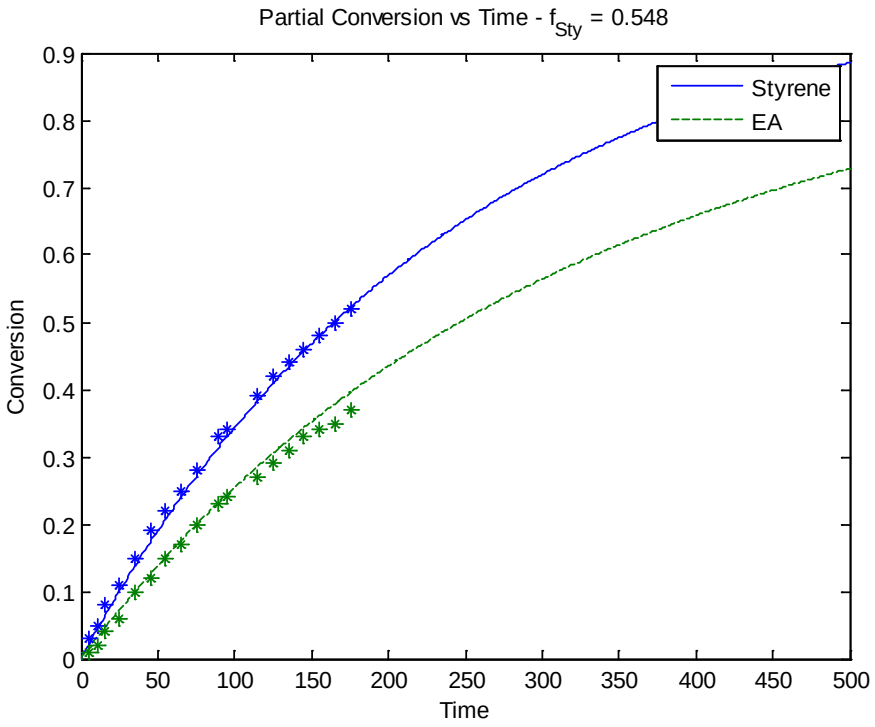

Figure 4. Simulation of the co-polymerization of Sty/EA, T = 70°C, $[BPO]_0$ = 0.047M, f_{Sty0} = 0.548.

3.2. Co-polymerization of methyl methacrylate and butyl acrylate

Methyl methacrylate was co-polymerized with butyl acrylate at 90°C/115°C/140°C using di-tert-butyl peroxide (dTBPO) as an initiator and tolene as a solvent (94). Approximately 0.006M of n-dodecyl mercaptan was used as a chain transfer agent in each of the 18 runs. The reactivity ratios used were taken from (12, 13): r_{MMA-BA} = 1.78938 and r_{BA-MMA} = 0.29763. Conversion and polymer composition data were obtained from nearly all of the

18 runs, whereas weight-average molecular weight data were presented for a few of the 90°C runs. Observation of Table 5 shows that there are many duplicate polymerizations: Runs 1/2, 6/7, 10/11, 15/16. As the data were similar and the simulation the same, only one plot of each duplicate is shown in the following analysis.

Table 5. Co-polymerization of MMA/BA with dTBPO as initiator and n-dodecyl mercaptan as CTA (94)

Run	**Temperature (°C)**	**f_{MMA0}**	**Toluene (wt%)**	**dTBPO (M)**
1	90	0.852	30	0.044
2	90	0.852	30	0.045
3	90	0.561	30	0.045
4	90	0.851	23	0.045
5	90	0.561	23	0.045
6	90	0.852	0	0.047
7	90	0.852	0	0.045
8	90	0.745	0	0.046
9	115	0.852	30	0.0062
10	115	0.851	30	0.045
11	115	0.852	30	0.045

12	115	0.852	23	0.0058
13	115	0.561	0	0.0063
14	115	0.852	0	0.0061
15	140	0.852	30	0.00050
16	140	0.852	30	0.00047
17	140	0.852	0	0.00049
18	140	0.745	0	0.00045

Figures 5 through 11 show the conversion vs. time predictions against the experimental data for runs 1, 7, 9, 11, 12, 14, and 15. Figures 12 through 18 are the polymer composition plots for runs 2, 3, 5, 10, 12, 13, and 16. The final three figures, Figures 19 to 21, represent the weight-average molecular weight data against conversion for runs 2, 5 and 8. These molecular weight figures show acceptable predictions for the course of the reaction. Each of the conversion and composition simulations proved very accurate under diverse conditions.

Depropagation was accounted for runs 15 through 18 (T = 140°C) as MMA is known to depropagate at elevated temperatures (164). In terms of depropagation parameters (see section 2.3.1), the data used to model this were given by (164): $R_1 = 0$, R_2

= 0.008, R_{11} = 0.085, R_{22} = 0. Basically, R_2 represents the depropagation of MMA from a penultimate unit of BA, whereas R_{11} represents the homo-depropagation of MMA.

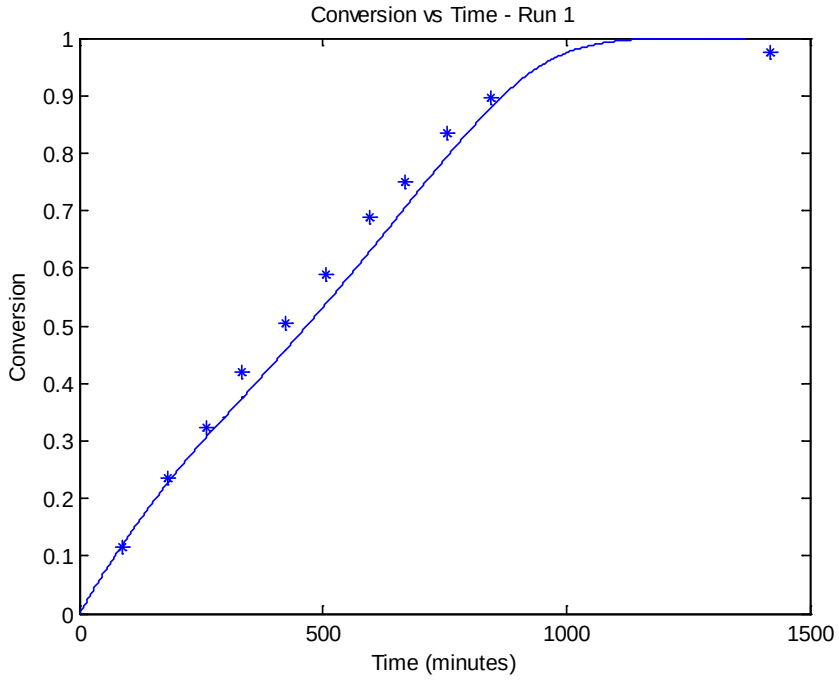

Figure 5. Simulation of the co-polymerization of MMA/BA, T = 90°C, $[dTBPO]_0$ = 0.044M, toluene = 30 wt%, f_{MMA0} = 0.852.

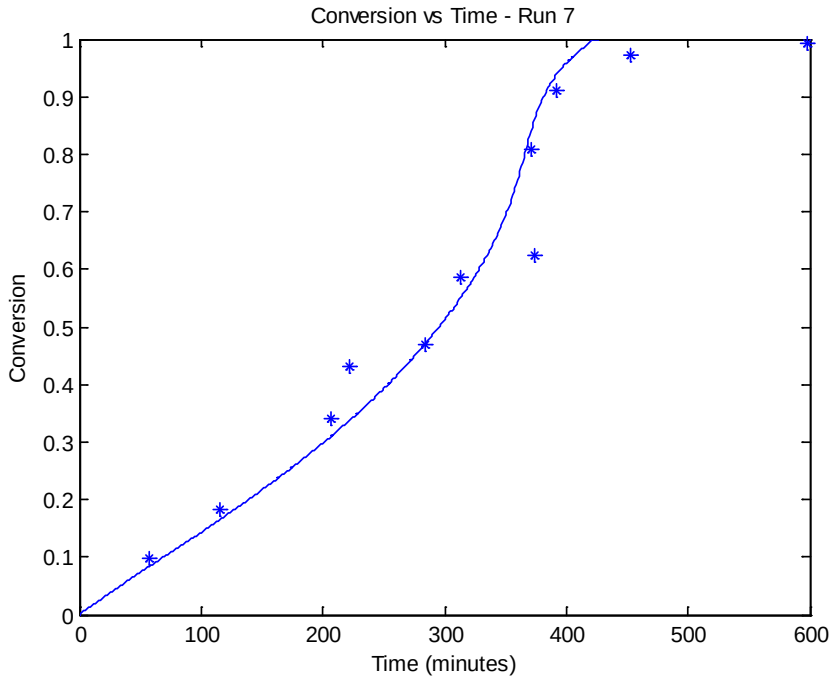

Figure 6. Simulation of the co-polymerization of MMA/BA, T = 90°C, $[dTBPO]_0$ = 0.045M, toluene = 0 wt%, f_{MMA0} = 0.852.

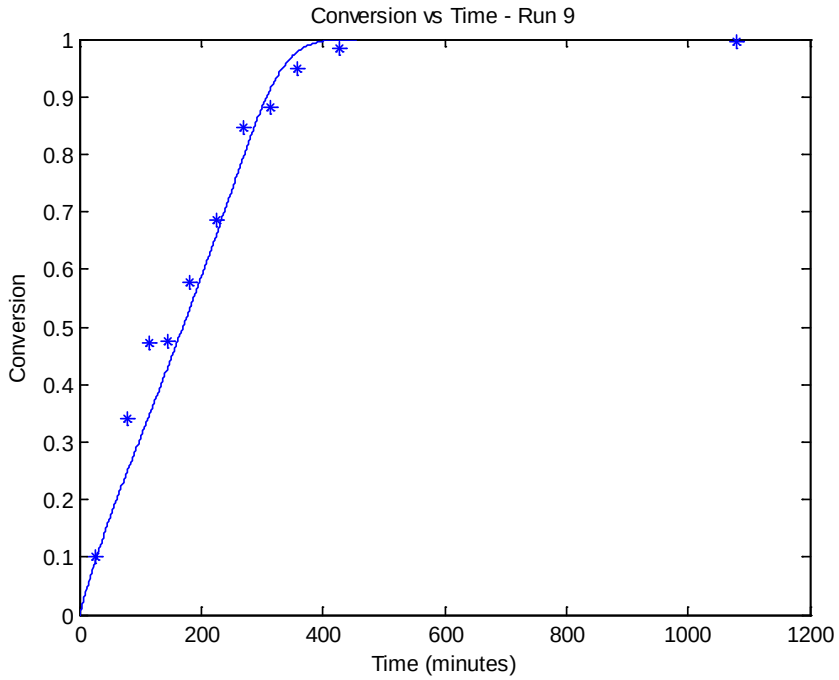

Figure 7. Simulation of the co-polymerization of MMA/BA, T=115°C, $[dTBPO]_0$= 0.0062M, toluene = 30 wt%, f_{MMA0} = 0.852.

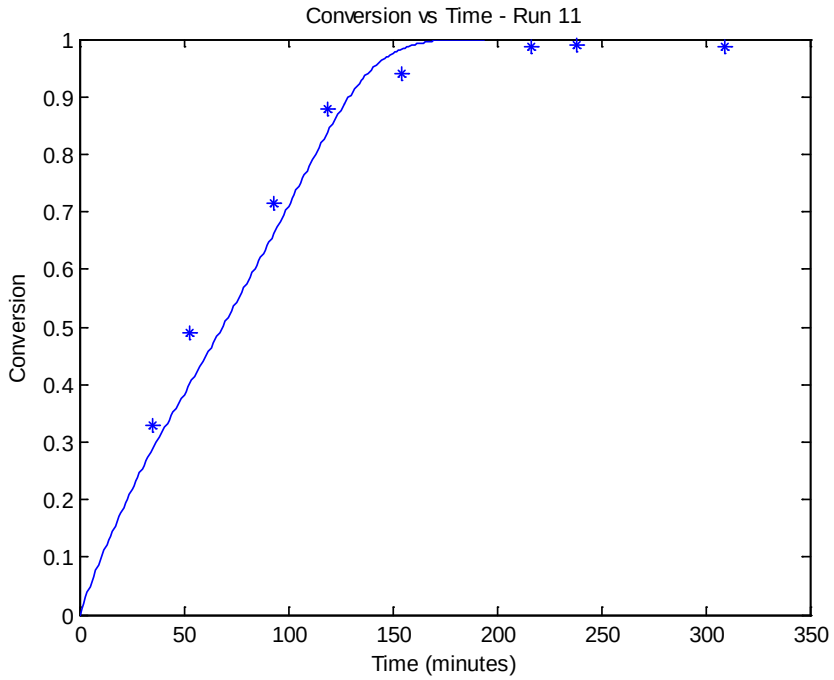

Figure 8. Simulation of the co-polymerization of MMA/BA, T= 115°C, $[dTBPO]_0$ = 0.045M, toluene = 30 wt%, f_{MMA0} = 0.852.

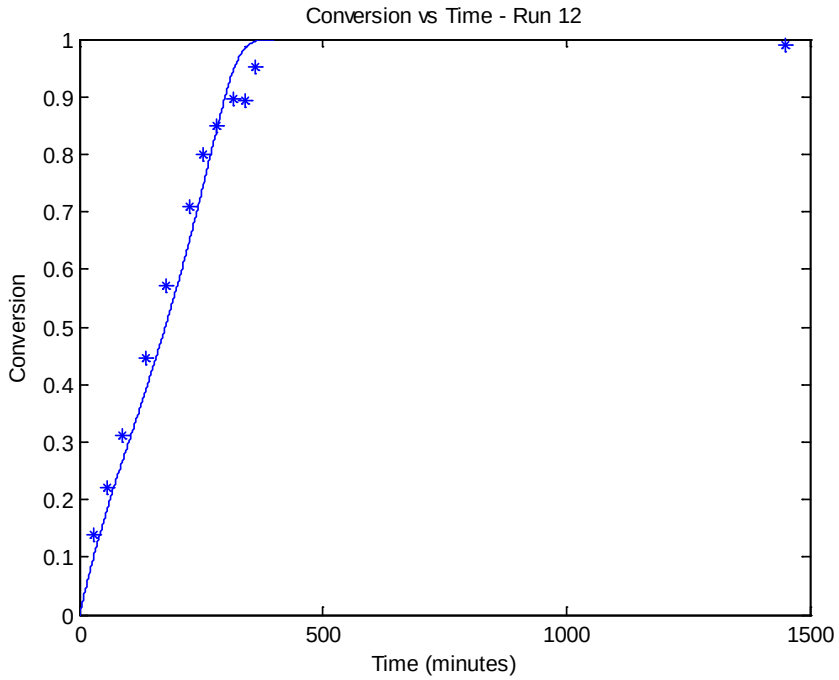

Figure 9. Simulation of the co-polymerization of MMA/BA, T=115°C, $[dTBPO]_0$= 0.0058M, toluene = 23 wt%, f_{MMA0} = 0.852.

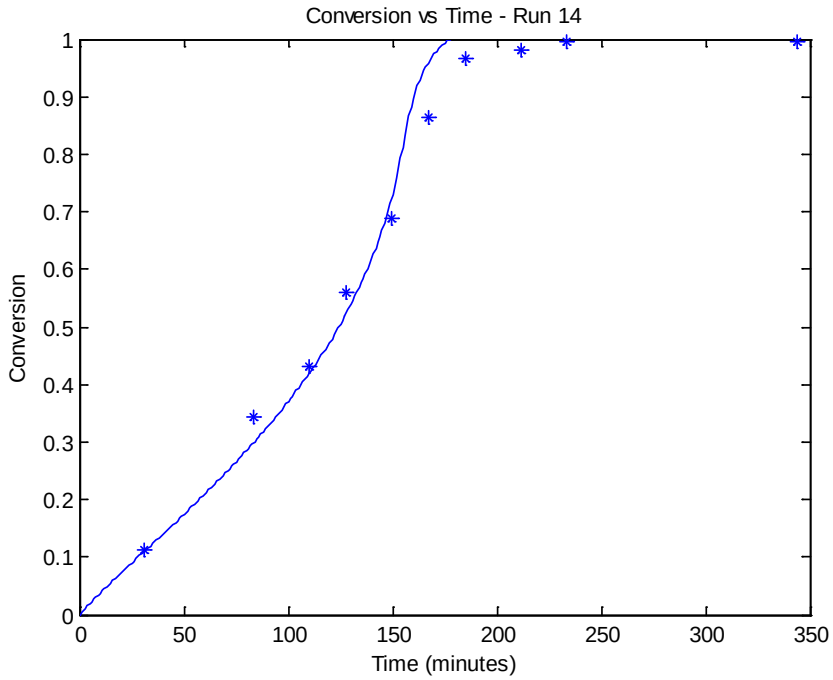

Figure 10. Simulation of the co-polymerization of MMA/BA, T=115°C, $[dTBPO]_0$=0.0061M, toluene = 0 wt%, f_{MMA0} = 0.852.

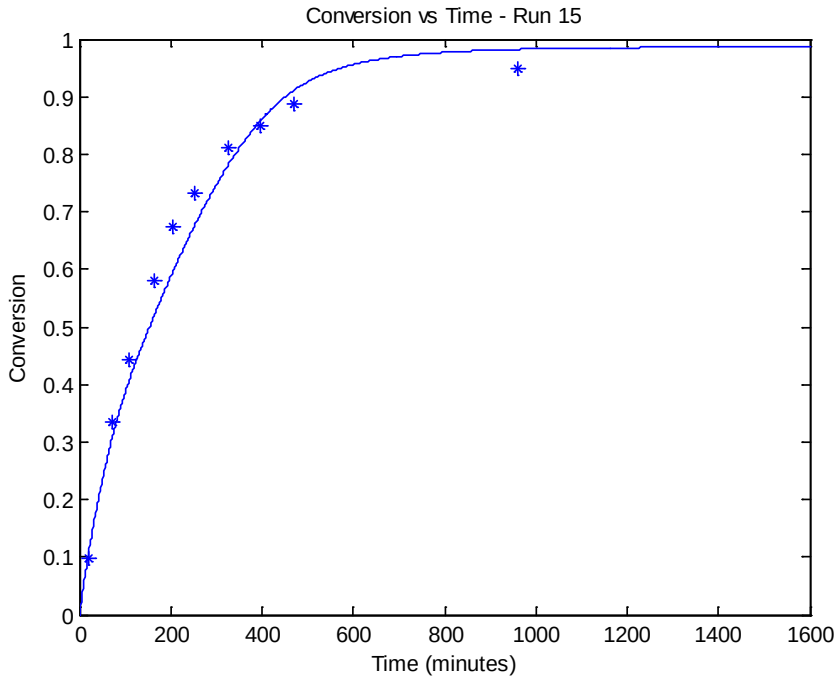

Figure 11. Simulation of the co-polymerization of MMA/BA, T=140°C, $[dTBPO]_0$=0.0005M, toluene = 30 wt%, f_{MMA0} = 0.852.

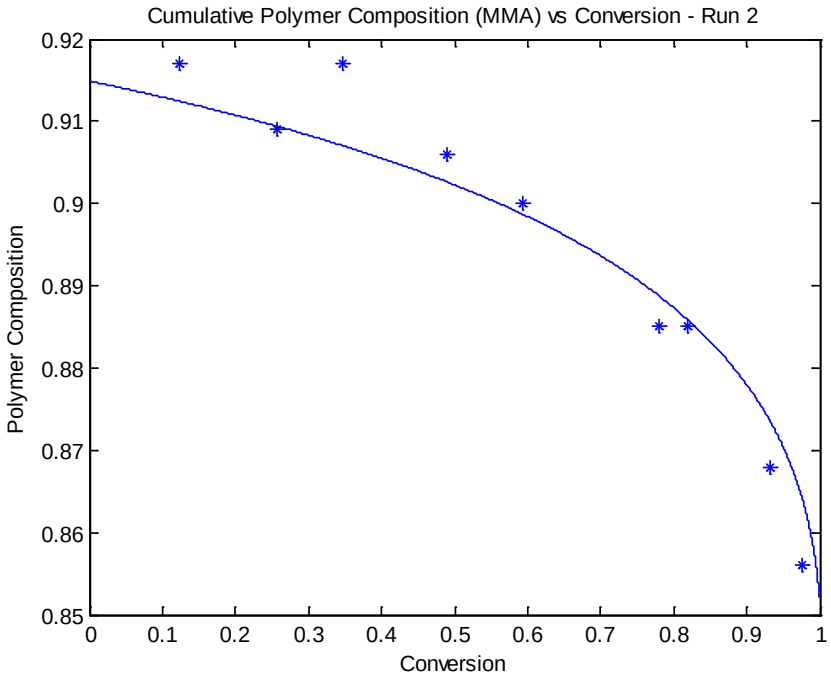

Figure 12. Simulation of the co-polymerization of MMA/BA, T= 90°C, $[dTBPO]_0$ = 0.045M, toluene = 30 wt%, f_{MMA0} = 0.852.

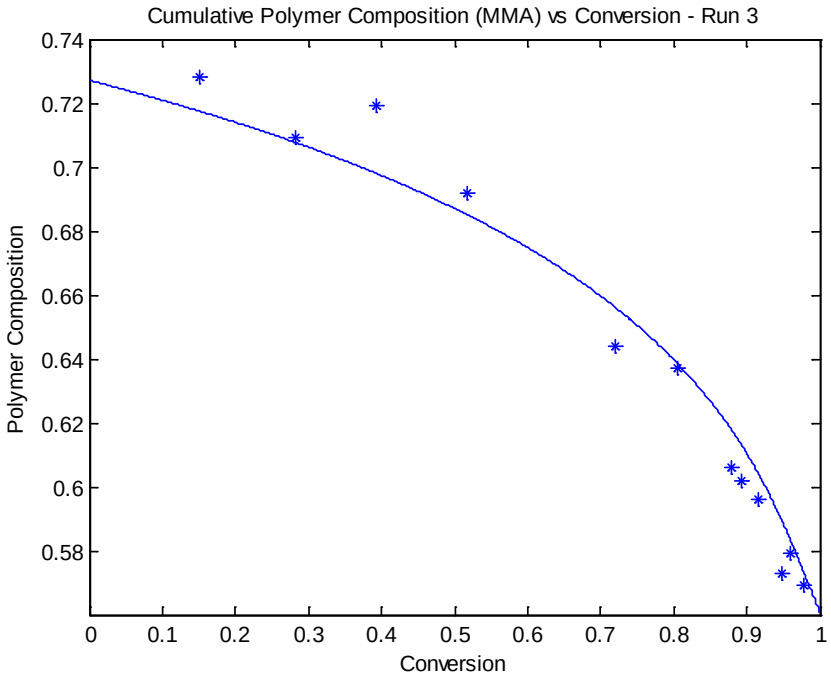

Figure 13. Simulation of the co-polymerization of MMA/BA, T= 90°C, $[dTBPO]_0$ = 0.045M, toluene = 30 wt%, f_{MMA0} = 0.561.

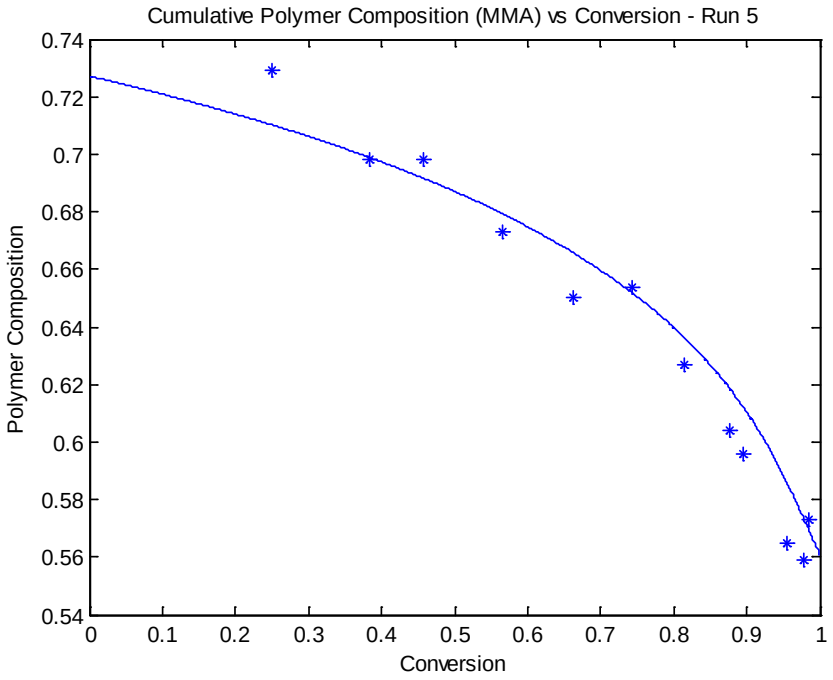

Figure 14. Simulation of the co-polymerization of MMA/BA, T= 90°C, $[dTBPO]_0$ = 0.045M, toluene = 23 wt%, f_{MMA0} = 0.561.

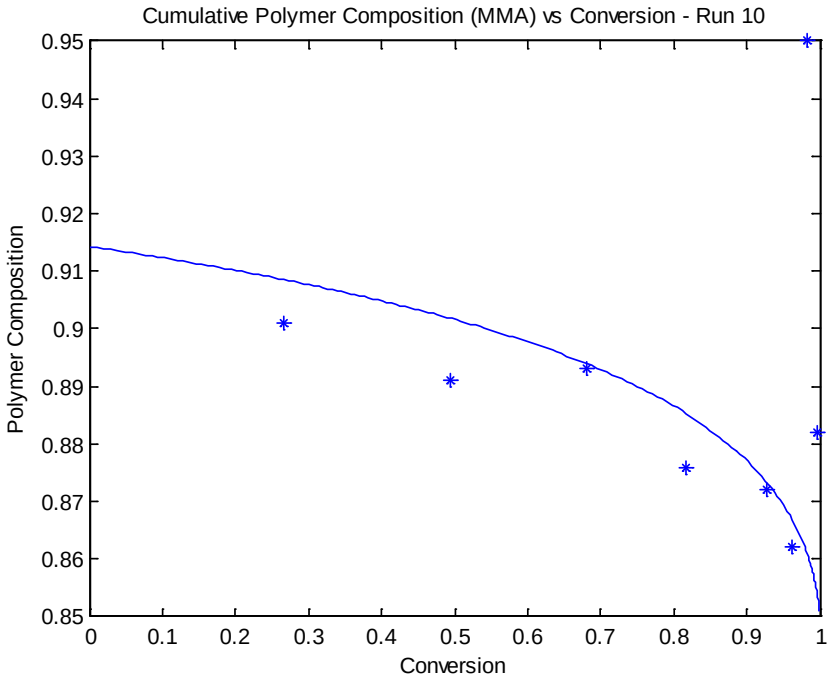

Figure 15. Simulation of the co-polymerization of MMA/BA, T=115°C, $[dTBPO]_0$= 0.045M, toluene = 30 wt%, f_{MMA0} = 0.851.

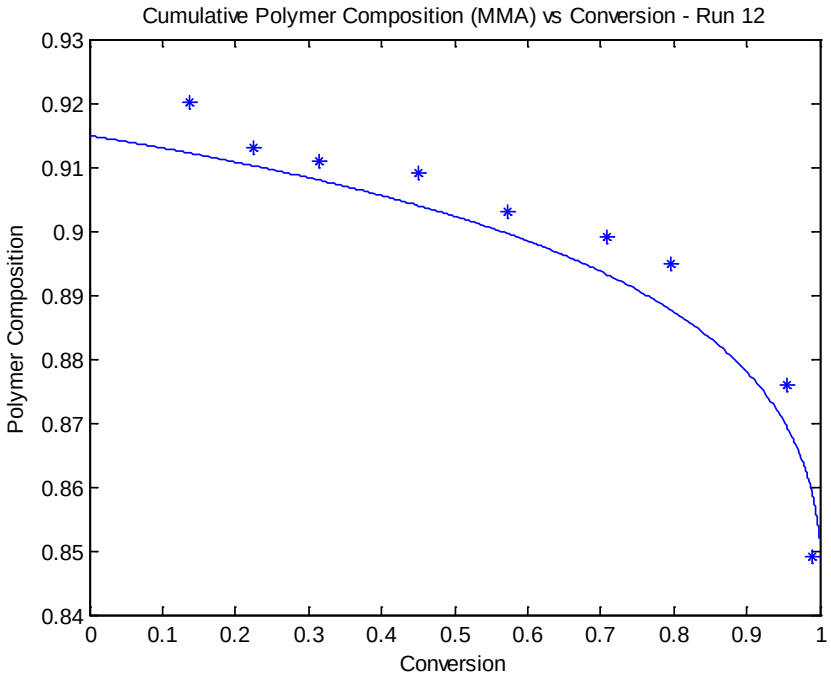

Figure 16. Simulation of the co-polymerization of MMA/BA, T=115°C, $[dTBPO]_0$=0.0058M, toluene = 23 wt%, f_{MMA0} = 0.852.

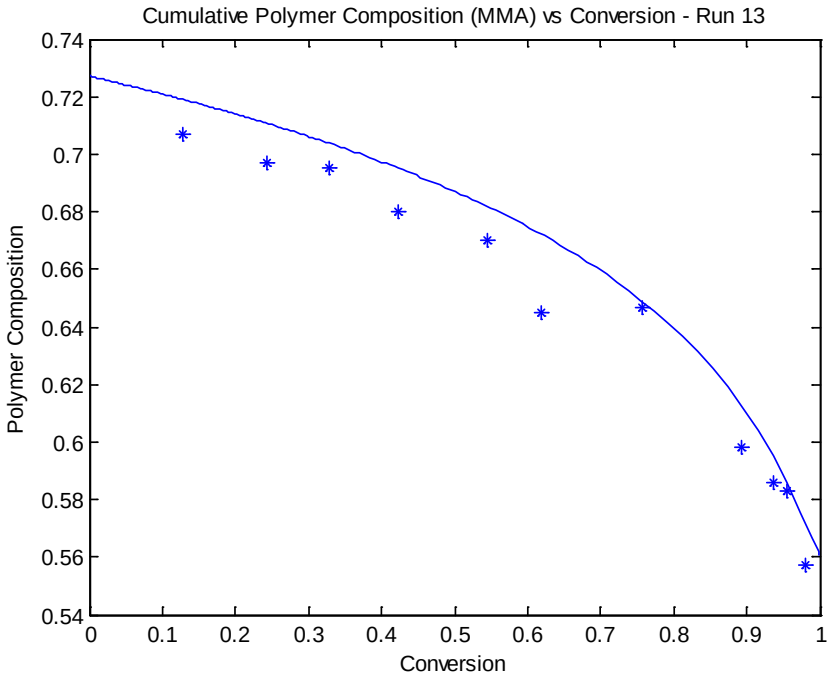

Figure 17. Simulation of the co-polymerization of MMA/BA, T=115°C, $[dTBPO]_0$=0.0063M, toluene = 0 wt%, f_{MMA0} = 0.561.

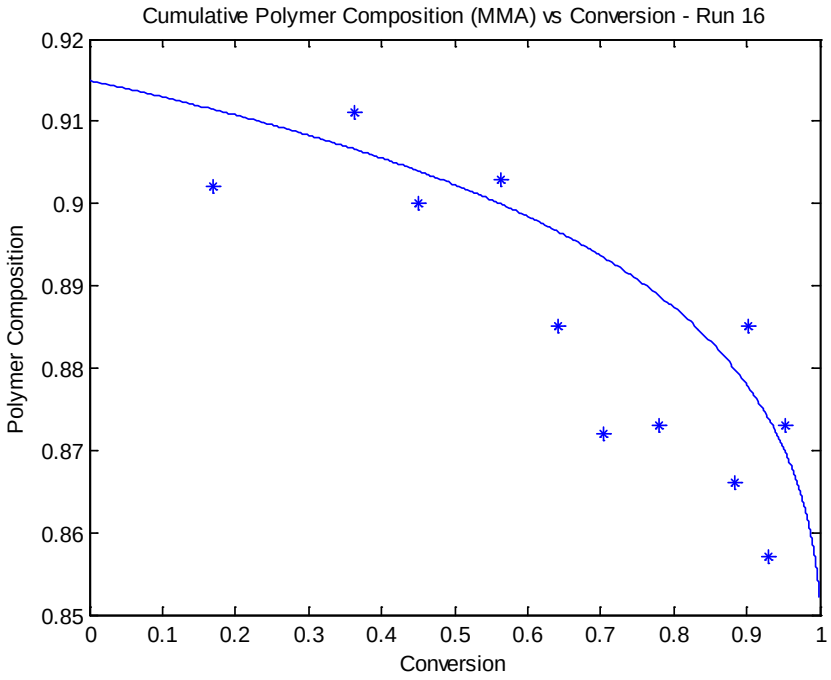

Figure 18 Simulation of the co-polymerization of MMA/BA, T=140°C, $[dTBPO]_0$=0.00047M, toluene = 30 wt%, f_{MMA0} = 0.852.

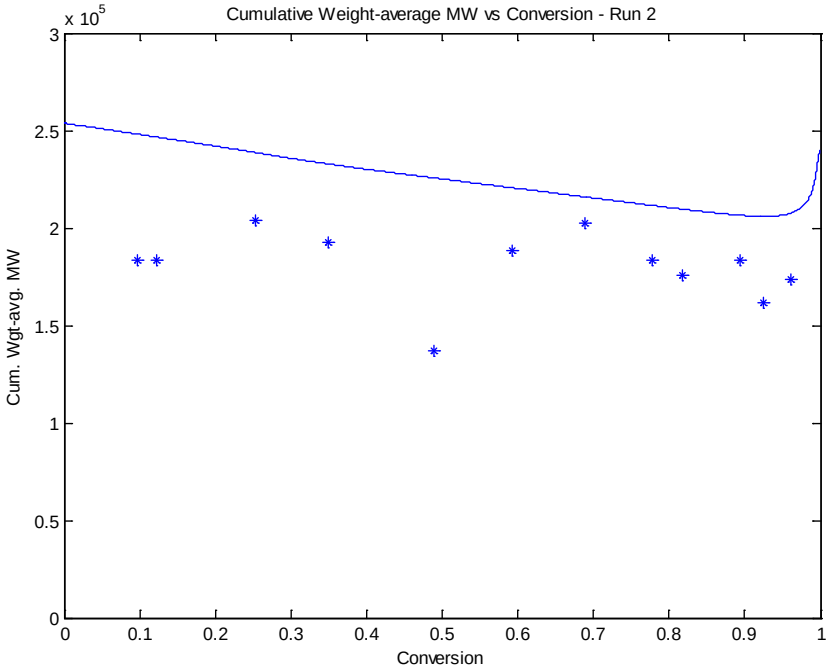

Figure 19. Simulation of the co-polymerization of MMA/BA, T= 90°C, $[dTBPO]_0$ = 0.045M, toluene = 30 wt%, f_{MMA0} = 0.852.

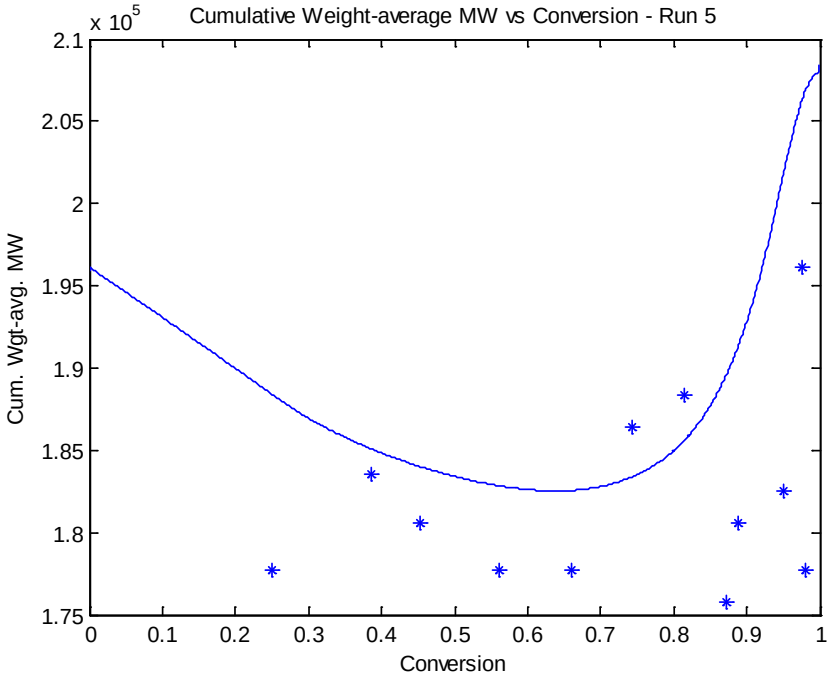

Figure 20. Simulation of the co-polymerization of MMA/BA, T= 90°C, $[dTBPO]_0$ = 0.045M, toluene = 23 wt%, f_{MMA0} = 0.561.

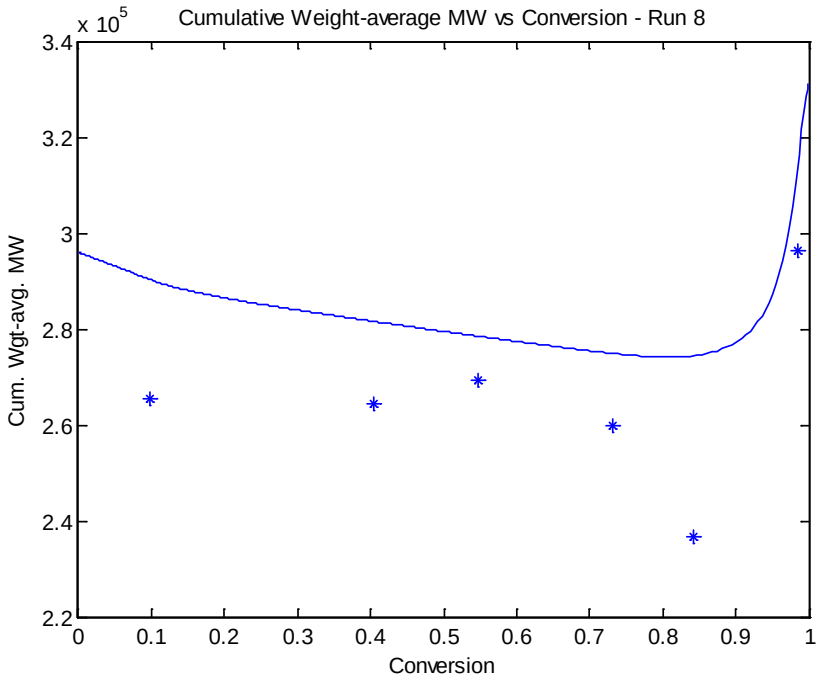

Figure 21. Simulation of the co-polymerization of MMA/BA, T= 90°C, $[dTBPO]_0$ = 0.046M, toluene = 0 wt%, f_{MMA0} = 0.745.

3.3. Co-polymerization of styrene and acrylonitrile

The co-polymerization of styrene (designated as monomer 1) and acrylonitrile (monomer 2) was simulated ten times at 60°C, each time with a different starting monomer mole fraction. The conversion was kept very low and triad fraction data against the mole fraction of styrene were plotted. Hill *et al.* (54) conducted the same runs and their experimental data are shown in the figures below. The reactivity ratios, $r_{Sty\text{-}AN} = 0.360$ and $r_{AN\text{-}Sty} = 0.078$, were taken from (59). Figure 22 shows the styrene-centered triad fractions and Figure 23 shows the AN-centered triad fraction (212 represents the triad fraction of AN-Sty-AN). As expected, both the simulations and the experimental data show that styrene is more reactive than AN. The simulations prove to be very accurate and follow the trends very well.

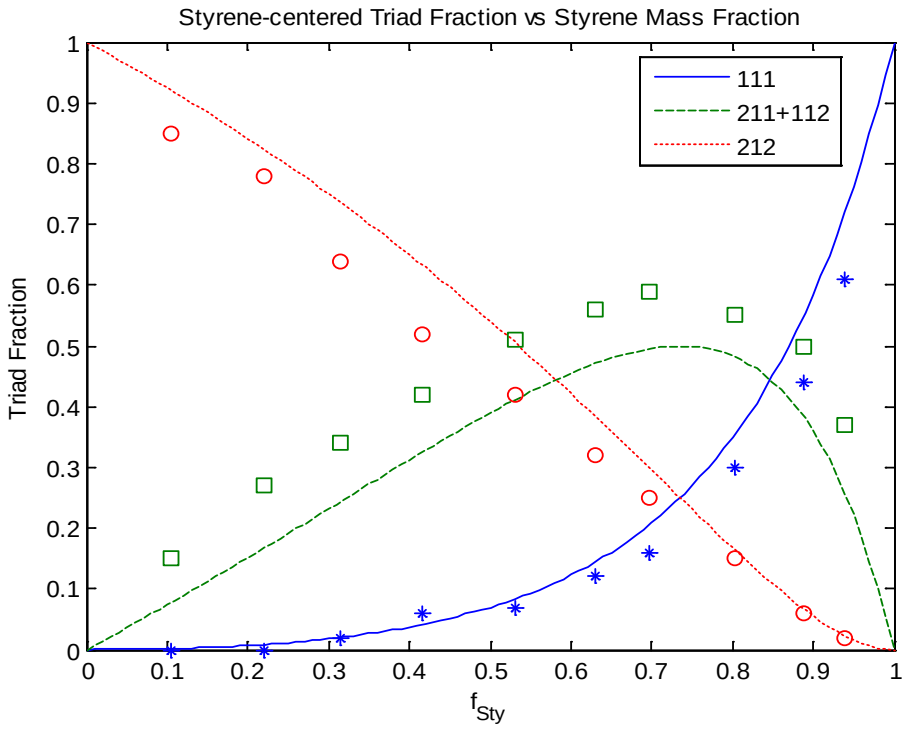

Figure 22. Simulation of the batch co-polymerization of Sty/AN, T = 60°C.

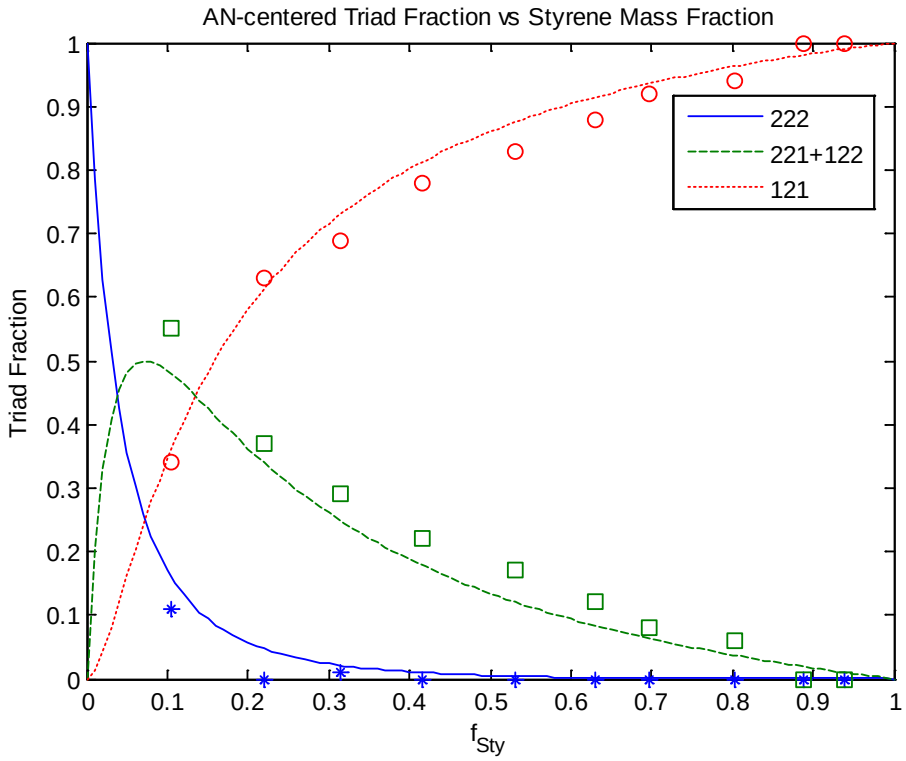

Figure 23. Simulation of the batch co-polymerization of Sty/AN, T = 60°C.

3.4. Co-polymerization of methyl methacrylate and methyl acrylate

Methyl methacrylate (monomer 1) and methyl acrylate (monomer 2) were co-polymerized at 50°C by (96) at six different monomer mole fractions. The triad fraction data against the MMA mole fraction at the initial stages of each of the reactions are shown in Figure 24 (MMA-centered) and Figure 25 (MA-centered). The reactivity ratios used come from the same paper as the experimental data being tested (96): $r_{MMA\text{-}MA}$ = 2.60 and $r_{MA\text{-}MMA}$ =

0.27. This means that the results of this section primarily demonstrate the functionality of our triad fraction calculations.

The modeling software shows a very good agreement with the experimental data in both simulations. Note that 212 in this case represents the triad fraction MA-MMA-MA.

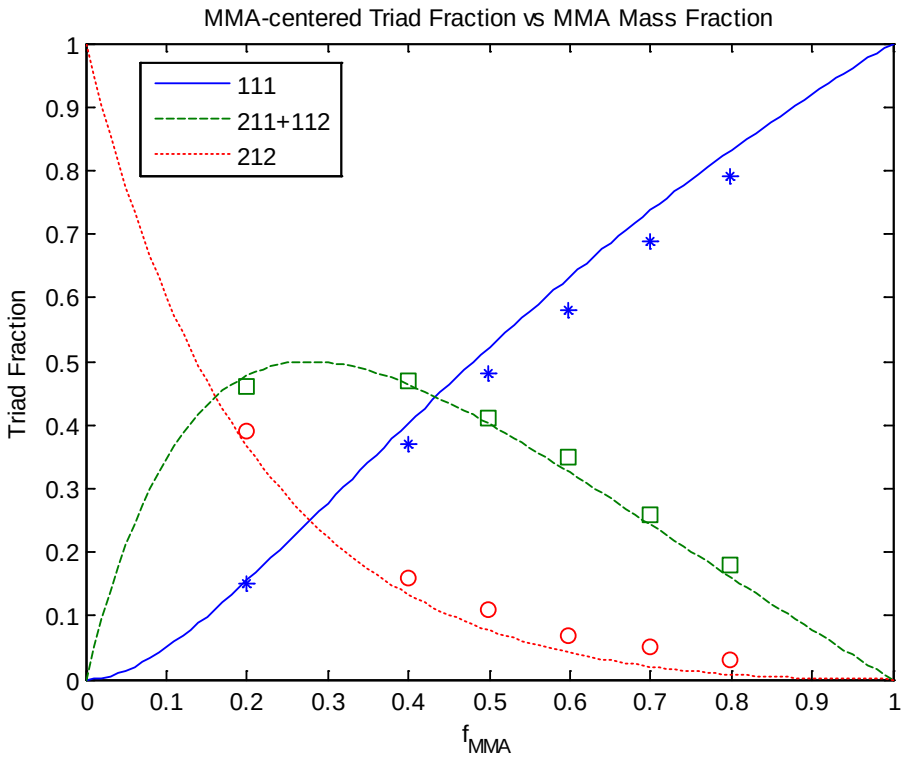

Figure 24. Simulation of the co-polymerization of MMA/MA, T = 50°C.

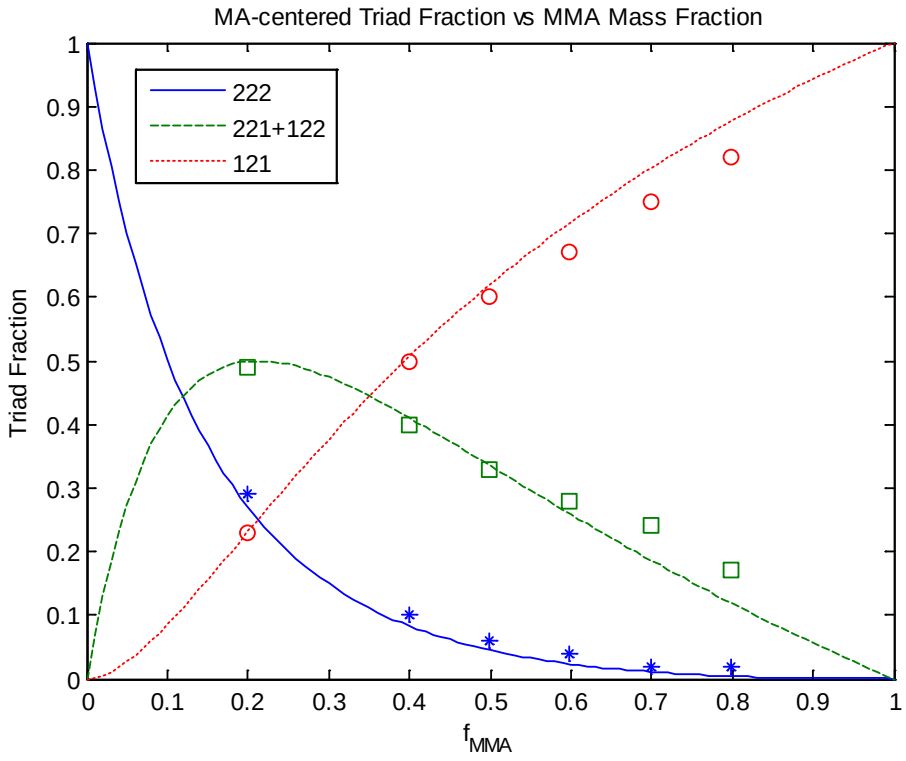

Figure 25. Simulation of the co-polymerization of MMA/MA, T = 50°C.

3.5. Co-polymerization of Alpha Methyl Styrene and Methyl Methacrylate

A co-polymerization of AMS and MMA was performed at lower temperatures by (87). Composition drift data were taken at 50°C, 60°C and 80°C. As AMS is known to depropagate at lower than average temperatures, simulations were carried out with and without depropagation to show the large effect that the reverse reaction has. The reactivity ratios as well as the cross- and homo-depropagation ratios were taken from (91):

$r_{AMS-MMA} = 0.734$ $r_{MMA-AMS} = 0.548$

$R_1 = \exp(-6222/T + 18.34)$ $R_2 = 0$

$R_{11} = 253469.8*\exp(-3489.1/T)*r_{AMS-MMA}$ $R_{22} = 0$

Figure 26 shows the instantaneous composition drift at 60°C, whereas Figure 27 shows the same effect at 80°C. The polymerizations were done at five different monomer mole fractions for each temperature. The accuracy of Krüger's model confirms the presence of depropagation and is very important for accurate multi-component modeling.

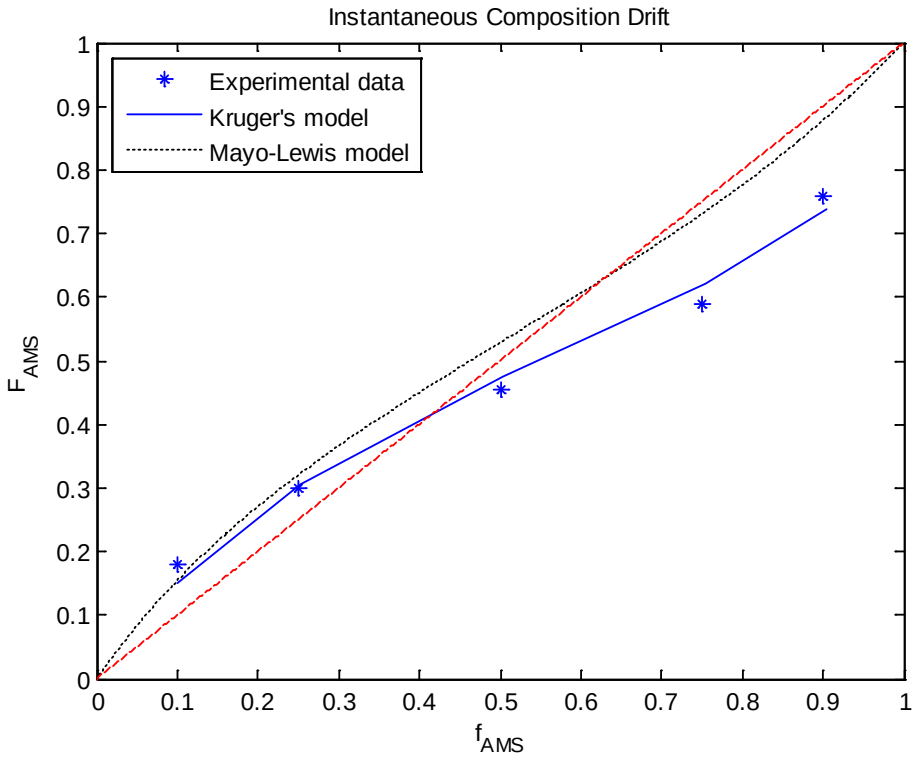

Figure 26. Simulation of the co-polymerization of AMS/MMA at 60°C.

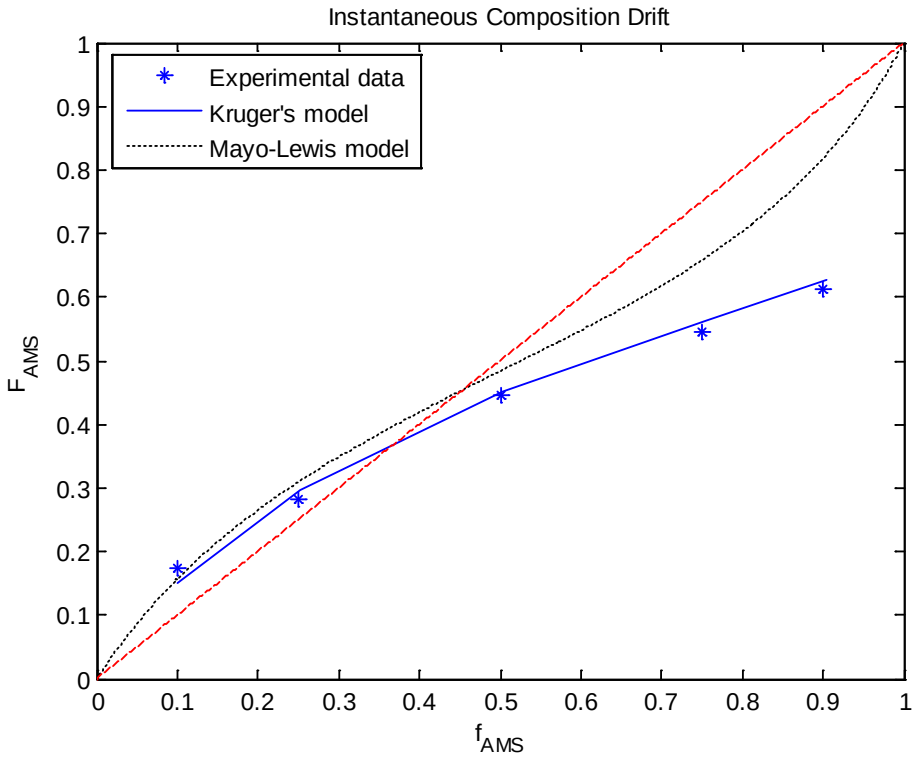

Figure 27. Simulation of the co-polymerization of AMS/MMA at 80°C.

3.6. Model Extensions/Refinements and Case Studies

3.6.1. Depropagation

The importance of depropagation can be seen in a conversion vs. time simulation of the co-polymerization of MMA and BA at 140°C with 30% by weight toluene (94). Figure 28 displays the simulation against literature data with the standard termination reaction constant between MMA and BA and the simulation with a severely increased termination reaction constant. The drastic increase had minimal effect on conversion. Figure 29 uses

the standard termination constant but accounts for depropagation of MMA at this elevated temperature.

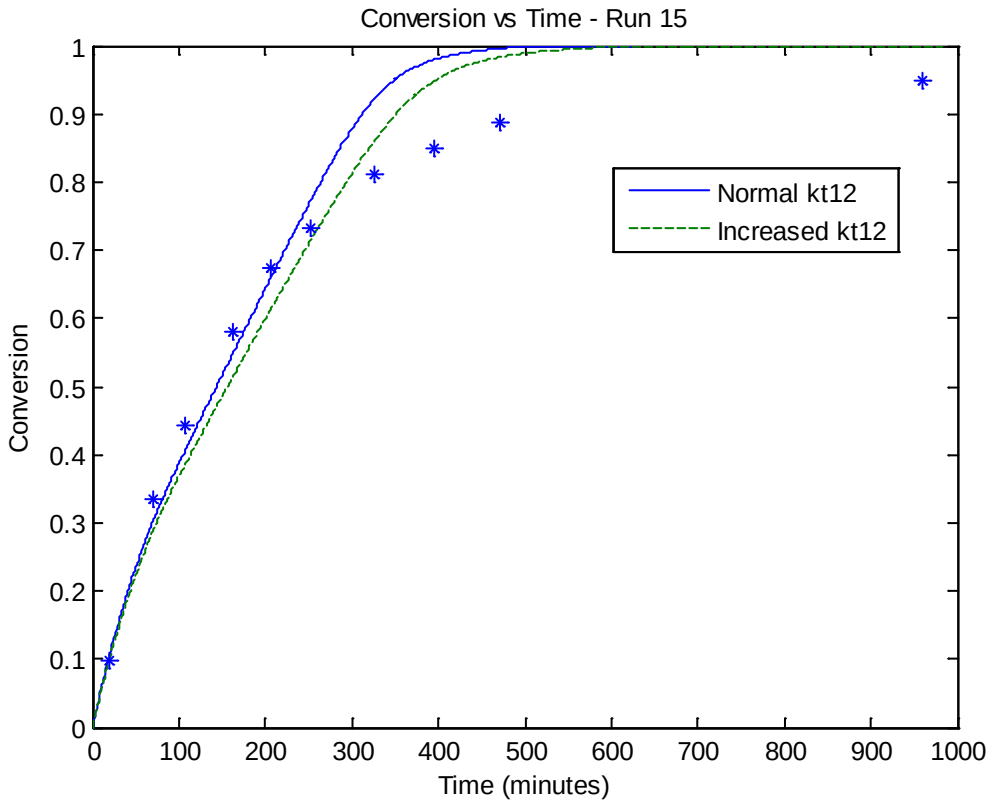

Figure 28. Simulation of the co-polymerization of MMA/BA, T=140°C, $[dTBPO]_0$=0.0005M, toluene = 30 wt%, f_{BA0} = 0.148.

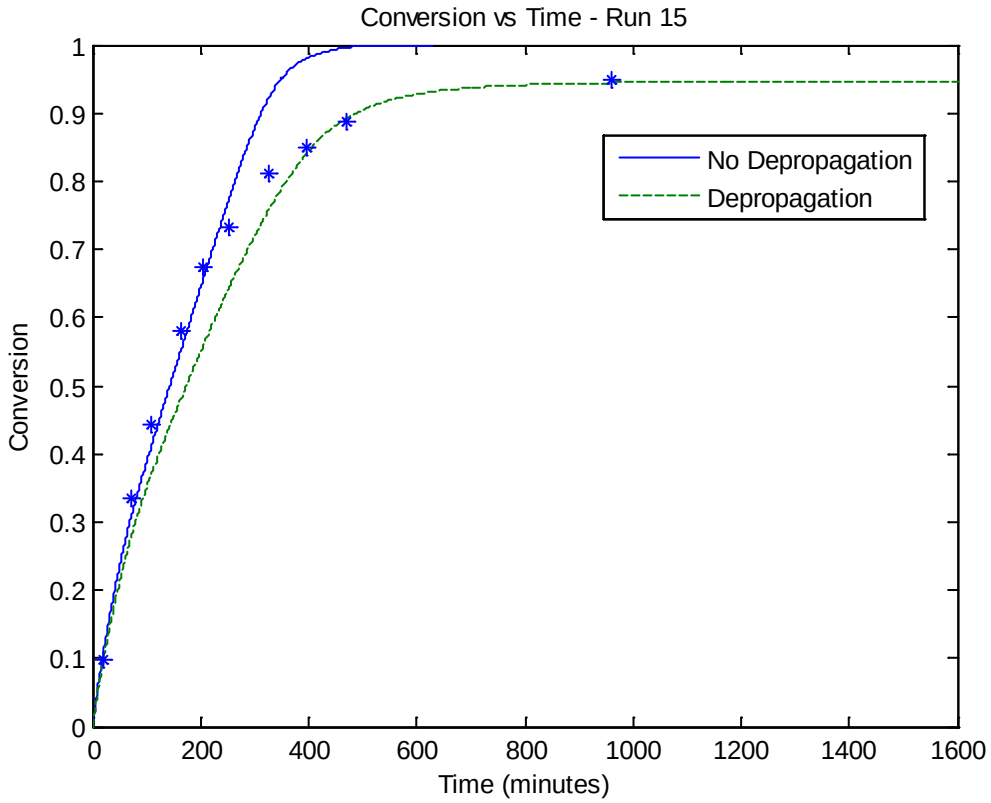

Figure 29. Simulation of the co-polymerization of MMA/BA, T= 140°C, $[dTBPO]_0$=0.0005M, toluene = 30 wt%, f_{BA0} = 0.148.

This shows that at elevated temperatures, depropagation is a fundamental modeling extension and requires adequate explanation. This alters the original propagation reactions and consequently, all of the monomer and radical balances. As such, the effects of depropagation are observed not only on conversion but also on polymer composition,

molecular weight, and sequence length distribution. The additional complexity arising to account for depropagation was briefly explained in section 2.3.1.

3.6.2. Case study 1: Homo-polymerization of butyl methacrylate

Butyl methacrylate was polymerized in solution at two different temperatures and three different monomer concentrations: 17 wt% at 110°C and 9/17/34 wt% at 132°C (161). The initiator, di-tert-butyl peroxide, was used at 1 wt% of monomer. Xylene was used as the solvent and no chain transfer agents or inhibitors were present. Monomer concentration and molecular weight data vs. time were extracted from (161).

This example has been included here to illustrate the sensitivity of monomer concentration and related variables when accounting for depropagation. An earlier paper by (103) had a depropagation rate constant slightly higher than that indicated by the results reported in (161); the difference being in the exponential term:

k_{dp} $k_p*(1.76-1.37*w_p)*10^6*\exp(-\mathbf{6145}/T)$ (from ref 103)

k_{dp} $k_p*(1.76-1.37*w_p)*10^6*\exp(-\mathbf{6240}/T)$ (from ref 161)

As one can see, Figure 30, representing the depropagation rate constant from (103), shows quite unfavorable results arising from the higher depropagation rate constant. Figure 31, however, produces a simulation much more true to the data obtained.

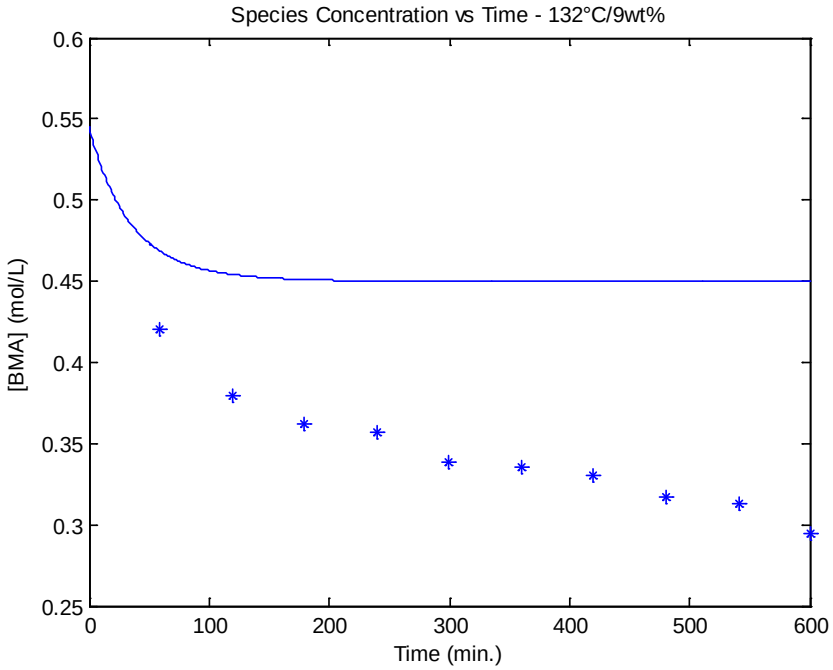

Figure 30. Simulation of the homo-polymerization of BMA, T = 132 °C, $[dTBPO]_0$ = 0.09 wt%, xylene = 91 wt%, k_{dp} from (103).

With only the depropagation rate constant exponential term changing slightly (the value in (103, 105) being only 1.26 times larger than that in (161, 162) at 132°C), the difference in final conversion achieved, or more specifically to the plots at hand, the difference in the total amount of monomer consumed, is quite significant. This shows how

precise the depropagation rate constant must be in order to accurately model depropagation.

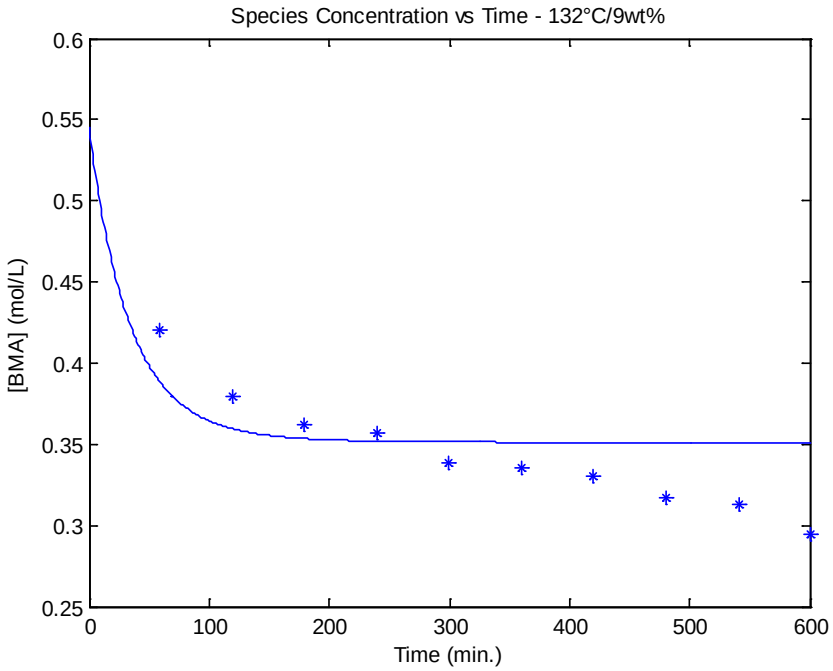

Figure 31. Simulation of the homo-polymerization of BMA, T = 132°C, $[dTBPO]_0$ = 0.09 wt%, xylene = 91 wt%, k_{dp} from (161).

sThe remainder of the simulations uses the more accurate depropagation rate constant. Figures 32 and 33 show other monomer concentration vs. time plots, all showing good results. Figure 34 shows molecular weight vs. time plots at 132°C. Molecular weight

data are much more difficult to predict (although the main trends are captured), given also the error in measuring such low molecular weight averages.

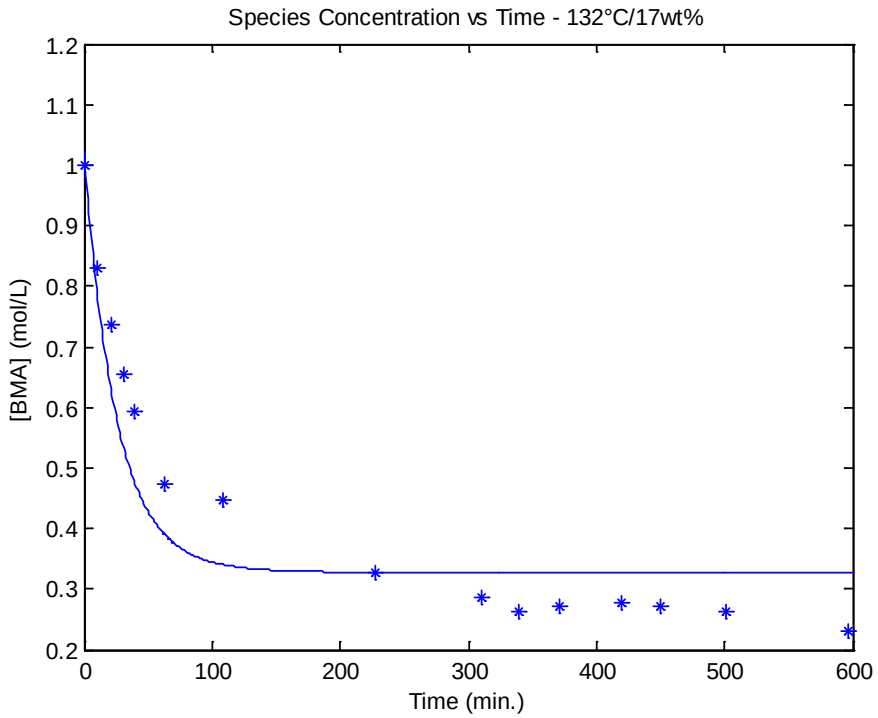

Figure 32. Simulation of the homo-polymerization of BMA, T = 132°C, $[dTBPO]_0$ = 0.17 wt%, xylene = 83 wt%.

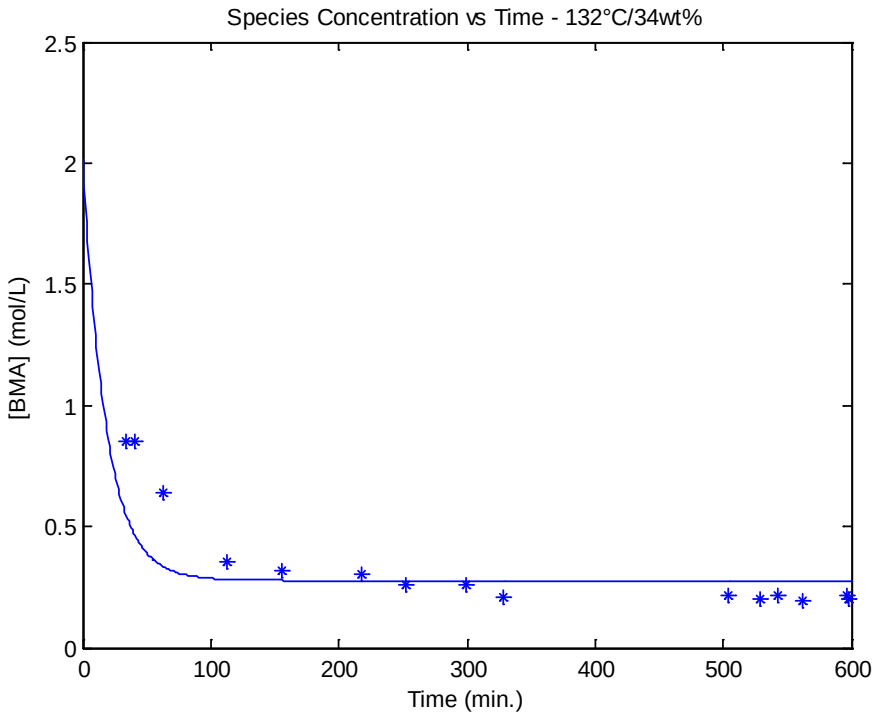

Figure 33. Simulation of the homo-polymerization of BMA, T = 132°C, $[dTBPO]_0$ = 0.34 wt%, xylene = 66 wt%.

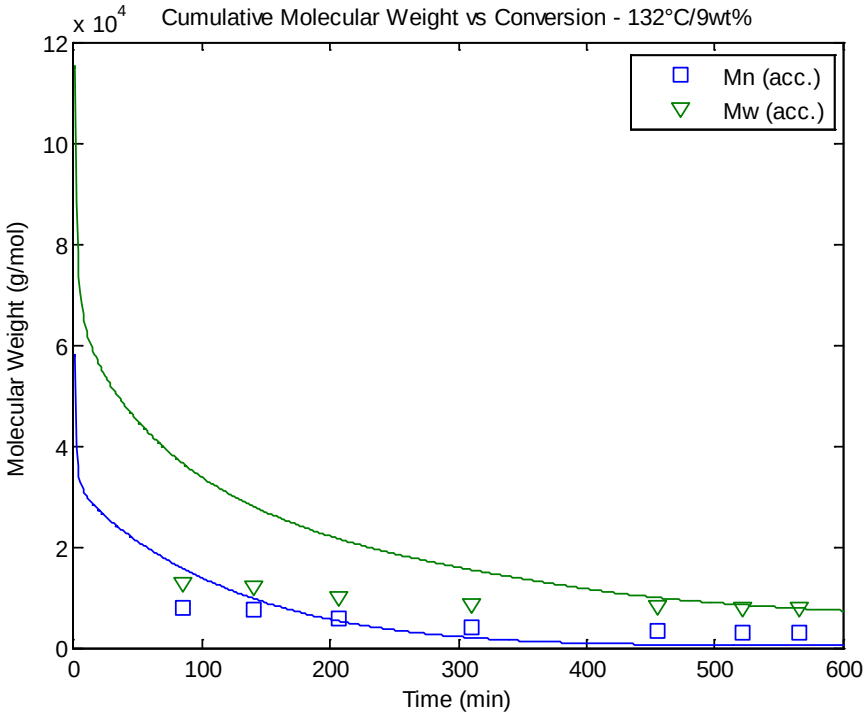

Figure 34. Simulation of the homo-polymerization of BMA, T = 132°C, $[dTBPO]_0$ = 0.09 wt%, xylene = 91 wt%.

3.6.3. Case study 2: Co-polymerization of alpha methyl styrene and styrene

This case study is another prime example demonstrating the importance of depropagation. Fischer (45) ran four co-polymerizations of AMS and styrene at different temperatures recording the composition drift throughout. The reactivity ratios and depropagation data are presented in Table 6 and were taken from (45):

Table 6. Kinetic data for the co-polymerizations of AMS and Styrene

T (°C)	$r_{AMS-Sty}$	$r_{Sty-AMS}$	K_{eq} (mol/L)*	R_2
60	0.15	1.00	7.1	0
90	0.30	1.09	17.2	0
110	0.40	1.13	28.5	0
150	0.80	1.20	67.0	0.8

* $k_{dp,AMS} = K_{eq} * k_{p,AMS}$

AMS is known to homo-depropagate at low temperatures. The same phenomenon is observed here as well. Figure 35 is the co-polymerization of AMS and styrene at 60°C. The small effect that the depropagation of AMS has is shown as the slight departure from the Mayo-Lewis curve. As expected, with each increase in temperature follows a greater difference between our model and the Mayo-Lewis prediction (see Figures 36 and 37 for 90°C and 110°C, respectively). By the time the co-polymerization reaches 150°C in Figure 38, the difference has become quite large. At that point, AMS has begun to depropagate from penultimate units of styrene as simulated by the cross-depropagation ratio, $R_2 = 0.8$. Another trend with increasing temperature is that the Mayo-Lewis curve nears the 45° line. This is a result of the change in reactivity ratios; $r_{AMS-Sty}$ and $r_{Sty-AMS}$

become closer and closer to unity as the steric hindrances of AMS become less predominant at high temperatures.

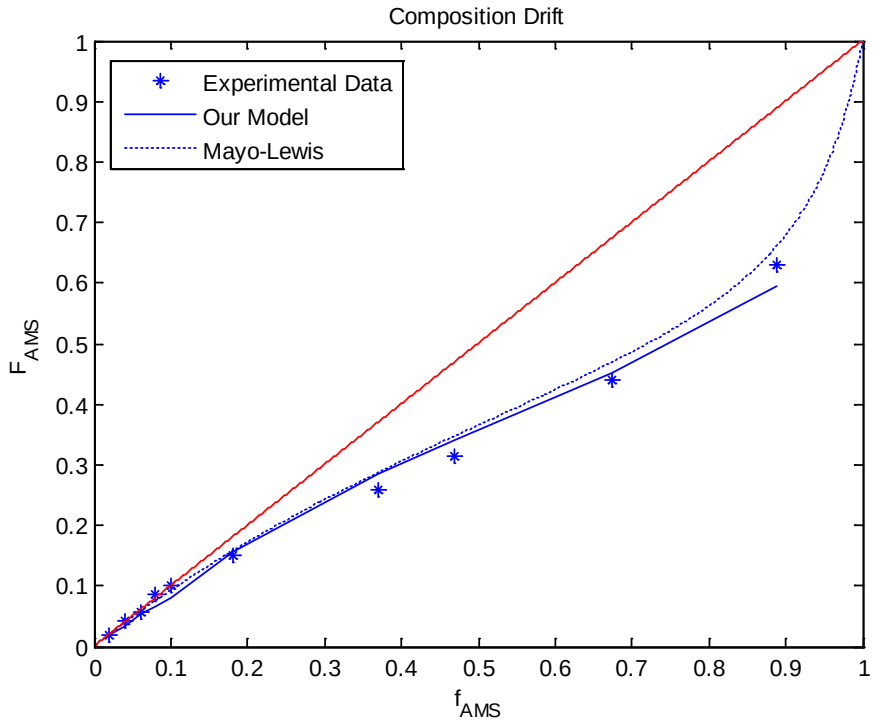

Figure 35. Simulation of the co-polymerization of AMS/Sty, T = 60°C.

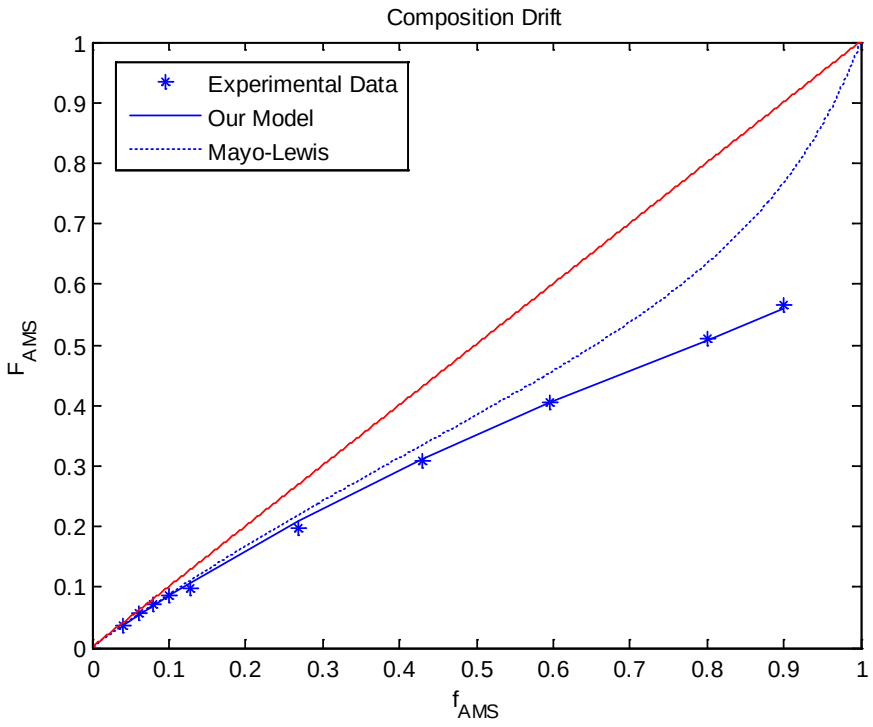

Figure 36. Simulation of the co-polymerization of AMS/Sty, T = 90°C.

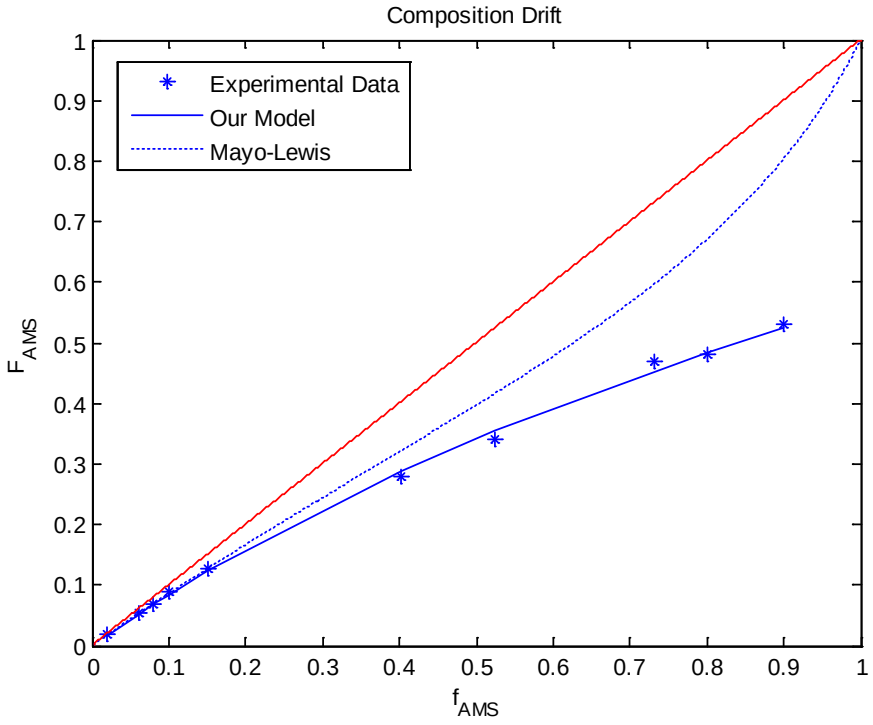

Figure 37. Simulation of the co-polymerization of AMS/Sty, T = 110°C.

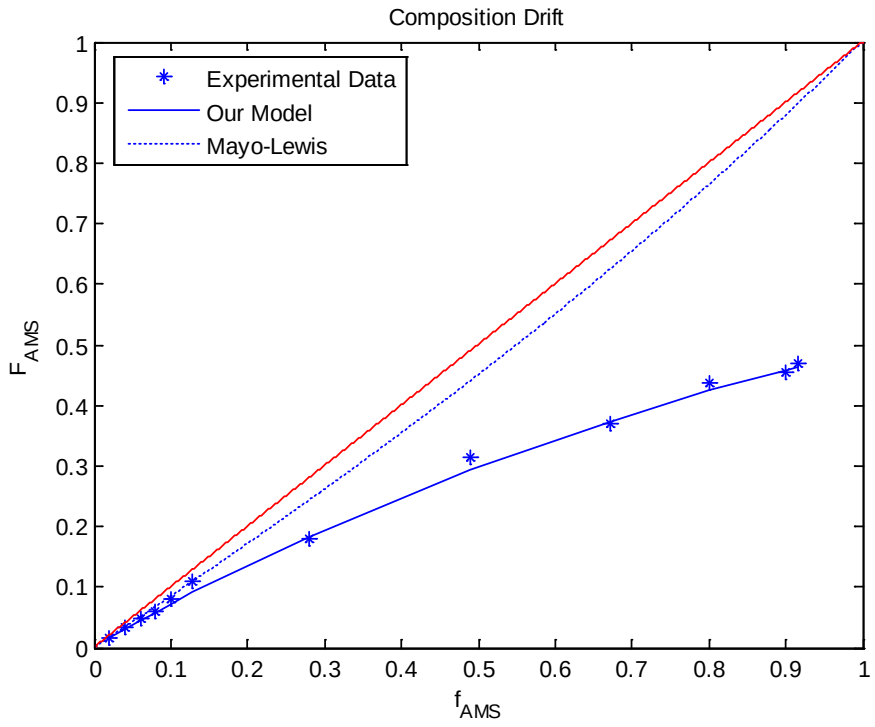

Figure 38. Simulation of the co-polymerization of AMS/Sty, T = 150°C.

3.6.4. Case study 3: Co-polymerization of AMS and MMA

Palmer *et al.* (90) conducted several bulk co-polymerizations of AMS and MMA at 115°C and 140°C using di-*tert*-butyl peroxide (dTBPO) as initiator. The reactivity and depropagation ratios for 140°C are $r_{AMS\text{-}MMA} = 0.003$, $r_{MMA\text{-}AMS} = 0.420$, $R_1 = 1.388$, $R_2 = 24.960$, $R_{11} = 0.163$ and $R_{22} = 0.192$; the kinetic data for 115°C have much less depropagation present: $r_{AMS\text{-}MMA} = 0.009$, $r_{MMA\text{-}AMS} = 0.404$, $R_1 = 0$, $R_2 = 11.28$, $R_{11} = 0.285$ and $R_{22} = 0.083$ (90). A summary of each experiment is presented in Table 7 with the corresponding figure numbers shown in the rightmost column.

Table 7. Reaction conditions for the co-polymerizations of AMS and MMA.

Run	**Temperature (°C)**	**Monomer composition (AMS/MMA wt%)**	**Initiator amount (wt%)**	**Figure number**
1	140	45/55	2	Figure 39
				Figure 40
				Figure 41
2	140	45/55	0.5	Figure 42
3	140	29/71	1	Figure 43
				Figure 44
4	115	45/55	8	Figure 45
5	115	45/55	2	Figure 46
				Figure 47

For each of the simulations, the polymer composition and molecular weight predictions were satisfactory. Monomer conversion data were also represented quite well by the modeling software.

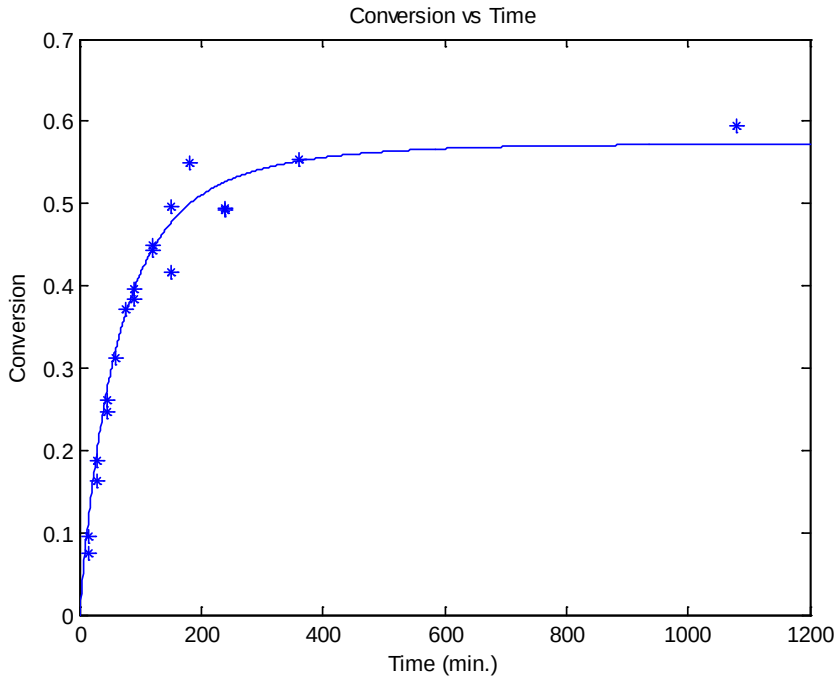

Figure 39. Simulation of the bulk co-polymerization of AMS/MMA, T = 140°C, $[dTBPO]_0$ = 2 wt%, f_{AMS0} = 45 wt%.

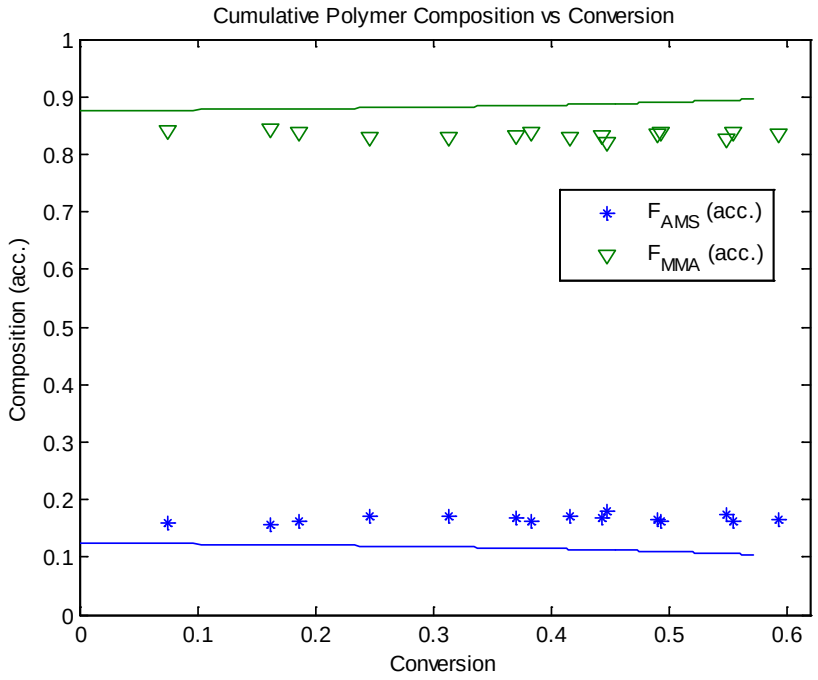

Figure 40. Simulation of the bulk co-polymerization of AMS/MMA, T = 140°C, $[dTBPO]_0$ = 2 wt%, f_{AMS0} = 45 wt%.

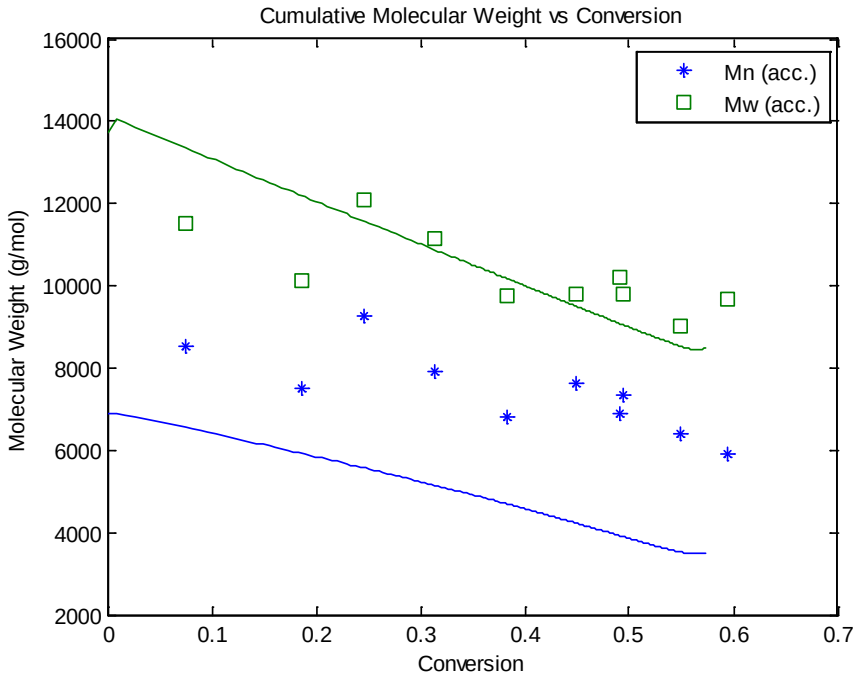

Figure 41. Simulation of the bulk co-polymerization of AMS/MMA, T = 140°C, $[dTBPO]_0$ = 2 wt%, f_{AMS0} = 45 wt%.

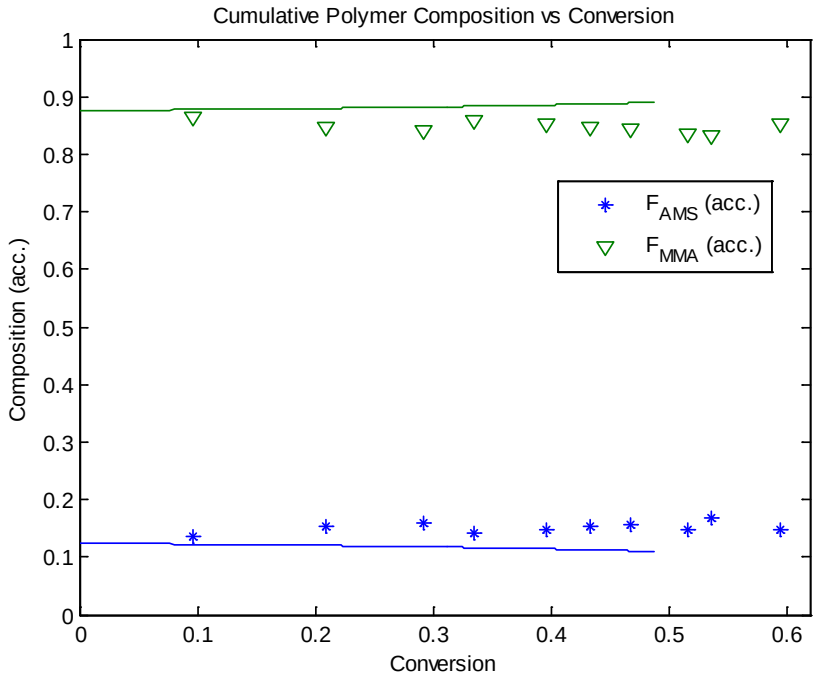

Figure 42. Simulation of the bulk co-polymerization of AMS/MMA, T = 140°C, $[dTBPO]_0$ = 0.5 wt%, f_{AMS0} = 45 wt%.

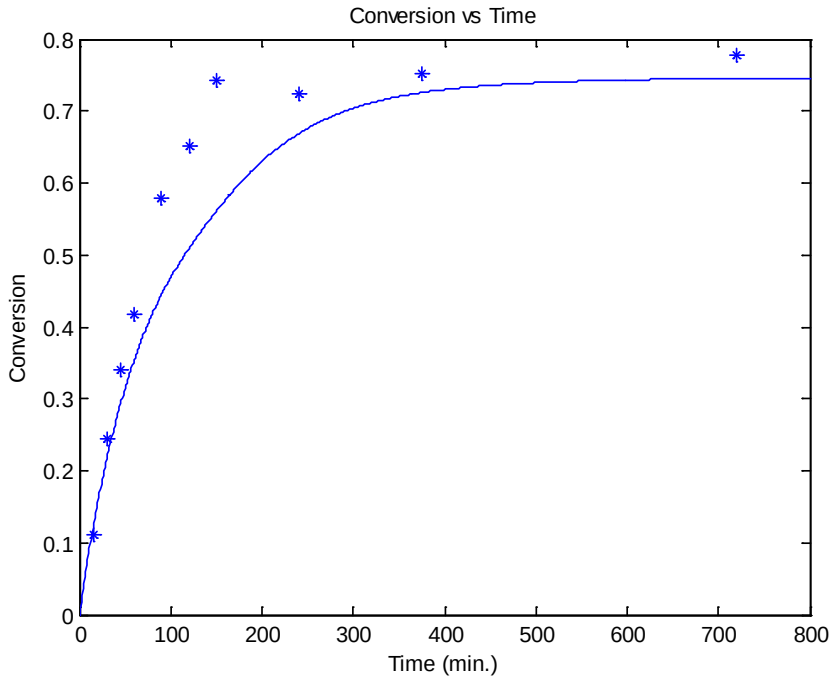

Figure 43. Simulation of the bulk co-polymerization of AMS/MMA, T = 140°C, $[dTBPO]_0$ = 1 wt%, f_{AMS0} = 29 wt%.

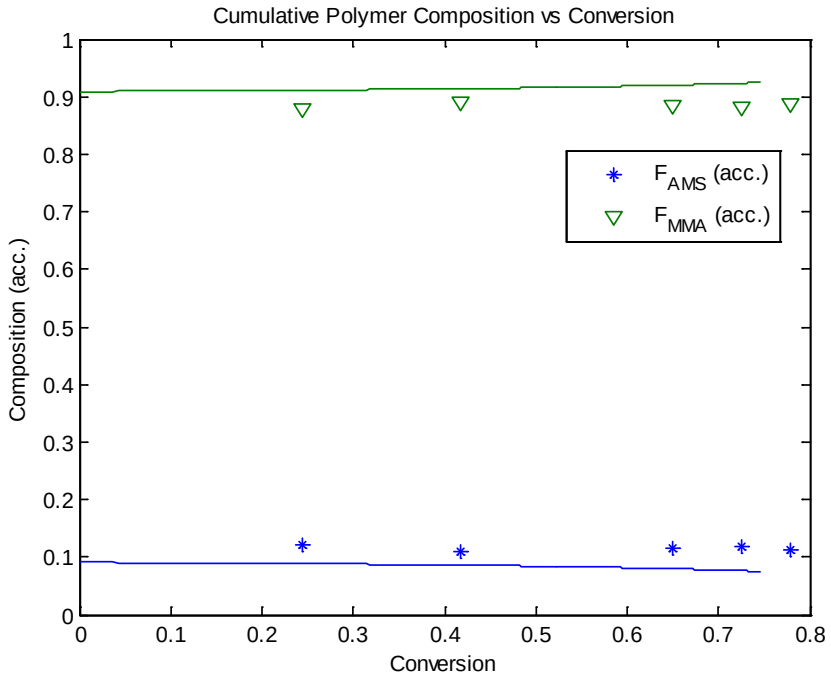

Figure 44. Simulation of the bulk co-polymerization of AMS/MMA, T = 140°C, $[dTBPO]_0$ = 1 wt%, f_{AMS0} = 29 wt%.

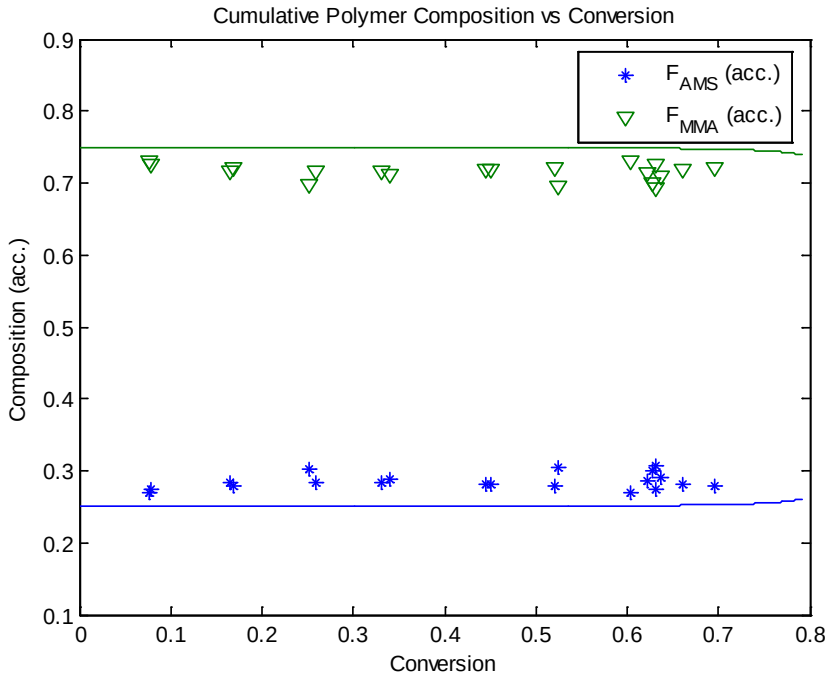

Figure 45. Simulation of the bulk co-polymerization of AMS/MMA, T = 115°C, $[dTBPO]_0$ = 8 wt%, f_{AMS0} = 45 wt%.

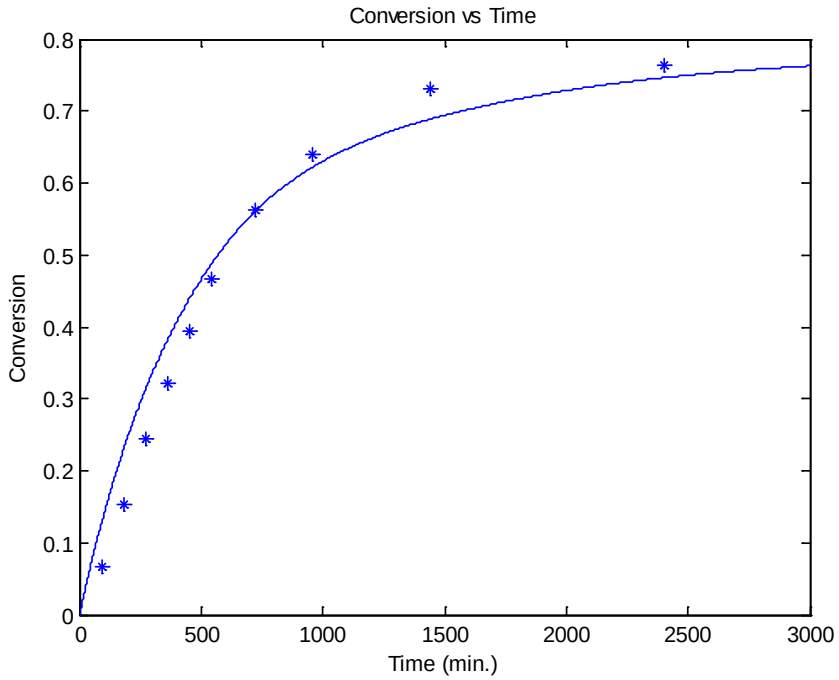

Figure 46. Simulation of the bulk co-polymerization of AMS/MMA, T = 115°C, $[dTBPO]_0$ = 2 wt%, f_{AMS0} = 45 wt%.

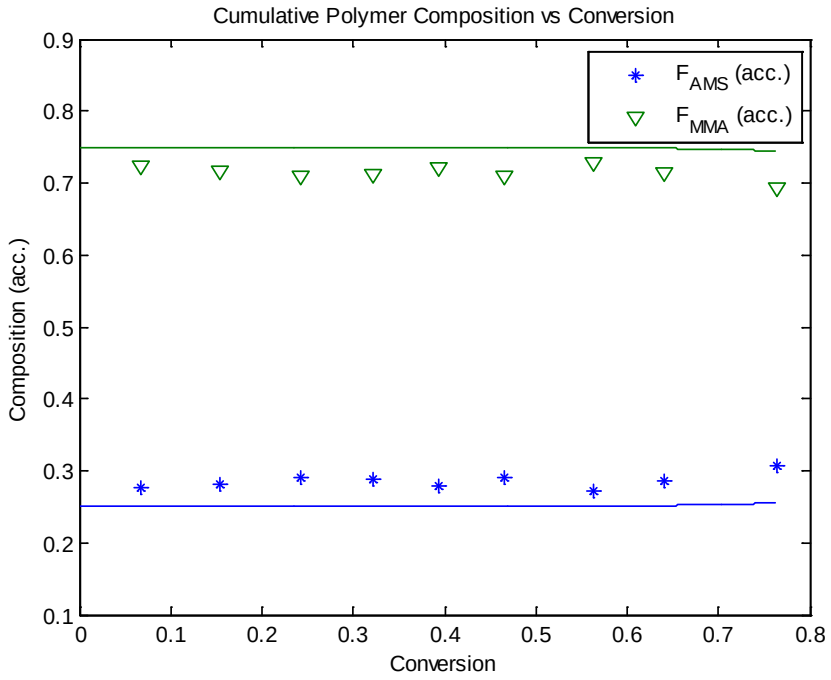

Figure 47. Simulation of the bulk co-polymerization of AMS/MMA, T = 115°C, $[dTBPO]_0$ = 2 wt%, f_{AMS0} = 45 wt%.

3.6.5. Case study 4: Co-polymerization of styrene and glycidyl methacrylate

Eight co-polymerizations of styrene and GMA were carried out at 170°C, 190°C and 230°C (97). Polymer composition data against monomer conversion were recorded. No initiator was present as styrene is known to self-initiate at elevated temperatures. Three of the experiments were carried out with 30 wt% xylene. Due to the effect that solvent has on monomer concentration, homo-depropagation of GMA was assumed to occur when

solvent was present. GMA has been cited to homo-depropagate following the rate constant.

$$k_{dp,GMA\text{-}homo} = 1.765e14*\exp((-1.7065e4)/(R*T)) \qquad \text{(refs.109, 110)}$$

Reactivity ratios were taken from both (85) as well as from (97), presented in Table 8. The corresponding figure number for each of the simulations is also cited in the table.

Table 8. Reaction conditions and kinetic data used for the co-polymerization of Styrene and GMA

Figure	**Temperature (°C)**	**Solvent**	$\mathbf{r_{Sty}}$	$\mathbf{r_{GMA}}$	**Source**
Figure 48	170	No	0.316	0.750	(97)
Figure 49	190	No	0.356	0.785	(97)
Figure 50	190	No	0.356	0.785	(97)
Figure 51	190	No	0.356	0.785	(97)
Figure 52	190	Yes	0.278	0.539	(85)
Figure 53	190	Yes	0.278	0.539	(85)

Figure 54	190	Yes	0.278	0.539	(85)
Figure 55	230	No	0.356	0.785	(97)

The reason for the discrepancy between the reactivity ratios is because (97) did not account for depropagation of GMA at elevated temperatures. As this is a co-polymerization, a reduction in the amount of depropagation, was used to account for the presence of styrene. Cross-depropagation of GMA from styrene was assumed negligible.

For each of the simulations presented in Figures 48 to 55, the results were quite accurate, another confirmation about the validity of the model.

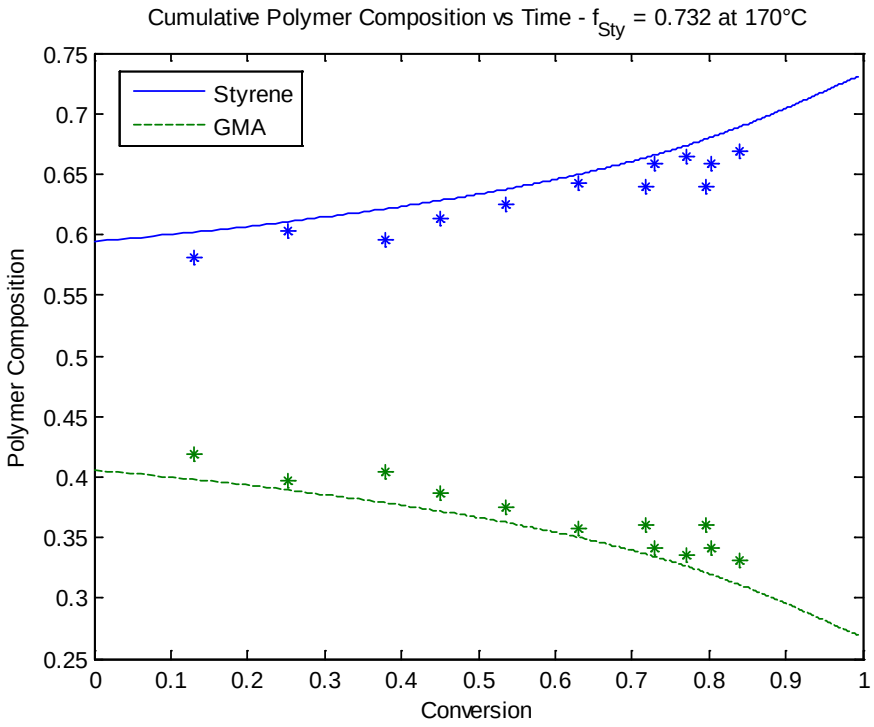

Figure 48. Simulation of the co-polymerization of Sty/GMA, T = 170°C, f_{Sty0} = 0.732.

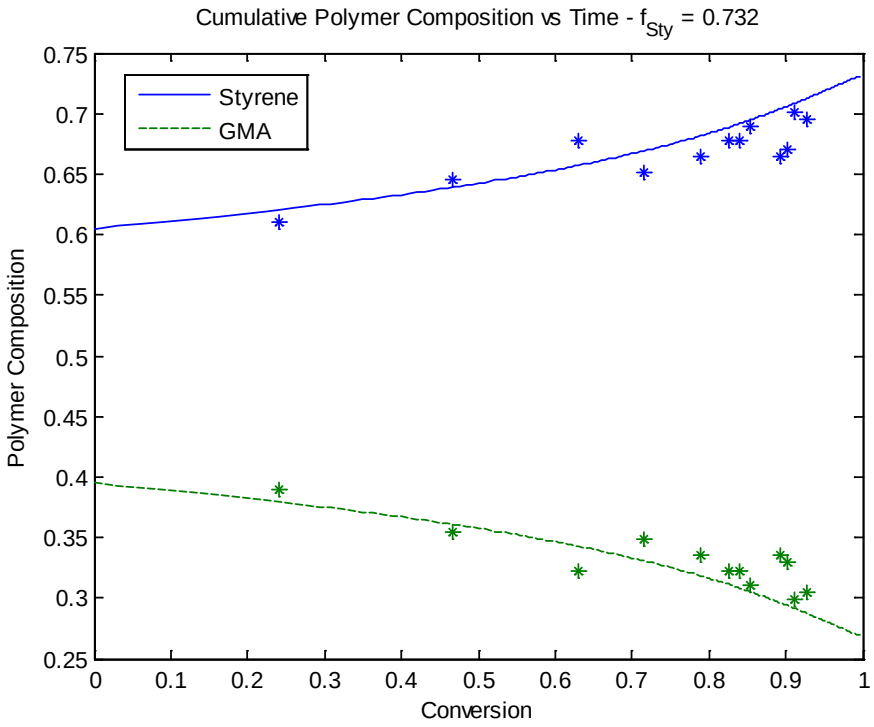

Figure 49. Simulation of the co-polymerization of Sty/GMA, T = 190°C, f_{Sty0} = 0.732.

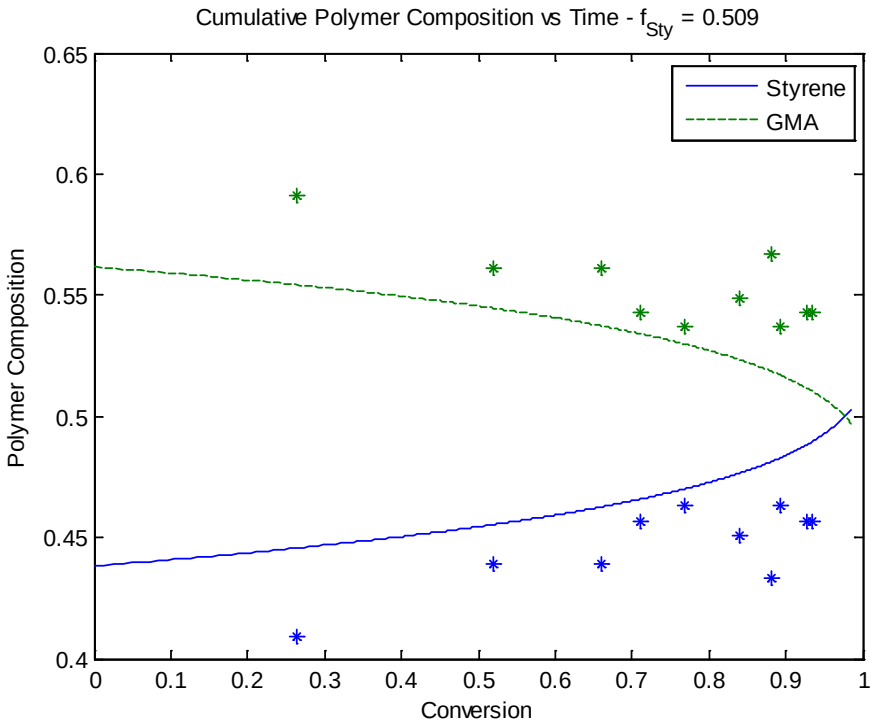

Figure 50. Simulation of the co-polymerization of Sty/GMA, T = 190°C, f_{Sty0} = 0.509.

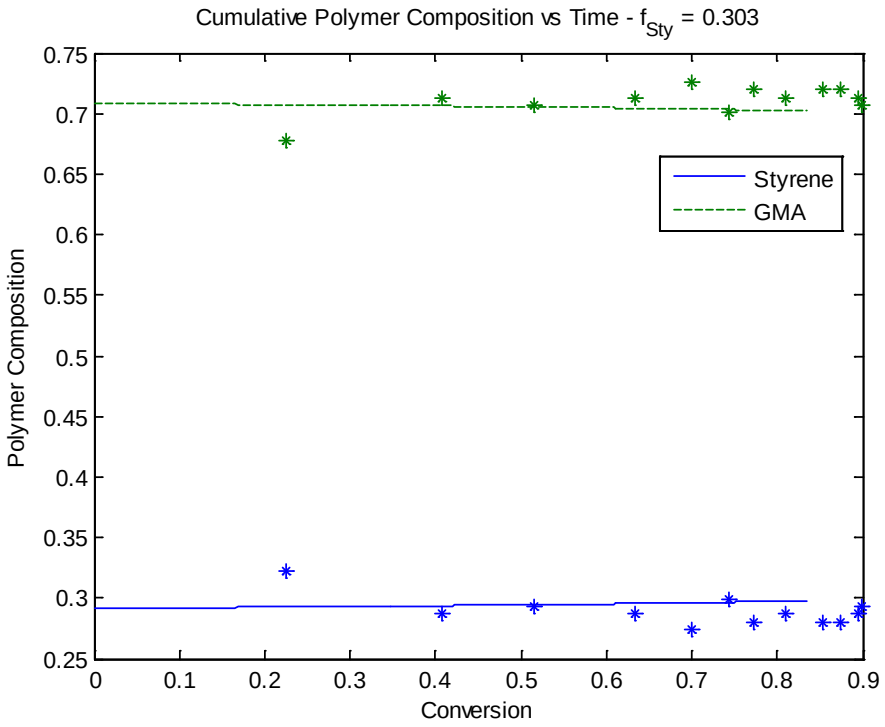

Figure 51. Simulation of the co-polymerization of Sty/GMA, T = 190°C, f_{Sty0} = 0.303.

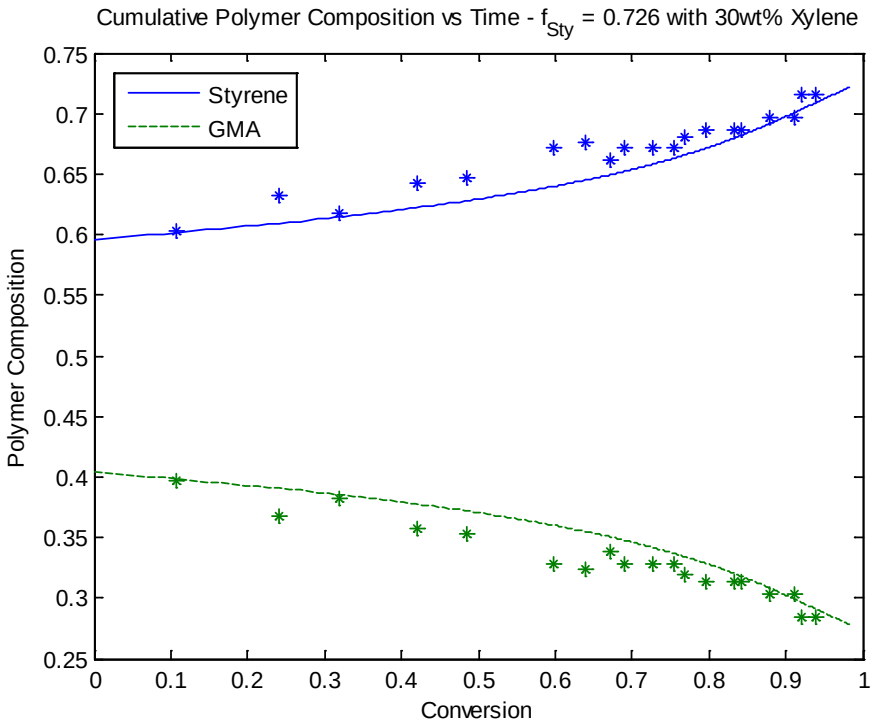

Figure 52. Simulation of the co-polymerization of Sty/GMA, T = 190°C, xylene = 30 wt%, f_{Sty0} = 0.726.

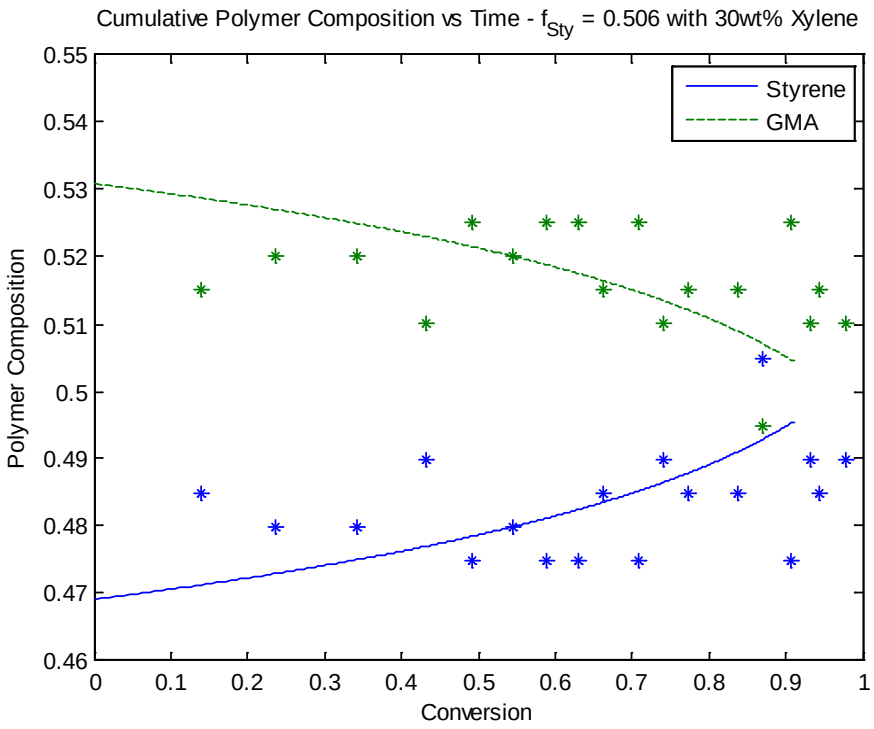

Figure 53. Simulation of the co-polymerization of Sty/GMA, T = 190°C, xylene = 30 wt% f_{Sty0} = 0.506.

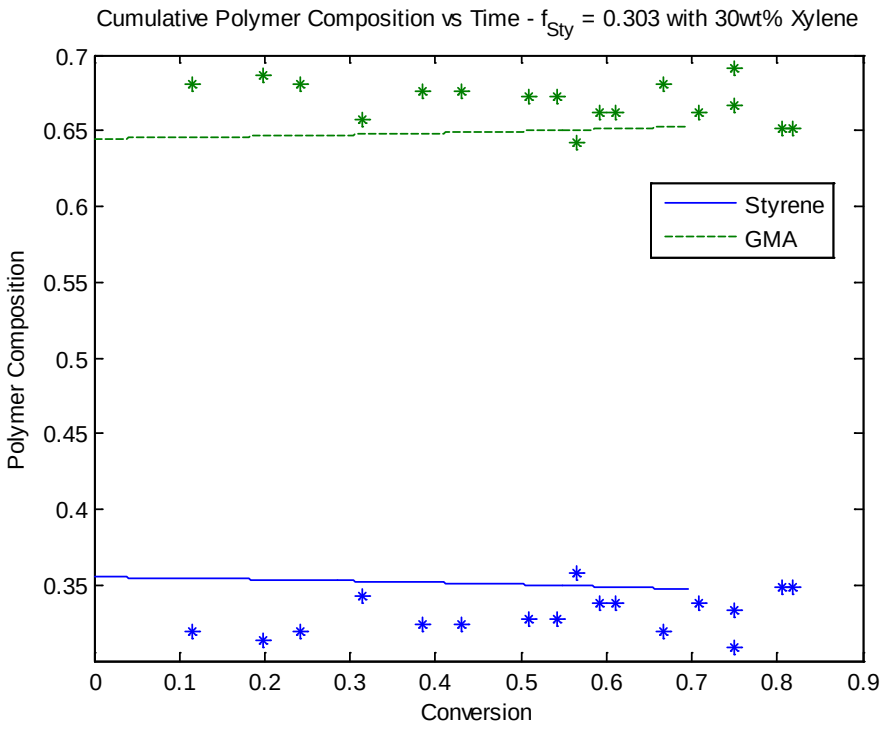

Figure 54. Simulation of the co-polymerization of Sty/GMA, T = 190°C, xylene = 30 wt%, f_{Sty0} = 0.303.

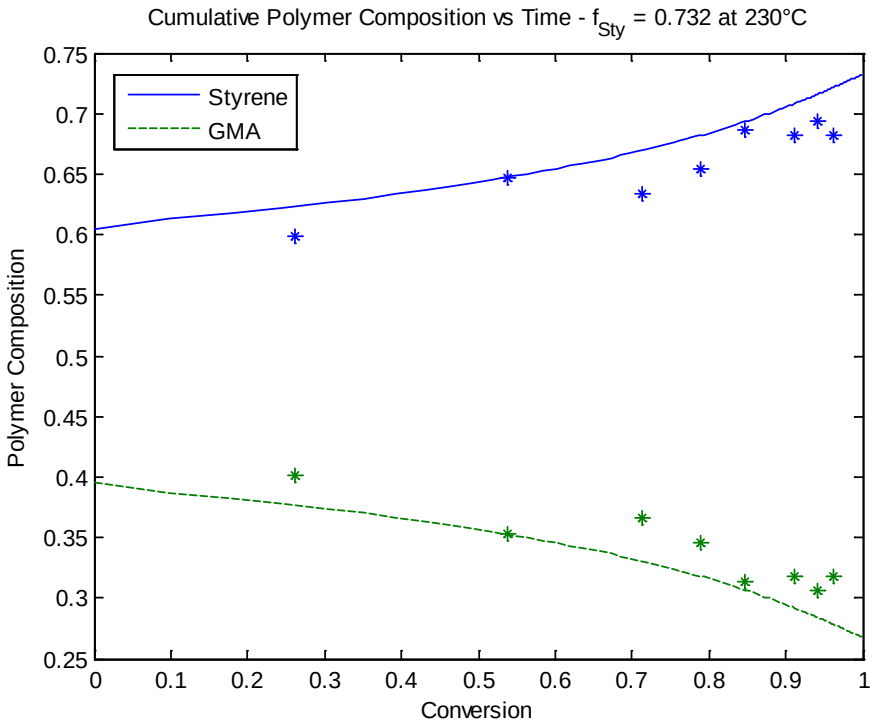

Figure 55. Simulation of the co-polymerization of Sty/GMA, T = 230°C, f_{Sty0} = 0.732.

Another co-polymerization of styrene and GMA at elevated temperatures was conducted by (23). Five semi-batch co-polymerizations were completed in total at 138°C using 2 wt% of tert-butyl peroxyacetate relative to monomer and 30 wt% xylene. The reactor was initially charged with the solvent; the monomers were fed evenly over 360 min and the initiator was fed evenly over 375 mins. The reactivity ratios used are $r_{Sty\text{-}GMA}$ = 0.306 and $r_{GMA\text{-}Sty}$ = 0.508 from (23). Only homo-depropagation of GMA was assumed.

Figures 56 and 57 show the concentration of each monomer in the system throughout polymerization with the simulations represented by the solid lines. Earlier, styrene and GMA were tested against polymer composition and performed quite well. Here, the same two monomers are tested against concentration data with very good results again. Kinetic data from GMA, as well as all other monomers in our database can be found in the appendices.

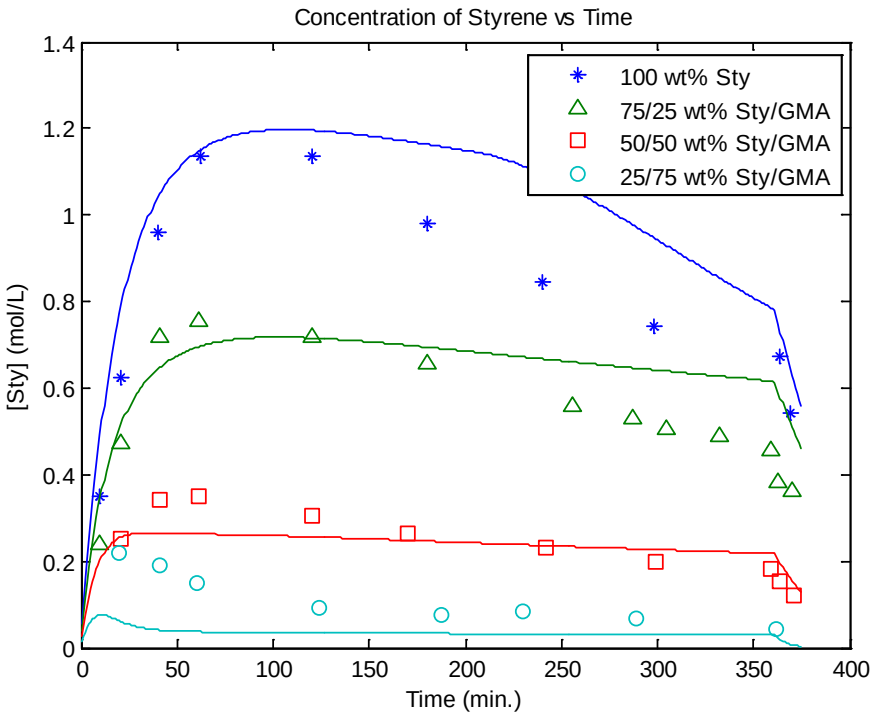

Figure 56. Simulation of the co-polymerization of Sty/GMA, T = 138°C, $[TBPA]_0$ = 2 wt%, xylene = 30 wt%.

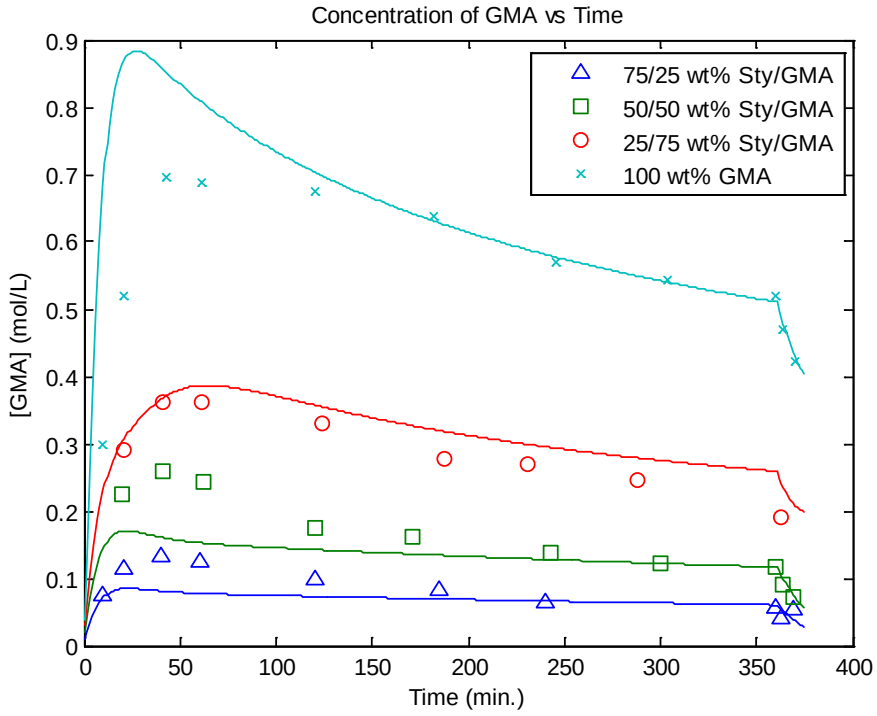

Figure 57. Simulation of the co-polymerization of Sty/GMA, T = 138°C, $[TBPA]_0$ = 2 wt%, xylene = 30 wt%.

3.6.6. Case study 5: Ter-polymerization of AMS, MMA and BA

The next case study presented is a ter-polymerization of AMS (monomer 1), MMA (monomer 2) and BA (monomer 3). The four experiments were conducted by McManus *et al.* (20) involving different monomer feed ratios at 140°C. Polymer composition data were taken for three of the experiments and molecular weight data, both number-average and weight-average, were measured for one of the runs. Again, dTBPO was used as the initiator at 0.5 wt%. The reactivity and depropagation ratios are shown in Table 9.

Table 9. Reactivity and depropagation ratios for the ter-polymerization of AMS, MMA and BA at 140°C

Reactivity Ratio		Source
$r_{AMS-MMA}$	0.003	(90)
r_{AMS-BA}	0.5575	(166)
$r_{MMA-AMS}$	0.420	(90)
r_{MMA-BA}	1.905	(166)
r_{BA-AMS}	0.143	(166)
r_{BA-MMA}	0.348	(166)
R_1	1.388	(90)
*R_2	11.28	(90)
R_{11}	0.163	(90)

*Value used for 120°C

In terms of reactivity ratios, we know from the one of the previous case studies that the values given by Palmer *et al.* (90) haven proven quite accurate when dealing with AMS and MMA at 140°C. In all other cases, the only values we have for a ter-polymerization of AMS, MMA and BA are given by Leamen *et al.* (166) and were used accordingly. This is a ter-polymerization with a non-depropagating monomer (BA). The

cross-depropagation ratio of AMS from MMA, R_2, was set to the 120°C value from Palmer *et al.* (90).

Figure 58 shows accurate predictions for polymer composition data against conversion, further indicating that the reactivity ratios are reasonable. Figure 59 depicts a satisfactory simulation of both number-average and weight-average molecular weights.

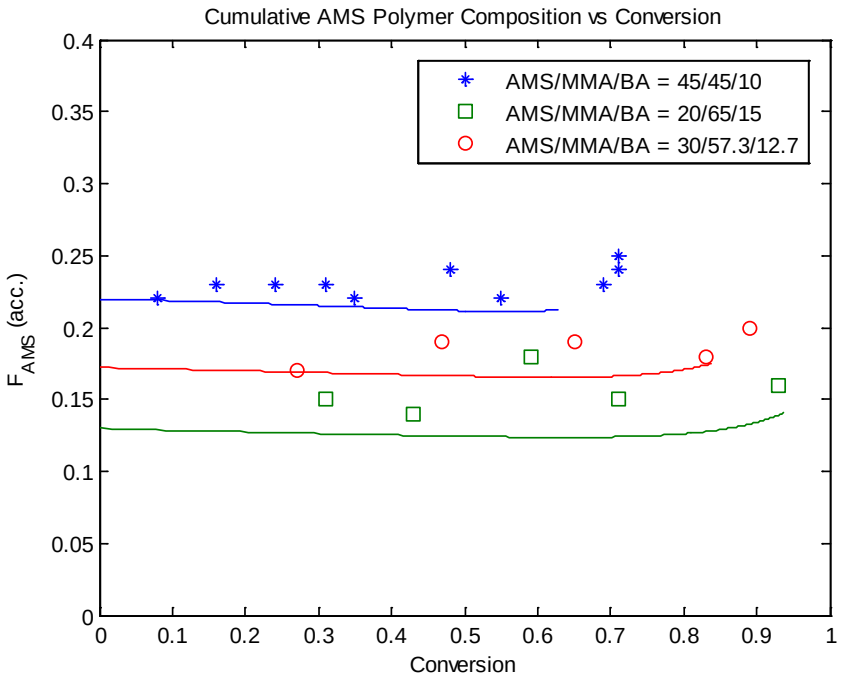

Figure 58. Simulation of the bulk ter-polymerization of AMS/MMA/BA, T = 140°C, $[dTBPO]_0$ = 0.5 wt%.

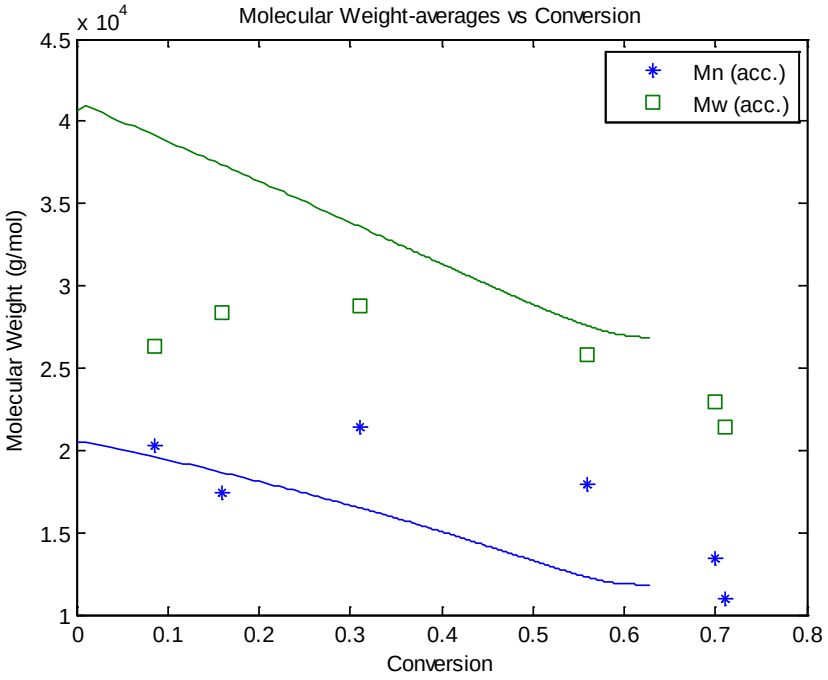

Figure 59. Simulation of the bulk ter-polymerization of AMS/MMA/BA, T = 140°C, $[dTBPO]_0$ = 0.5 wt%, $f_{AMS0} = f_{MMA0}$ = 45 wt%.

3.6.7. Backbiting of butyl acrylate

Rantow *et al.* (152) performed two homo-polymerizations of BA at 160°C and 180°C with 60% xylene by weight. No initiator was used as BA can self-initiate at elevated temperatures (152, 163). Figures 60 through 63 each compare the homo-polymerization of BA with and without backbiting. As the data illustrate, modeling without backbiting and beta-scission results in a simulation that follows polymerization behavior very poorly. The

reason for such a large difference in the two predictions is that the tertiary radical formed in backbiting is much more stable and results in a slower rate of reaction.

This can be seen directly in Figure 60 as the simulation without backbiting reaches complete conversion almost instantly whereas the simulation with backbiting only reaches 81% conversion after 100 min. Figure 61 is at a higher temperature but still, the reaction is only moderately faster; a conversion of 86% is reached after 100 min. This is a result of the increased amount of backbiting at higher temperatures. Plessis *et al.* (167) supported this theory as they observed that the level of branching measured from ^{13}C-NMR spectroscopy was shown to increase as temperature increased.

Figures 62 and 63 are the molecular weight predictions at 160°C and 180°C, respectively. The backbiting simulation follows the data trend with accuracy, whereas the prediction without backbiting (and beta-scission) is too high. The backbiting simulation is much more accurate due to β-fragmentation. Each time the tertiary radical chain splits, a second chain is created and the molecular weight drops accordingly.

Figures 64 and 65 represent the average number of short chain branches per chain throughout the reaction (CBC). In spite of the discrepancy between the data and our

simulation (given that the measurement has quite a lot of error in it as well), the model still follows the same decreasing trend as the reaction proceeds. As there were no experimental data for the average number of terminal double bonds per chain (TDBC), Figures 66 and 67 are just the model simulations. As temperature increases from 160°C to 180°C, several trends can be seen. The molecular weight drops, as expected, CBC decreases and TDBC increases. When the temperature is increased, the number of polymer chains increases due to the increased rate of initiator decomposition as well as the increased amount of beta-scission. As CBC is the number average per chain, the reason for the decrease is simply that the number of chains increased more than the average number of short chain branches. When β-scission occurs, the short chain branch is no longer formed as the midchain radical is converted into a secondary radical and a dead polymer chain with a terminal double bond; thus, the decrease in CBC and the increase in TDBC can both be explained by an increased amount of beta-fragmentation.

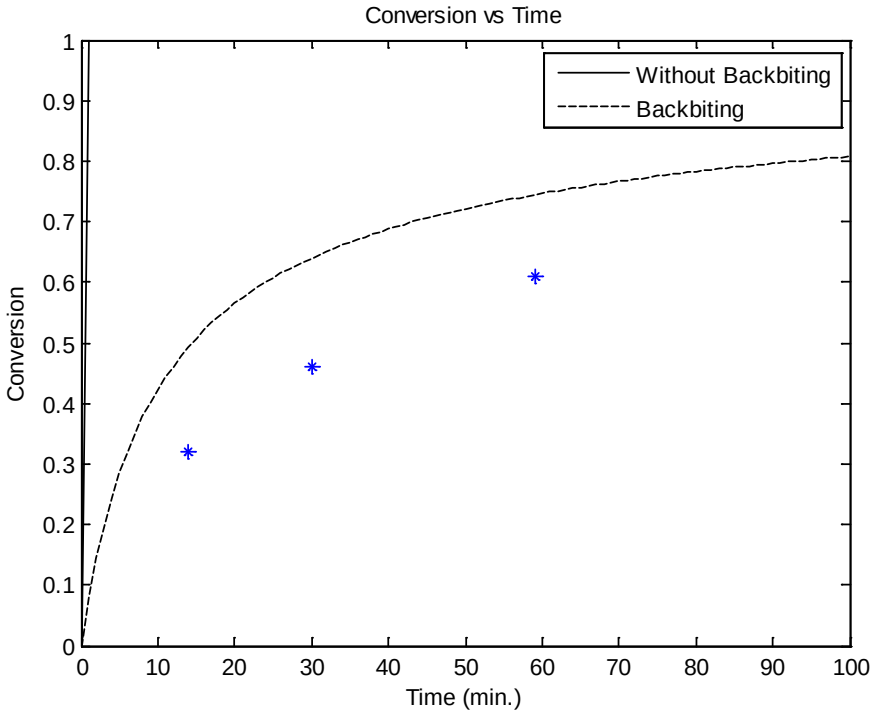

Figure 60. Simulation of the homo-polymerization of BA at 160°C with no initiator and 60 wt% xylene.

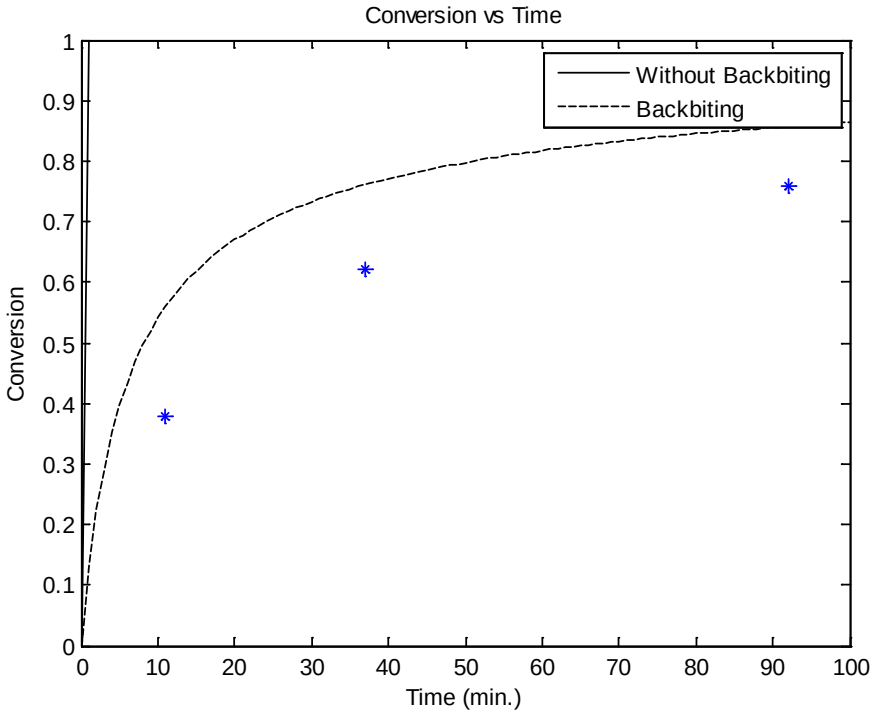

Figure 61. Simulation of the homo-polymerization of BA at 180°C with no initiator and 60 wt% xylene.

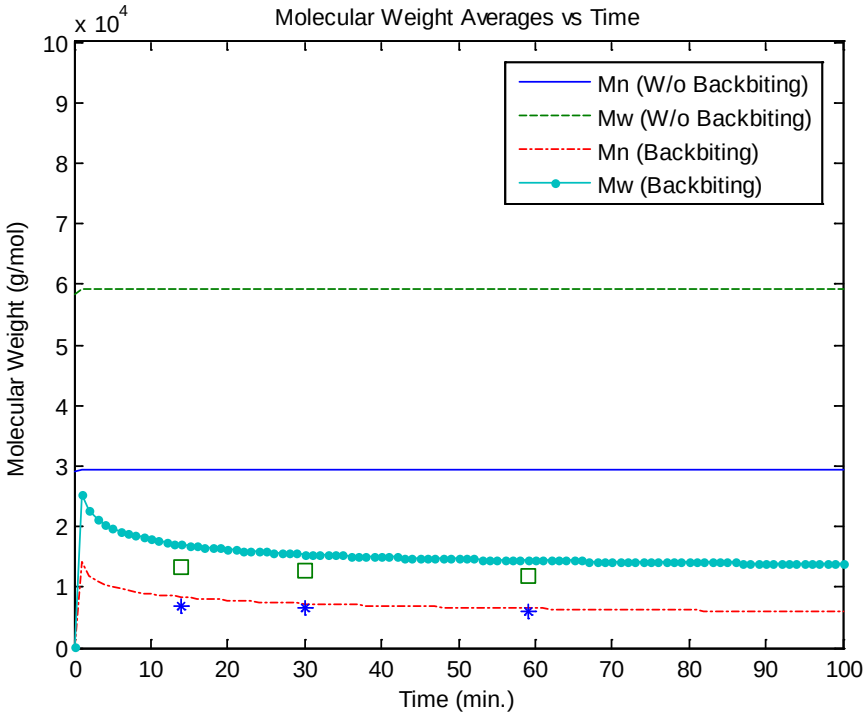

Figure 62. Simulation of the homo-polymerization of BA at 160°C with no initiator and 60 wt% xylene.

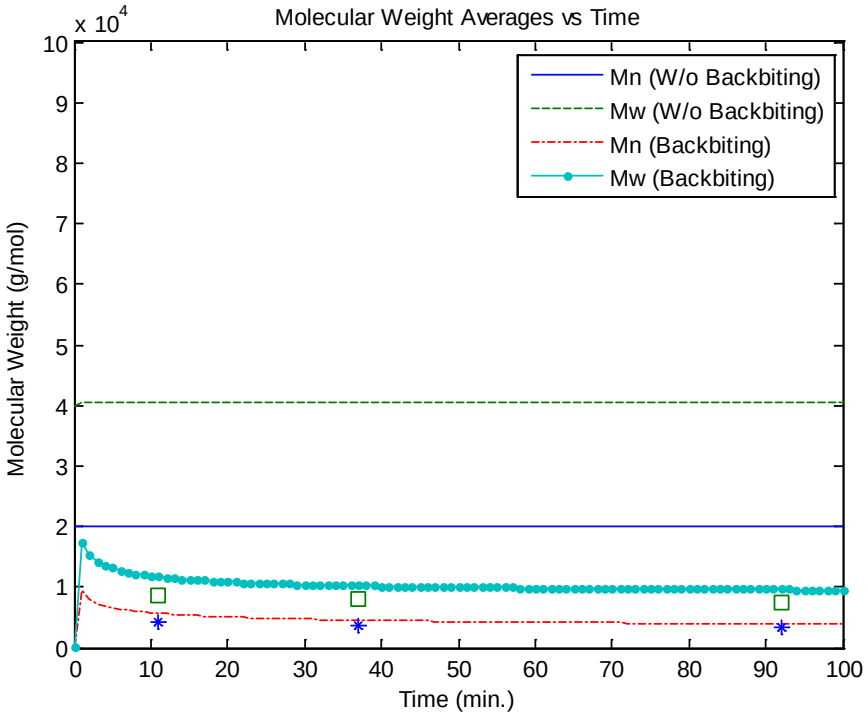

Figure 63. Simulation of the homo-polymerization of BA at 180°C with no initiator and 60 wt% xylene.

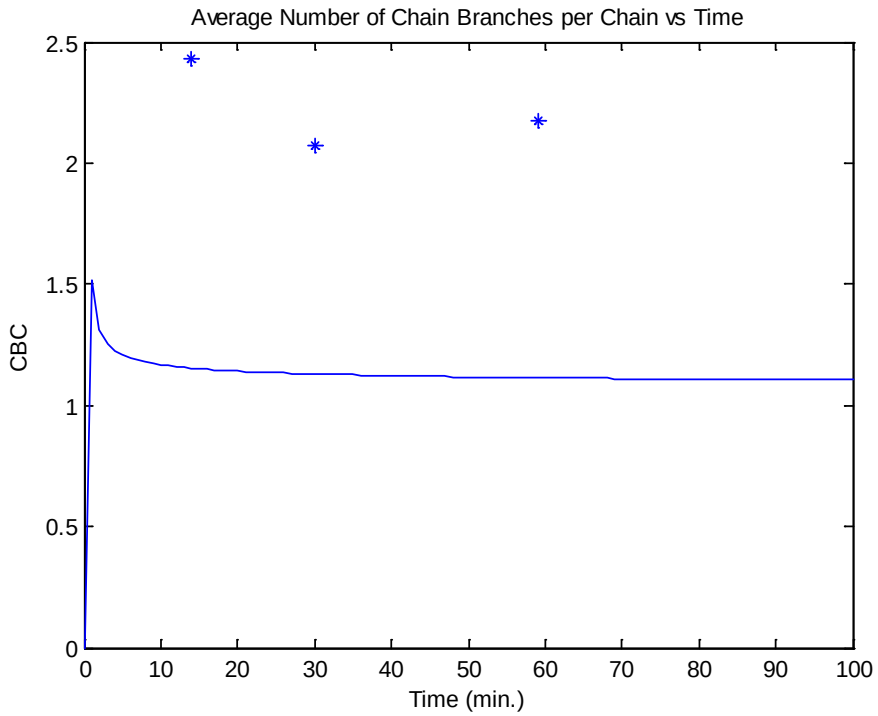

Figure 64. Simulation of the homo-polymerization of BA at 160°C with no initiator and 60 wt% xylene.

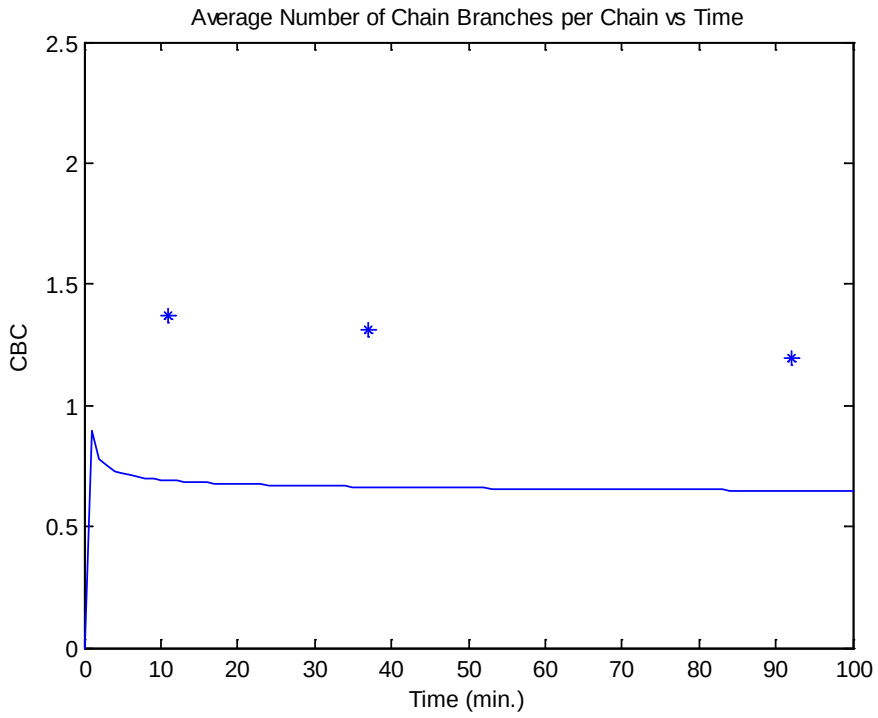

Figure 65. Simulation of the homo-polymerization of BA at 180°C with no initiator and 60 wt% xylene.

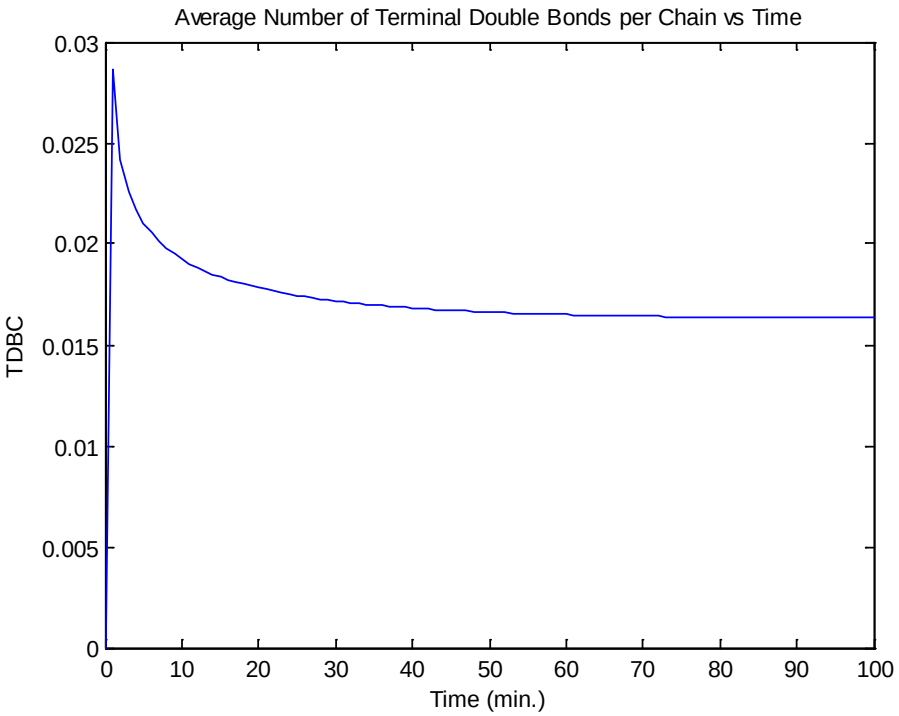

Figure 66. Simulation of the homo-polymerization of BA at 160°C with no initiator and 60 wt% xylene.

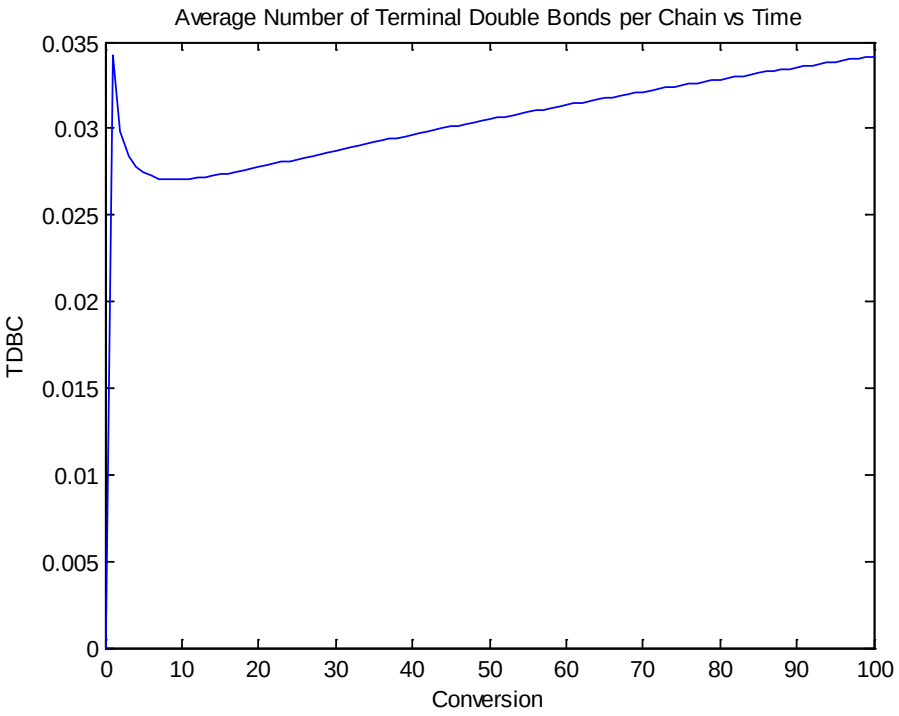

Figure 67. Simulation of the homo-polymerization of BA at 180°C with no initiator and 60 wt% xylene.

3.6.8. Case study 8: Co-polymerization of butyl acrylate and butyl methacrylate

Three co-polymerizations and two homo-polymerizations were conducted by (103). The inlet monomer mole fractions of BMA for the five reactions were 100 wt%, 75 wt%, 50 wt%, 25 wt% and 0 wt%. The reactor was initially charged with 30% xylene by weight. The monomer and initiator were then fed constantly over 360 and 375 min, respectively. The final amount of monomers and initiator fed were equal to 68.3 wt% and 1.7 wt%, respectively. The reactivity ratios used were $r_{BA\text{-}BMA} = 0.8268 \exp(282.1/T)$ and $r_{BMA\text{-}BA} =$

1.5815 exp (-564.8/T), obtained from (89). The homo-depropagation rate constant of BMA was equal to k_{pBMA} x (1.76-1.37 wp 10^6 exp (-6240/T)), taken from (161); cross-depropagation was assumed negligible.

As these experiments were run at elevated temperatures, backbiting, beta-scission and depropagation all have to be modeled properly to produce accurate simulations. Backbiting was only assumed to occur when BA was the terminal and pen-penultimate unit of the chain, whereas depropagation of BMA only occurred when BMA was the terminal and penultimate unit. With backbiting and β-scission limited, the reaction will proceed much quicker and with higher molecular weights than if it had been a homo-polymerization of butyl acrylate.

Figures 68 and 69 are the concentrations of BMA and BA monomers, respectively. As depropagation kinetics have been researched far more extensively than the relatively new backbiting phenomenon, it is not surprising that the concentration of BMA simulations performed much better than the BA predictions. Some improvement is required, but the overall accuracy is on par with the simulations by (103). This just means that BA behavior is still relatively unexplained and further refinement is required for better model simulations.

Figure 70 is the weight-average molecular weight vs. time for four of the polymerizations. The model is very accurate at each monomer feed ratio. It is also evident that indeed the molecular weights do increase with less butyl acrylate and consequently less beta-scission overall. Figure 71 is the cumulative polymer composition of BMA vs. time for each of the co-polymerizations. The model performs very well against the data for all three experiments. Finally, Figure 72 is the polymer weight fraction vs. time for the 50/50 wt% polymerization. Again, the simulation is very precise.

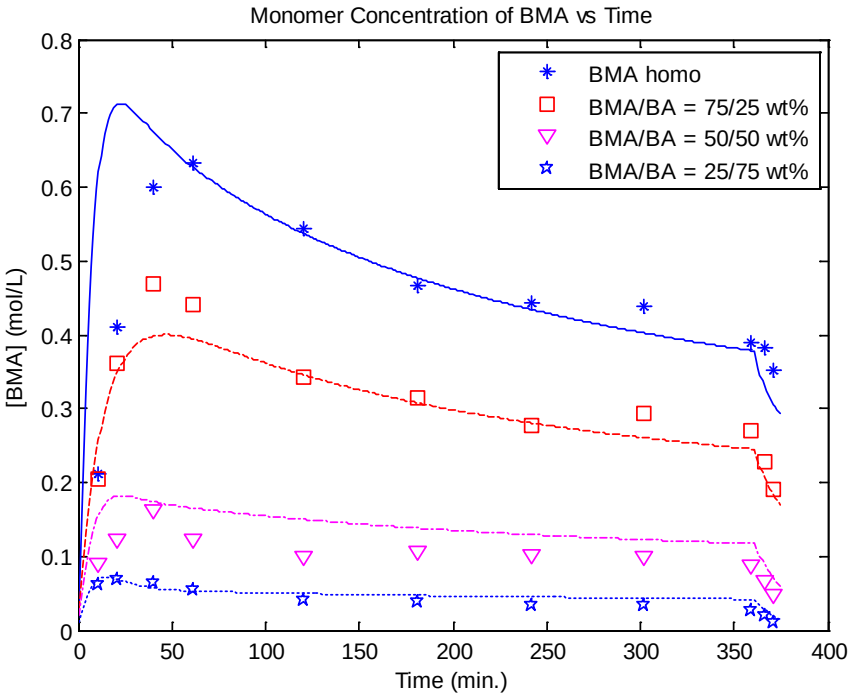

Figure 68. Simulation of the co-polymerizations of BMA/BA, T = 138°C, $[dTBPO]_0$ = 1.7 wt%, xylene = 30 wt%.

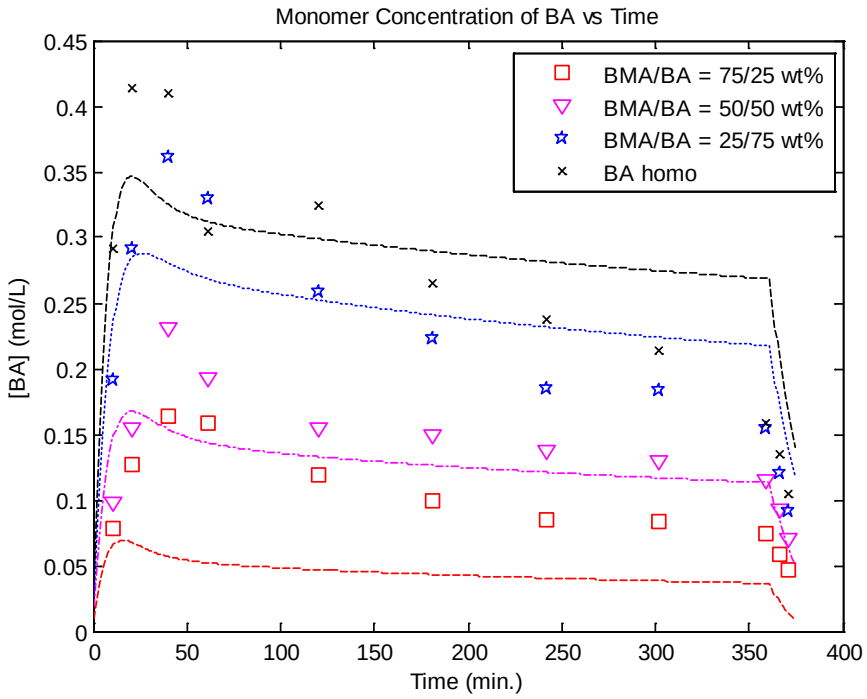

Figure 69. Simulation of the co-polymerizations of BMA/BA, T = 138°C, $[dTBPO]_0$ = 1.7 wt%, xylene = 30 wt%.

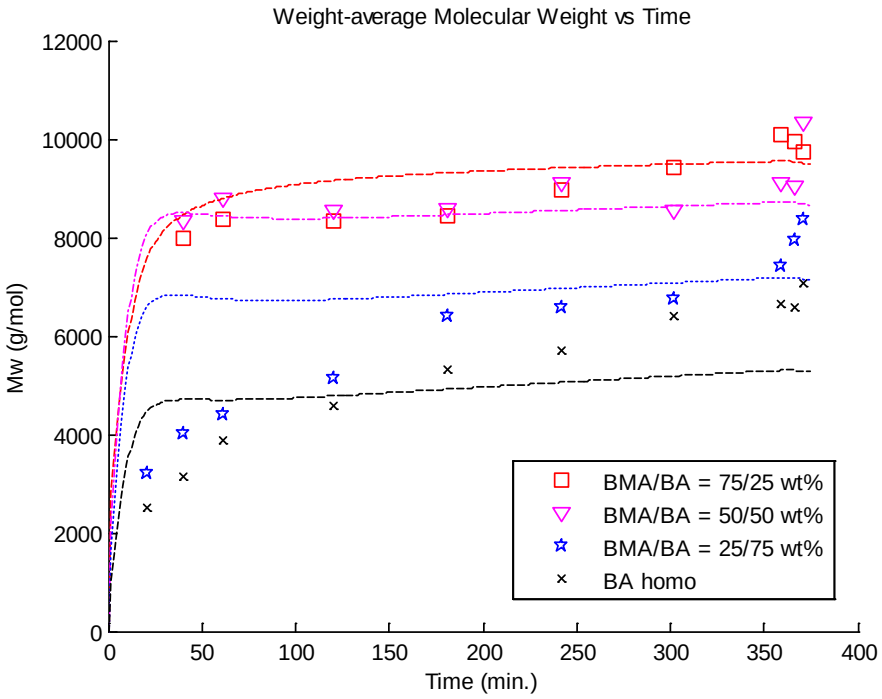

Figure 70. Simulation of the co-polymerizations of BMA/BA, T = 138°C, $[dTBPO]_0$ = 1.7 wt%, xylene = 30 wt%.

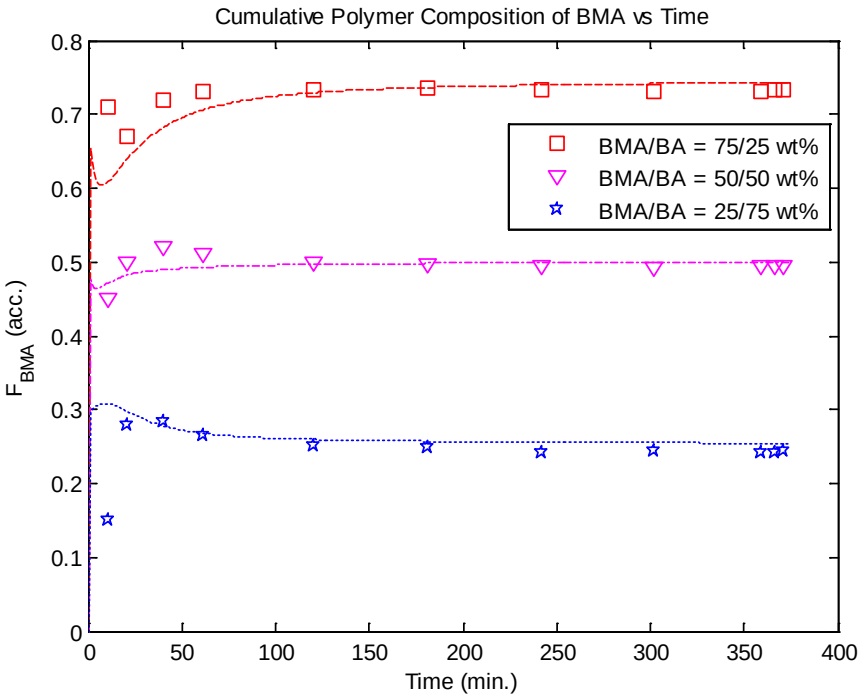

Figure 71. Simulation of the co-polymerizations of BMA/BA, T = 138°C, $[dTBPO]_0$ = 1.7 wt%, xylene = 30 wt%.

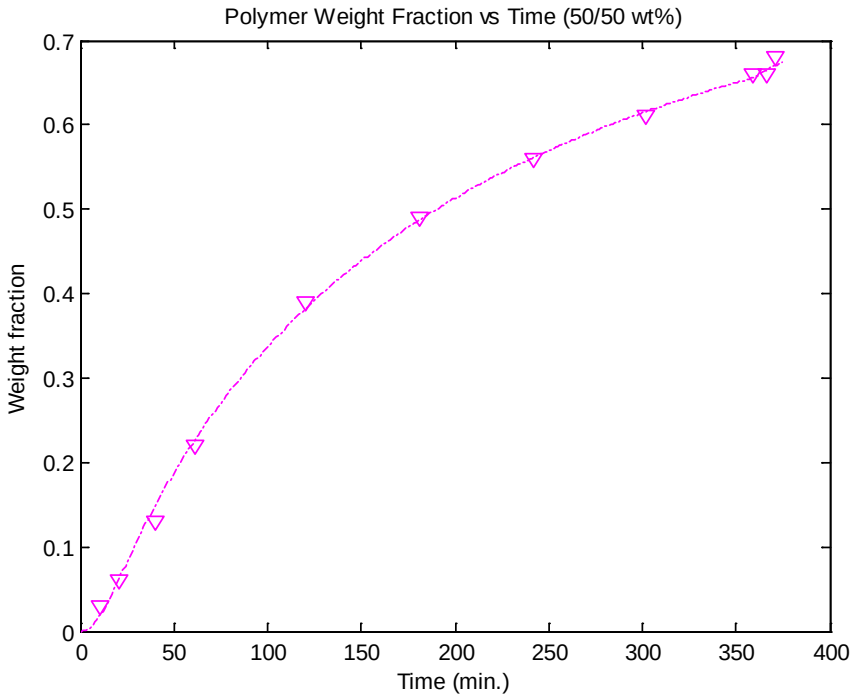

Figure 72. Simulation of the co-polymerization of BMA/BA, T = 138°C, $[dTBPO]_0$ = 1.7 wt%, xylene = 30 wt%, f_{BA0} = 50 wt%.

3.6.9. Case study 9: Co-polymerization of styrene and butyl acrylate

Recently, Wang (23) published experimental data on the semi-batch co-polymerization of styrene and BA at 138°C. Three different initial monomer mole fractions were examined: 75/25 wt%, 50/50 wt% and 25/75 wt% of styrene and butyl acrylate, respectively. Thirty weight-percent of xylene was charged into the reactor at time zero. The monomers and di-tert butyl peroxyacetate (TBPA) were fed evenly for 360 and 375 min, respectively. The reactivity ratios were taken from (83) as $r_{Sty\text{-}BA}$ = 0.956 and $r_{BA\text{-}Sty}$ = 0.183.

The simulations of monomer concentration for the monomer mole fraction of 75 wt% styrene in Figures 73 and 74 show very good representation of the data. The molecular weight prediction for this monomer feed overshot the data by about 20%, not that large a margin. The modeling software (23) used also overshot the data, meaning that the data might be slightly under the value of the true molecular weight.

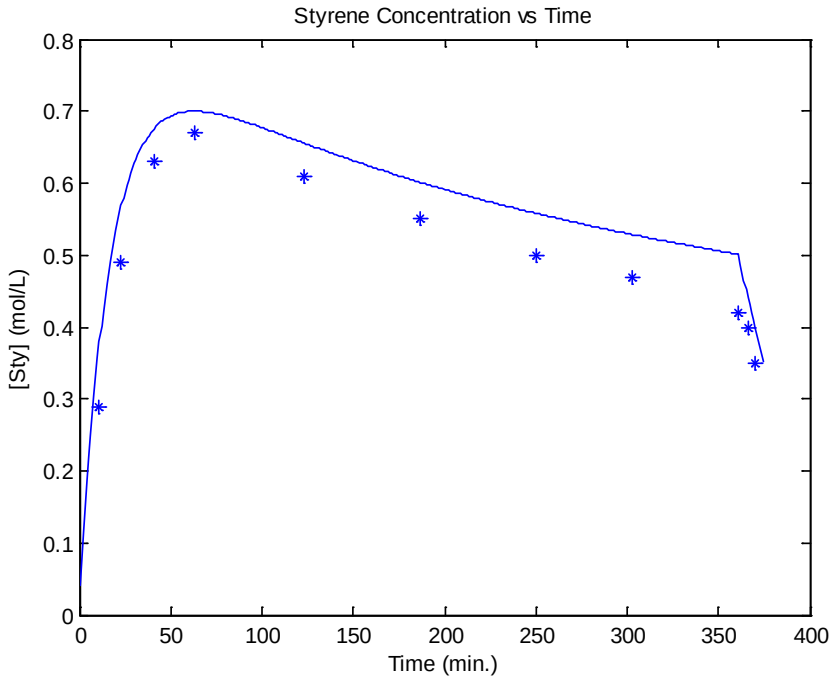

Figure 73. Simulation of the semi-batch co-polymerization of Sty/BA, T = 138°C, $[TBPA]_0$ = 2 wt%, xylene = 30wt%, f_{Sty0} = 75 wt%.

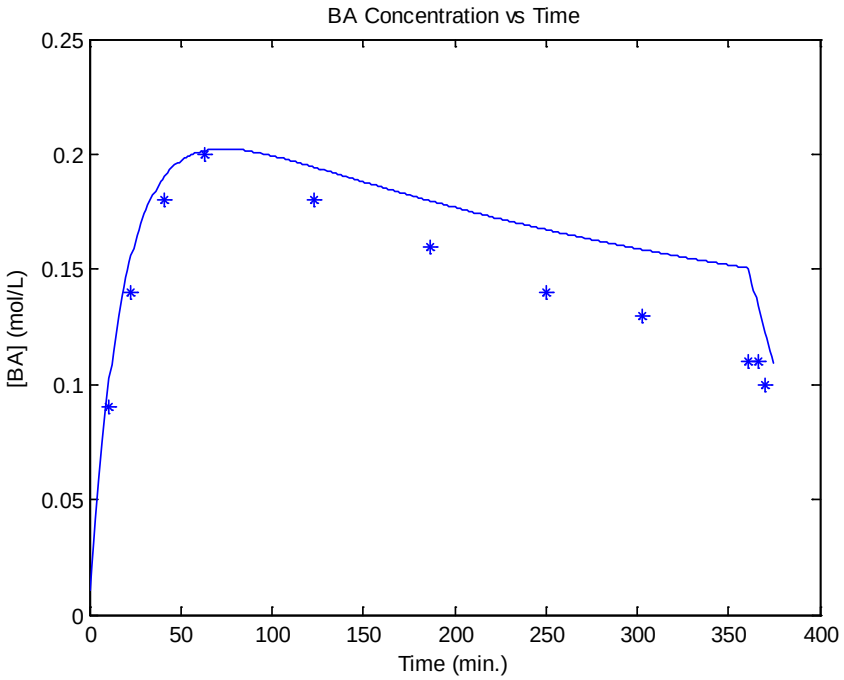

Figure 74. Simulation of the semi-batch co-polymerization of Sty/BA, T = 138°C, $[TBPA]_0$ = 2 wt%, xylene = 30wt%, f_{Sty0} = 75 wt%.

3.6.10. Case study 10: Ter-polymerization of styrene, BMA and BA

With this case study, the model was expanded once again to account for backbiting and beta-scission of one monomer (BA), depropagation of another (BMA), and normal free radical polymerization of the third, all at once. The semi-batch ter-polymerization data are from (23) and cover polymer composition and monomer concentration vs. time. The four ter-polymerizations were run using the same method as in the previous section; the monomer and initiator were fed evenly over six hours with an extra 15 min of feed time

for the initiator, TBPA. The starting monomer mole fractions examined were as follows: 33/33/33, 25/50/25, 15/70/15, 15/15/70 wt% of Sty/BMA/BA. The reactivity ratios are in Table 10; only homo-depropagation of BMA was assumed to occur as was the case in case study 8, $k_{dpBMA} = k_{pBMA}$ x (1.76 - 1.37 wp 10^6 exp(-6240/T)) (161, 162).

Table 10. Reactivity ratios for the ter-polymerization of Styrene, Butyl Methacrylate and Butyl Acrylate at 138°C

Reactivity ratios		**Source**
r_{Sty-BA}	0.956	(83)
r_{BA-Sty}	0.183	(83)
$r_{Sty-BMA}$	0.61	(105)
$r_{BMA-Sty}$	0.42	(105)
r_{BA-BMA}	1.5815*exp(-564.8/T)	(89)
r_{BMA-BA}	0.8268*exp(282.1/T)	(89)

Figures 75 through s78 show cumulative polymer composition vs. time for each of the polymerizations. Each simulation is very accurate, verifying the reactivity ratios used. Figures 79, 80 and 81 are the monomer concentration simulations for styrene, BMA and BA, respectively. The simulations for styrene follow the data well, but each slightly overestimates the data with the exception of the fourth run. As styrene is present in the

least amount, even a slight deviation from the data appears much larger than it actually is. Both the monomer concentrations of the BMA and BA, however, are quite accurate and follow the pattern established by the data. For such a complex ter-polymerization with depropagation and backbiting, the model performed extremely well and could very well predict an experiment with three monomers at an elevated temperature.

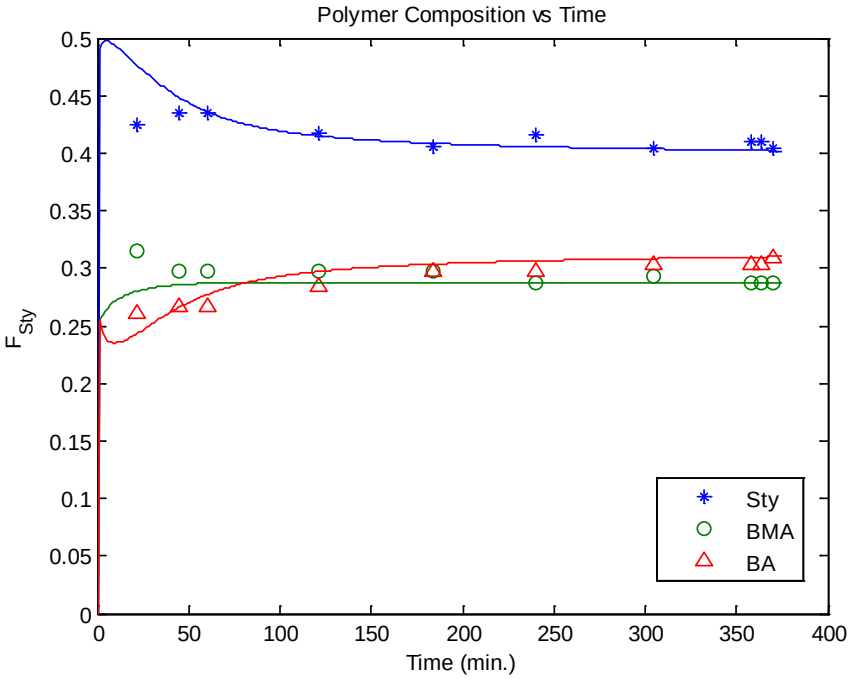

Figure 75. Simulation of the semi-batch ter-polymerization of Sty/BMA/BA, T = 138°C, $[TBPA]_0$ = 2 wt%, xylene = 30 wt%, $f_{Sty0} = f_{BMA0}$ = 33 wt%.

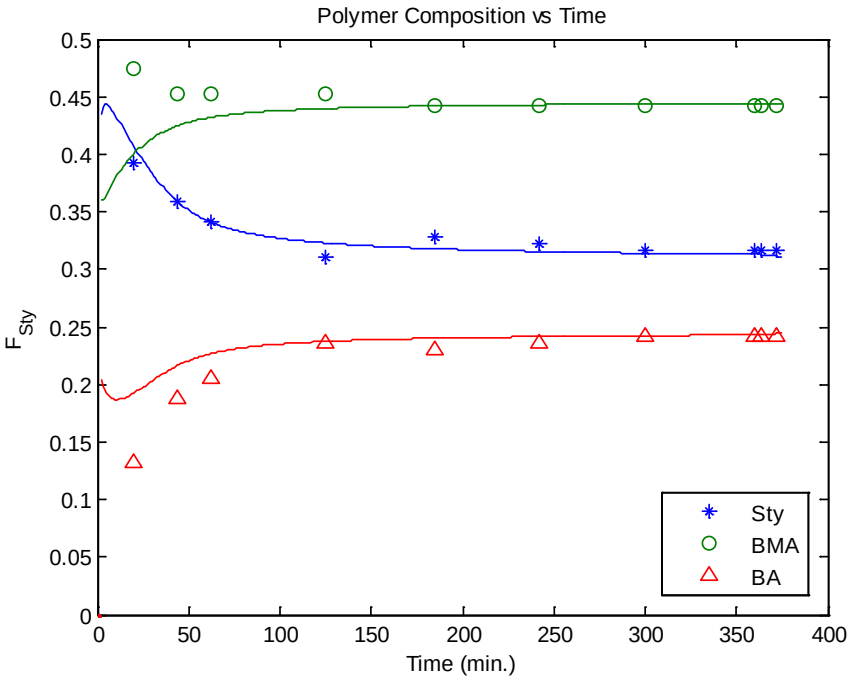

Figure 76. Simulation of the semi-batch ter-polymerization of Sty/BMA/BA, T = 138°C, $[TBPA]_0$ = 2 wt%, xylene = 30 wt%, $f_{Sty0} = f_{BA0}$ = 25 wt%.

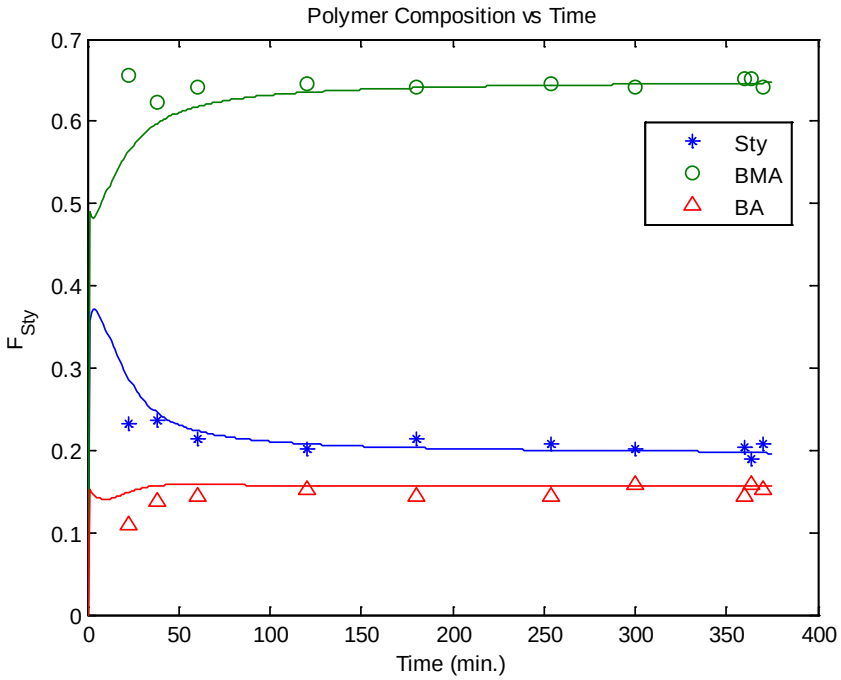

Figure 77. Simulation of the semi-batch ter-polymerization of Sty/BMA/BA, T = 138°C, $[TBPA]_0$ = 2 wt%, xylene = 30 wt%, $f_{Sty0} = f_{BA0}$ = 15 wt%.

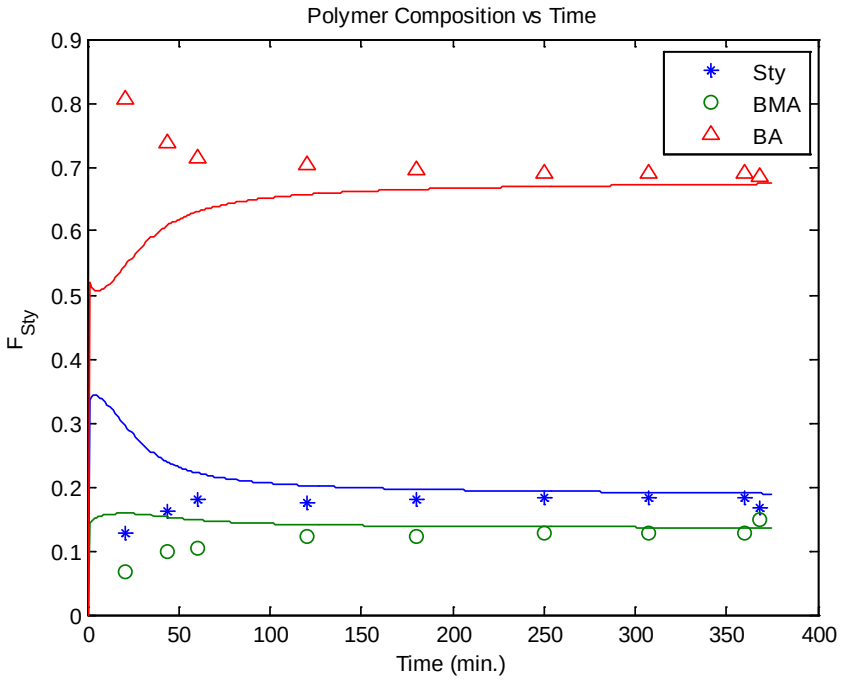

Figure 78. Simulation of the semi-batch ter-polymerization of Sty/BMA/BA, T = 138°C, $[TBPA]_0$ = 2 wt%, xylene = 30 wt%, $f_{Sty0} = f_{BMA0}$ = 15 wt%.

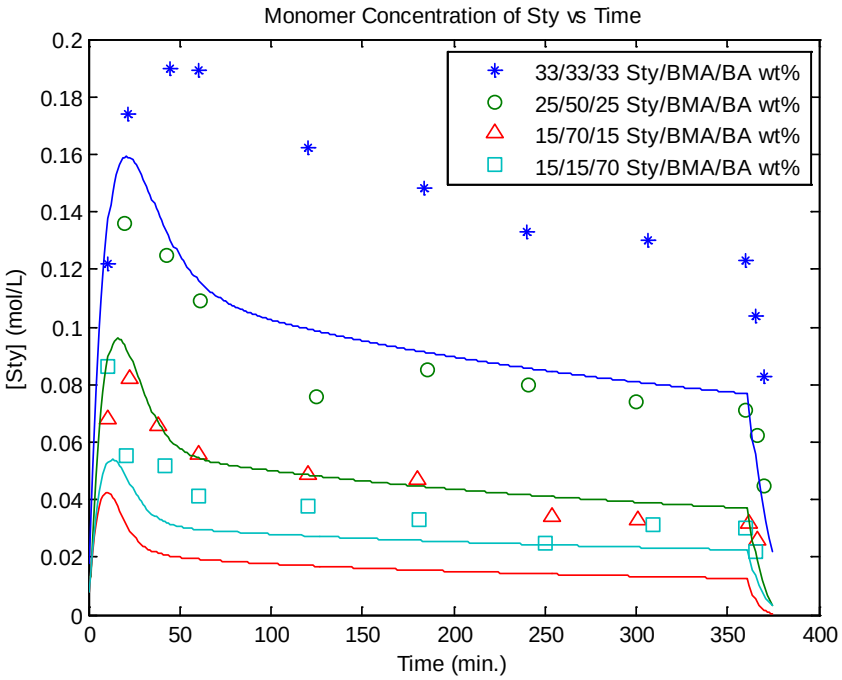

Figure 79. Simulation of the semi-batch ter-polymerization of Sty/BMA/BA, T = 138°C, $[TBPA]_0$ = 2 wt%, xylene = 30 wt%.

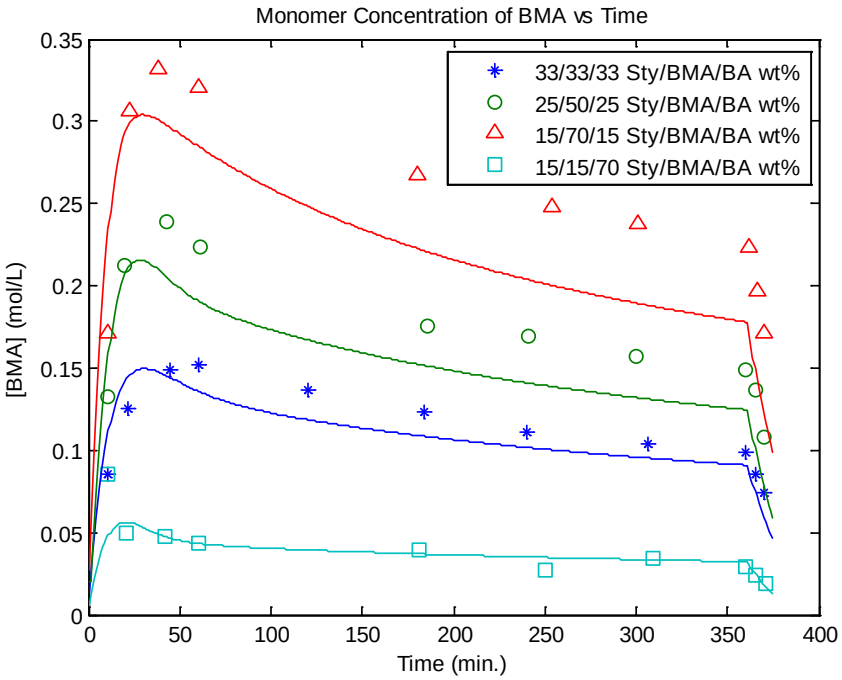

Figure 80. Simulation of the semi-batch ter-polymerization of Sty/BMA/BA, T = 138°C, $[TBPA]_0$ = 2 wt%, xylene = 30 wt%.

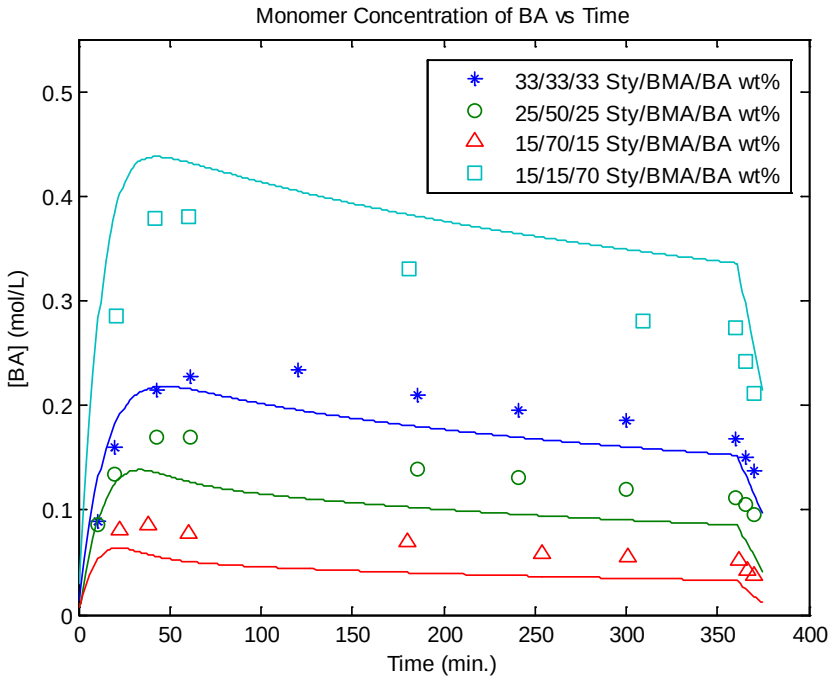

Figure 81. Simulation of the semi-batch ter-polymerization of Sty/BMA/BA, T = 138°C, $[TBPA]_0$ = 2 wt%, xylene = 30 wt%.

4. Conclusions

A general, flexible, multi-component free-radical polymerization model has been tested over a wide range of recipes and operating conditions in order to check its reliability in Part 1 of this series of two papers (1). Part 2 represents a refinement and expansion of the detailed and extensive mathematical model presented in Part 1 for free-radical, bulk and/or solution multi-component polymerizations. The expansion is mainly with respect to depropagation, thus making the model more fluent at elevated polymerization

temperatures and, in parallel, with additional features as backbiting (with systems involving butyl acrylaye). To give an indication of the magnitude of information in this Part of the series, Part 2 contains 10 tables in the main text, with general information from the literature, with an additional 25 far more important tables in the appendices, full of items comprising the extensive polymerization database; 81 figures/plots with experimental data and model predictions; and 168 references. The extensive simulation results of both Part 1 (1) and Part 2 (herein) all rely solely on a unique monomer/polymer database of physico-chemical properties and other characteristics, with no further parameter adjustment. The dtabase items are all cited in detail in the tables of the appendices of the current paper (Part 2).

Acknowledgements

The authors wish to acknowledge financial support from the Natural Sciences and Engineering Research Council (NSERC) of Canada, and the Canada Research Chair (CRC) program. Also, thanks go to various industrial contacts, for the countless lively discussions on modeling over numerous years. Finally, a huge ‘thank you’ to Lyn Roberts, who has been the epitome of efficiency and a model managing editor for JMS PAC over many years, and therefore a significant contributor to the success of the journal. Lyn, I (AP) have seen and dealt with many journals; you certainly put the great majority

of all other editors/managing editors/editors-in-chief (and editorial offices, in general) to shame.

References

1. Jung, W., Riahinezhad, M., Duever, T. A., Penlidis, A. (2015) J. Macromol. Sci., Pure & Appl. Chem., Part A, 52(9): 659-698.
2. Jung, W. (2008) MASc thesis, Dep. Chem. Eng., Uni. Waterloo.
3. Dorschner, D. (2010) MASc thesis, Dep. Chem. Eng., Uni. Waterloo.
4. Sahloul, N. A. (2004) PhD thesis, Dep. Chem. Eng., Uni. Waterloo.
5. Alfrey, T., Goldfinger, G. (1944) J. Chem. Phys., 12: 205-209.
6. Alfrey, T., Goldfinger, G. (1946). J. Chem. Phys., 14: 115-116.
7. Walling, C., Briggs, E. R. (1945) J. Am. Chem. Soc., 67: 1774-1778.
8. Valvassori, A., Sartori, G. (1967) Adv. Polym. Sci., 5(1): 28-58.
9. Galbraith, M. N., Moad, G., Solomon, D. H., Spurling, T. H. (1987) Macromol., 20: 675-679.
10. Hamielec, A. E., MacGregor, J. F., Penlidis, A., Comprehensive Polymer Science Encyclopedia, Pergamon Press: Oxford, Chap. 2, 17-31, 1987.
11. Hamielec, A. E., MacGregor, J. F., Penlidis, A. (1987) Makromol. Chem. Macromol. Symp. 10-11: 521-570.
12. Dubé, M. A., Penlidis, A. (1995) Polym., 36(3): 587-598.

13. Dubé, M. A., Penlidis, A. (1995) Macromol. Chem. Phys., 196: 1102-1112.

14. Hocking, M. B., Klimchuk, K. A. (1996) J. Polym. Sci. Part A: Polym. Chem., 34: 2481-2497.

15. Dubé, M. A., Penlidis, A. (1996) AIChE, 42(7): 1985-1994.

16. Dubé M. A., Soares J. B. P., Penlidis A., Hamielec A. E. (1997) Ind. Eng. Chem. Res., 36(4): 966-1015.

17. McManus, N. T., Kim, J. D., Penlidis, A. (1998) Polym. Bull., 41: 661-668.

18. Gao, J., Penlidis, A. (2000) Macromol. Chem. Phys., 201: 1176-1184.

19. Keramopoulos, A., Kiparissides, C. (2003) J. Appl. Polym. Sci., 88: 161-176.

20. McManus, N. T., Hsieh, G., Penlidis, A. (2004) Polym., 45: 5837-5845.

21. Leamen, M. J., McManus, N. T., Penlidis, A. (2005). J. Polym. Sci. Part A: Polym. Chem., 43: 3868-3877.

22. Li, D., Hutchinson, R. A. (2007) Macromol. Rapid Commun., 28: 1213-1218.

23. Wang, W. (2010) PhD thesis, Dep. Chem. Eng., Queen's Uni.

24. Branson, H., Simha, R. (1943) J. Chem. Phys., 11(6): 297-298.

25. Mayo, F. R., Lewis, F. M. (1944) J. Am. Chem. Soc., 66: 1594-1601.

26. Simha, R., Branson, H. (1944) J. Chem. Phys., 12(6): 253-267.

27. Wall, F. T., (1944) J. Am. Chem. Soc., 66: 2050-2057.

28. Stockmayer, W. H. (1945) J. Chem. Phys., 13(6): 199-207.

29. Merz, E., Alfrey, T., Goldfinger G. (1946) J. Polym. Sci., 1(2): 75-82.

30. Skeist, I. (1946) J. Am. Chem. Soc., 68: 1781-1784.

31. Walling, C. (1949) J. Am. Chem. Soc., 71: 1930-1935.

32. Mayo, F. R., Walling, C. (1950) Chem. Rev., 46: 191-287.

33. Bradbury, J. H., Melville, H. W. (1954) Proc. Royal Soc. London Series A. Math. Phys. Sci., 222(1151), 456-470.

34. Lowry, G. G. (1960) J. Polym. Sci., 42: 463-477.

35. Harwood, H. J., Ritchey, W. M. (1964) Polym. Lett., 2: 601-607.

36. Meyer, V. E., Lowry, G. G. (1965) J. Polym. Sci. Part A: Gen. Pap., 3(8): 2843-2851.

37. Otsu, T., Ito, T., Imoto, M. (1965) Polym. Lett., 3: 113-117.

38. Otsu, T., Ito, T., Imoto, M. (1966) J. Polym. Sci. Part A-1, 4: 733-736.

39. Cameron, G. G., Kerr, G. P. (1967) Eur. Polym. J., 3: 1-4.

40. Chan, R. K. S., Meyer, V. E. (1968) J. Polym. Sci. Polym. Symp., 25: 11-21.

41. Harwood, H. J. (1968) J. Polym. Sci. Part C: Polym. Lett., 25: 37-45.

42. Howell, J. A., Izu, M., O'Driscoll, K. F. (1970) J. Polym. Sci. Part A: Polym. Chem., 8: 699-710.

43. Izu M., O'Driscoll, K. F. (1970 J. Polym. Sci. Part A: Polym. Chem., 8: 1675-1685.

44. Wittmer, P. (1971) Adv. Chem. Ser., 99: 140-174.

45. Fischer J. P. (1972) Die Makromolekulare Chemie, 155: 211-225.

46. Johnston, N. W. (1973) Macromol., 6(3): 453-456.

47. Chow, C. D. (1975) J. Polym. Sci. Polym. Chem. Ed., 13: 309-313.

48. Gaddam, N. B., Xavioir, S. F., Goel, T. C. (1977) J. Polym. Sci. Polym. Chem. Ed., 15:1473-1478.

49. Johnson, M., Karmo, T. S., Smith, R. R. (1978) Eur. Polym. J., 14: 409-414.

50. Dionisio, J. M., O'Driscoll, K. F. (1979) J. Polym. Sci. Polym. Lett. Ed., 17: 701-707.

51. Patino-Leal, H., Reilly, P. M., O'Driscoll, K. F. (1980) J. Polym. Sci. Polym. Lett. Ed., 18: 219-227.

52. Reilly, P. M., Patino-Leal, H. (1981) Technometrics, 23(3): 221-231.

53. Borchardt, J. K. (1982) Polym. Preprints, 23(2): 209-211.

54. Hill, D. J. T., O'Donnel, J. H., O'Sullivan, P. W. (1982) Macromol., 15: 960-966.

55. Duever, T. A., O'Driscoll, K. F., & Reilly, P. M. (1983) J. Polym. Sci. Polym. Chem. Ed., 21: 2003-2010.

56. Lord, M. G. (1984) MSc thesis, Dep. Chem. Eng. McMaster Uni.

57. Teramachi, S., Hasegawa, A., Uchiyama, N. (1984) J. Polym. Sci. Polym. Lett. Ed., 22: 71-76.

58. Borchardt, J. K. (1985) J. Macromol. Sci. Chem., 22(12): 1711-1733.

59. Garcia-Rubio, L. H., Lord, M. G., MacGregor, J. F., Hamielec, A. E. (1985) Polym., 26: 2001-2013.

60. Balaraman, K. S., Nadkarni, V. M., Mashelkar, R. A. (1986) Chem. Eng. Sci., 41(5): 1357-1368.

61. Catala, M., Nonn, A., Pujol, J. M., Brossas, J. (1986) Polym. Bull., 15: 311-315.

62. Krüger, H., Bauer, J., Rübner, J. (1987) Makromolekulare Chemie, 188: 2163-2175.

63. Tacx, J. C. J. F., Ammerdorffer, J. L., German, A. L. (1988) Polym., 29: 2087-2094.

64. Dubé, M. A. (1989) PhD thesis, Dep. Chem. Eng., Uni. Waterloo.

65. O'Driscoll, K. F., Huang, J. (1989) Eur. Polym. J., 25(7/8): 629-633.

66. O'Driscoll, K. F., Huang J. (1990) Eur. Polym. J., 26: 643-647.

67. Davis, T. P., O'Driscoll, K. F., Piton, M. C., Winnik, M. A. (1990) Macromol., 23: 2113-2119.

68. Dubé, M. A., Penlidis, A., O'Driscoll, K. F. (1990a) Chem. Eng. Sci., 45(8): 2785-2792.

69. Dubé, M. A., Penlidis, A., O'Driscoll, K. F. (1990b) Can. J. Chem. Eng. 68: 974-987.

70. Dubé, M. A., Rilling, K., Penlidis, A. (1991) J. Appl. Polym. Sci., 43: 2137-2145.

71. Dubé, M. A., Sanayei, R. A., Penlidis, A., O'Driscoll, K. F., Reilly, P. M. (1991) J. Polym. Sci. Part A Polym. Chem., 29: 703-708.

72. Kapur, G. S., Brar, A. S. (1992) Makromolekulare Chemie, 193: 1773-1781.

73. Englemann, U., Schmidt-Naake, G. (1993) Makromolekulare Chemie Theory and Simulations, 2: 275-297.

74. Reilly, P. M., Reilly, H. V., Keeler, S. E. (1993) Applied Statistics, 42(4), 693-701.

75. Switata-Zeliazkow, M. (1993) Makromolekulare Chemie, 194(5): 1505-1511.

76. Xie, T. Y., Hamielec, A. E. (1993) Makromolekulare Chemie Theory and Simulations, 2(3): 455-483.

77. Kim, J. D. (1994) MSc thesis, Dep. Chem. Eng., Uni. Waterloo.

78. Vivaldo-Lima, E., Hamielec, A. E., Wood, P. E. (1994) Polym. React. Eng., 2(1&2): 87-162.

79. Liu, Y., Mao, R., Huglin, M. B., Holmes, P. A. (1995) Polym., 26: 4287-4292.

80. Rossignoli, P. J., Duever, T. A. (1995) Polym. React. Eng., 3(4): 361-395.

81. McManus, N. T., Penlidis, A. (1996) J. Polym. Sci. Part A, 34: 237-248.

82. Brar, A. S., Dutta, K. (1998). Macromol., 31: 4695-4702.

83. Gao, J., Penlidis, A. (1998) J. Macromol. Sci. Macromol. Chem. Phys., Revs., C38(4): 651-780.

84. Polic, A. L., Duever, T. A., Penlidis, A. (1998) J. Polym. Sci. Part A Polym. Chem., 36: 813-822.

85. Brandrup, J., Immergut, E. H., Grulke, E. A., Bloch, D., Polymer Handbook. 4th Ed. New York: John Wiley & Sons, 1999.

86. Chambard, G., Klumperman, B., German, A. L. (1999) Polym., 40: 4459-4463.

87. Martinet, F., Guillot, J. (1999) J. Appl. Polym. Sci., 72: 1611-1625.

88. McManus, N. T., Dubé, M. A., Penlidis, A. (1999) Polym. React. Eng., 7(1): 131-145.

89. Hakim, M., Verhoeven, V., McManus, N. T., Dubé, M. A., Penlidis, A. (2000) J. Appl. Polym. Sci., 77: 602-609.

90. Palmer, D. E., McManus, N. T., Penlidis, A. (2000) J. Polym. Sci. Part A Polym. Chem., 38: 1981-1990.

91. Palmer, D. E., McManus, N. T., Penlidis, A. (2001) J. Polym. Sci. Part A Polym. Chem., 39: 1753-1763.

92. Buback, M., Feldermann, A., Barner-Kowollik, B., Lacik, I. (2001) Macromol., 34: 5439-5448.

93. Scholtens, C. A., Meuldijk, J., Drinkenburg, A. A. H. (2001) Chem. Eng. Sci., 56: 955-962.

94. Dubé, M. A., Hakim, M., McManus, N. T., Penlidis, A. (2002) Macromol. Chem. Phys., 203: 2446-2453.

95. Grady, M. C., Simonsick, W. J., Hutchinson, R. A. (2002) Macromol. Symp., 182: 149-168.

96. Kim, Y., Harwood, H. J. (2002) Polym., 43: 3229-3237.

97. Wolf, A., Bandermann, F., Schwede, C. (2002) Macromol. Chem. Phy., 203(2): 393-400.

98. Fernandez-Garcia, M., Fernandez-Sanz, M., Madruga, E. L. (2003) J. Polym. Sci. Part A, 42: 130-136.

99. Cheong, S. I., Penlidis, A. (2004) J. Appl. Polym. Sci., 93: 261-270.

100. Sahloul, N. A., Penlidis, A. (2004) Adv. Polym. Tech., 23(3): 186-195.

101. Sahloul, N. A., Penlidis, A. (2005) Polym.-Plastics Tech. Eng., 44: 771-782.

102. Sahloul, N. A., Emwas, N. A., Power, W., Penlidis, A. (2005) J. Macromol. Sci. Part A. Pure Appl. Chem., 42: 1369-1385.

103. Li, D., Grady, M. C., Hutchinson, R. A. (2005) Ind. Eng. Chem. Res, 44(8): 2506-2517.

104. Jianying, H., Jiayan C., Jiaming, Z., Yihong, C., Lizong, D., Yousi, Z. (2006) J. Appl. Polym. Sci., 100: 3531-3535.

105. Li, D., Li, N., Hutchinson, R. A. (2006) Macromol., 39: 4366-4373.

106. Abdollahi, M., Mehdipour-Ataei, S., Ziaee, F. (2007) J. Appl. Polym. Sci., 105: 2588-2597.

107. Mun, G. A., Nurkeeva, Z. S., Beissegul, A. B., Dubalazov, A. V., Urkimbaeva, P. I., Park, K., Khutoryanskiy, V. V. (2007) Macromol. Chem. Phys., 208: 979-987.

108. Fujisawa, T., Penlidis, A. (2008) J. Macromol. Sci. Part A. Pure Appl. Chem., 45: 115-132.

109. Wang, W., Hutchinson, R. A. (2008a) Macromol. Symp., 261: 64-73.

110. Wang, W., Hutchinson, R. A. (2008b) Macromol., 41: 9011-9018.

111. Popescu, D., Hoogenboom, R., Keul, H., Möller, M. (2010) J. Polym. Sci. Part A. Polym. Chem., 48: 2610-2621.

112. Bywater S. (1955). Photosensitized polymerization of methyl methacrylate in dilute solution above 100°C. Trans. Faraday Soc., 51: 1267-1273.

113. McCormick, H. W. (1957) J. Polym. Sci., 25(111): 488-490.

114. Nair, A. S., Muthana, M. S. (1961) Makromol. Chem., 47: 114-127.

115. Carlsson, D. J., Howard, J. A., Ingold, K. U. (1966) J. Am. Chem. Soc., 88(20): 4725-4726.

116. Raghuram, P. V. T., Nandi, U. S. (1967) J. Polym. Sci. Part A-1, 5: 2005-2012.

117. Raghuram, P. V. T., Nandi, U. S. (1970) J. Polym. Sci. Part A-1, 8: 3079-3088.

118. Hui, A. W., Hamielec, A. E. (1972) J. Appl. Polym. Sci., 16: 749-769.

119. Friis, N., Nyhagen, L. (1973) J. Appl. Polym. Sci., 17: 2311-2327.

120. Arai, K., Saito, S. (1976) J. Chem. Eng. Japan, 9(4): 302-313.

121. Husain, A., Hamielec, A. E. (1978) J. Appl. Polym. Sci., 22: 1207-1223.

122. Garcia-Rubio, L. H., Hamielec, A. E., MacGregor, J. F. (1979) J. Appl. Polym. Sci., 23: 1413-1429.

123. Marten, F. L., Hamielec, A. E. (1982) J. Appl. Polym. Sci., 27: 489-505.

124. Stickler, M. (1983) Makromol. Chem., 184: 2563-2579.

125. Stickler, M., Panke, D., Hamielec, A. E. (1984) J. Polym. Sci. Polym. Chem. Ed., 22: 2243-2253.

126. Buback, M. Degener B., Huckestein, B. (1989) Makromol. Chem. Rapid Commun., 10: 311-316.

127. Buback, M. (1990) Makromol. Chem., 191: 1575-1587.

128. Kumar, V. R., Gupta, S. K. (1991) Polym., 32(17): 3233-3243.

129. Kuindersma, M. E. (1992) MSc thesis, Dep. Chem. Eng., Uni. Waterloo.

130. Gao, J. (1992) MSc thesis, Dep. Chem. Eng., Uni. Waterloo.

131. Buback, M., Gilbert, R. G., Hutchinson, R. A., Klumperman, B., Kuchta, F., Manders, B. G., O'Driscoll, F., Russell, G. T., Schweer, J. (1995) Macromol. Chem. Phys., 196: 3267-3280.

132. Hutchinson, R. A., Paquet, D. A. Jr., McMinn, J. H., Fuller, R. E. (1995) Macromol., 28: 4023-4028.

133. Beuermann, S., Paquet, D. A., McMinn, J. H., Hutchinson, R. A. (1996) Macromol., 29: 4206-4215.

134. Gao, J., Penlidis, A. (1996) J. Macromol. Sci. Macromol. Chem. Phys., Revs., C36(2): 199-404.

135. Lyons, R. A., Hutovic, J., Piton, M. C., Christie, D. I., Clay, P. A., Manders, B. G., Kable, S. H., Gilbert, R. G. (1996) Macromol., 29: 1918-1927.

136. Gao, J., McManus, N. T., Penlidis, A. (1997) Macromol. Chem. Phys., 198: 843-859.

137. Beuermann, S., Paquet, D. A., McMinn, J. H., Hutchinson, R. A. (1997) Macromol., 30: 194-197.

138. Hutchinson, R. A., Beuermann, S., Paquet, D. A., McMinn, J. H. (1997) Macromol., 30: 3490-3493.

139. Buback, M., Kurz, C., Schmaltz, C. (1998) Macromol. Chem. Phys., 199: 1721-1727.

140. Maeder, S., Gilbert, R. G. (1998) Macromol., 31: 4410-4418.

141. Beuermann, S., Buback, M., Schmaltz, C. (1999) Ind. Eng. Chem. Res., 38: 3338-3344.

142. Buback, M., Klingbeil, S., Sandmann, J., Sderra, M., Vögele, H. P., Wackerbarth, H., Wittkowski, L. (1999) Phys. Chem., 210: 199-221.

143. Dhib, R., Gao, J., Penlidis, A. (2000) Polym. React. Eng., 8(4): 299-464.

144. Asua, M., Beuermann, S., Buback, M., Castignolles, P., Charleux, B., Gilbert, R. G., Hutchinson, R. A., Leiza, J. R., Nikitin, A. N., Vairon, J., Van Herk, A. M. (2004) Macromol. Chem. Phys., 205: 2151-2160.

145. Nising, P., Meyer, T. (2004) Ind. Eng. Chem. Res., 43(23): 7220-7226.

146. Peck, A. N. F., Hutchinson, R. A. (2004) Macromol., 37: 5944-5951.

147. Gao, J., Hungenberg, K. D., Penlidis, A. (2004) Macromol. Symp., 206, 509-522.

148. Quan, C., Soroush, M., Grady, M. C., Hansen, J. E., Simonsick, W. J. (2005) Macromol., 38: 7619-7628.

149. Vargün, E., Usanmaz, A. (2005) J. Polym. Sci. Part A Polym. Chem., 43: 3957-3965.

150. Willemse, R. X. E., Van Herk, A. M., Panchenko, E., Junkers, T., Buback, M. (2005) Macromol., 38(12): 5098-5103.

151. Buback, M., Junkers, T. (2006) Macromol. Chem. Phys., 207: 1640-1650.

152. Rantow, F. S., Soroush, M., Grady, M. C., Kalfas, G. A. (2006) Polym., 47: 1423-1435.

153. Matthews, B., Villa C., Pierini, P. (2007) Macromol. Sympo., 259: 94-101.

154. Nikitin, A. N., Hutchinson, R. A., Buback, M., Hesse, P. (2007) Macromol., 40: 8631-8641.

155. Chen, S., Hu, T., Tian, Y., Chen, L., Pojman, A. (2007) J. Polym. Sci. Part A Polym. Chem., 45: 873-881.

156. Ahmad, N., Charleux, B., Farcet, C., Ferguson, C. J., Gaynor, S. G., Hawkett, B. S., Heatley, F., Klumperman, B., Konkolewicz, D., Lovell, P. A., Matyjaszewski, K., Venkatesh, R. (2009) Macromol. Rapid Commun., 30: 2002-2021.

157. Barth, J., Buback, M., Hesse, P., Sergeeva, T. (2009) Macromol. Rapid Commun., 30: 1969-1974.

158. Castignolles, P. (2009) Macromol. Rapid Commun., 30: 1995-2001.

159. Nikitin, A. N., Hutchinson, R. A. (2009) Macromol. Rapid Commun., 30: 1981-1988.

160. Van Herk. A. M. (2009). Historic account of the development in the understanding of the propagation kinetics of acrylate radical polymerizations. Macromol. Rapid Commun., 30: 1964-1968.

161. Wang, W., Hutchinson, R. A., Grady, M. C. (2009a) Ind. Eng. Chem. Res., 48: 4810-4816.

162. Wang, W., Nikitin, A. N., Hutchinson, R. A. (2009b) Macromol. Rapid Commun., 30: 2022-2027.

163. Zorn, A., Junkers, T., Barner-Kowollik, C. (2009) Macromol. Rapid Commun., 30: 2028-2035.

164. Leamen, M. J. (2005) PhD thesis, Dep. Chem. Eng., Uni. Waterloo.

165. Moad, G., Solomon, D. H., The Chemistry of Free Radical Polymerization. Oxford: Pergamon, 1995.

166. Leamen, M. J., McManus, N. T., Penlidis, A. (2006) Chem. Eng. Sci., 61: 7774-7785.

167. Plessis, C., Arzamendi, G., Alberdi, J. M., Van Herk, A. M., Leiza, J. R., Asua, J. M. (2003) Macromol. Rapid Commun., 24(2): 173-177.

168. Mahabadi, H. K., O'Driscoll, K. F. (1978) J. Polym. Sci. Polym. Let. Ed., 16: 351-356.

Appendices

Appendix I. Initiator Database

This section has the kinetic data used for each of the available initiators. Certain parameters vary from monomer to monomer due to different interactions; the values for each monomer as well as the general value (used for any monomer not specified) are included in each of the initiator tables. All of the values used below are constant and remain unchanged from simulation to simulation. Without this, there would be no confidence in the simulation package for accurate use in industry and/or academia. Each of the values shown was originally taken from the comprehensive WATPOLY simulator database created by Gao and Penlidis (18, 83, 134). Since then, a select few have been

refined through simulation trials, sensitivity analyses or parameter estimation to create an enhanced mathematical model program.

Table A-1. Kinetic database for AIBN

Parameter	Monomer	Value	Unit	Description
Mw	General	164.21	g/mol	Initiator molecular weight
k_d	Styrene	$6.33*10^{16}\exp(-3.0719*10^4/RT)$	L/min	Decomposition rate constant
	EA	$7.7803*10^{16}\exp(-3.0704*10^4/RT)$		
	General	$6.23*10^{16}\exp(-3.0704*10^4/RT)$		
f	Styrene	0.6		Initiator efficiency
	BMA	0.42		
	General	0.0247exp(-2166/RT)		
V_{fi}	Styrene	0.04	V	Critical free volume for diffusion-control
	BA	0.15		
	EA	0.825exp(-1175/RT)		
	BMA	0.09		
	General	0.6365exp(-1368.8/RT)		
C	Styrene	0.5		Rate of decrease of f
	BA	1		

	EA	1		
	General	0.685		

Table A-2. Kinetic database for BPO

Parameter	Monomer	Value	Unit	Description
Mw	General	242.23	g/mol	Initiator molecular weight
k_d	MMA	$6.23*10^{16}\exp(-3.0704*10^4/RT)$	L/min	Decomposition rate constant
	EA	$7.7803*10^{16}\exp(-3.0704*10^4/RT)$		
	General	$6.429*10^{15}\exp(-3.01*10^4/RT)$		
f	Styrene	0.75		Initiator efficiency
	BMA	0.6		
	HEA	0.8		
	General	0.0247exp(-2166/RT)		
V_{fi}	Styrene	0.15	V	Critical free volume for diffusion-control
	BA	0.15		
	EA	0.825exp(-1175/RT)		
	BMA	0.075		
	General	0.6365exp(-1368.8/RT)		
C	Styrene	0.25		Rate of decrease of f
	BA	1		

	EA	1		
	General	0.685		

Table A-3. Kinetic database for TBPA (tert-butyl peroxyacetate)

Parameter	Monomer	Value	Unit	Description
Mw	General	132.16	g/mol	Initiator molecular weight
k_d	Styrene	$4.068*10^{17}\exp(-3.52*10^4/RT)$	L/min	Decomposition rate constant
	BA	$4.068*10^{17}\exp(-3.52*10^4/RT)$		
	BMA	$4.068*10^{17}\exp(-3.52*10^4/RT)$		
	General	$1.67*10^{16}\exp(-3.29*10^4/RT)$		
f	Styrene	0.515		Initiator efficiency
	BMA	0.515		
	General	0.6		
V_{fi}	Styrene	0.015	V	Critical free volume for diffusion-control
	BMA	0.015		
	General	0.15		
C	General	1		Rate of decrease of f

Table A-4. Kinetic database for TBPB (tert-butyl peroxybenzoate)

Parameter	Monomer	Value	Unit	Description
Mw	General	194.23	g/mol	Initiator molecular weight
k_d	General	$3.716*10^{16}\exp(-3.321*10^4/RT)$	L/min	Decomposition rate constant
f	Styrene	0.9		Initiator efficiency
	General	0.5		
V_{fi}	General	0.15	V	Critical free volume for diffusion-control
C	General	0.25		Rate of decrease of f

Table A-5. Kinetic database for dTBPO (di-tert-butyl peroxide)

Parameter	Monomer	Value	Unit	Description
Mw	General	146.23	g/mol	Initiator molecular weight
k_d	MMA	$1.68*10^{16}\exp(-3.5*10^4/RT)$[1]	L/min	Decomposition rate constant
	General	$7.29*10^{16}\exp(-3.56*10^4/RT)$		
f	MMA	0.7		Initiator efficiency
	BA	0.3		
	General	0.5		
V_{fi}	General	0.15	V	Critical free volume for diffusion-control
C	General	0.25		Rate of decrease of f

[1]Ref (145)

Appendix II. Monomer Database

The complete monomer database used in each of the simulations is shown below. The kinetic parameters that are unreferenced come from WATPOLY (Gao and Penlidis (134, 83, 18)). Again, these values are constant for each of the simulations shown herein and in Jung (2).

Table A-6. Kinetic database for acrylic acid

Parameter	Value	Unit	Description
Mw	72.06	g/mol	Molecular weight of the monomer
T_{gm}	189.65	K	Glass transition temp. of the monomer
T_{gp}	379	K	Glass transition temperature of the polymer
C_{pm}	502	cal/kg/K	Heat capacity of the monomer
C_{pp}	432.69	cal/kg/K	Heat capacity of the polymer
ΔH	$-1.85*10^4$	cal/mol	Heat of reaction
ρ_m	1.0776-0.001328(T-273.15)	kg/L	Density of the monomer
ρ_p	1.442	kg/L	Density of the polymer
k_p	$3.72*10^9\exp(-5600/RT)$	L/mol/min	Rate of propagation
k_t	$6*10^9$	L/mol/min	Rate of termination
$k_{td,ratio}$[1]	0.2		Disproportionation to combination ratio
k_{fm}	$1.72*10^9\exp(-1.11*10^4/RT)$	L/mol/min	Transfer to monomer rate

k_{fp}	0	L/mol/min	Transfer to polymer rate
k_{pin}	0	L/mol/min	Internal double bond rate of propagation
k_{pte}	0	L/mol/min	Terminal double bond rate of propagation
Δ	0.001	L/g	Reaction radius for segmental diffusion
V_{fc}	3.0956exp(-1683.2/RT)	L	Critical free volume
V_{fm}	0.025	L	Free volume of the monomer
α_m	0.001	L/K	Thermal expansion coeff. of the monomer
V_{fp}	0.025	L	Free volume of the polymer
α_p	0.0048	L/K	Thermal expansion coeff. of the polymer
B	1		Rate of decrease of k_p
m	0.5		Gel-effect model parameter
n	1.75		Gel-effect model parameter
A	1.75		Rate of decrease of k_t
K_3	$5*10^6$		Onset pt. of translational diffusion-control
n_s	120		Avg. number of monomer units per chain
l_0	$6.2*10^{-8}$	cm	Length of monomer unit per chain
k_{th}	0	$L^2/mol^2/min$	Thermal (/self) initiation rate

[1] $k_{td,ratio} = \frac{k_{td}}{k_t}$

Table A-7. Kinetic database for Acrylonitrile

Parameter	Value	Unit	Description
Mw	53.06	g/mol	Molecular weight of the monomer
T_{gm}	190	K	Glass transition temp. of the monomer
T_{gp}	337.15	K	Glass transition temperature of the polymer
C_{pm}	430	cal/kg/K	Heat capacity of the monomer
C_{pp}	301	cal/kg/K	Heat capacity of the polymer
ΔH	$-1.781*10^4$	cal/mol	Heat of reaction
ρ_m	0.82754-0.0011(T-273.15)	kg/L	Density of the monomer
ρ_p	1.175-0.00131(T-273.15)	kg/L	Density of the polymer
k_p	$6*10^9 exp(-7105.3/RT)$	L/mol/min	Rate of propagation
k_t	$2.5*10^{12} exp(-3996/RT)$	L/mol/min	Rate of termination
$k_{td,ratio}$	0.08		Disproportionation to combination ratio
k_{fm}	$1.2*10^8 exp(-1.033*10^4/RT)$	L/mol/min	Transfer to monomer rate
k_{fp}	0	L/mol/min	Transfer to polymer rate
k_{pin}	0	L/mol/min	Internal double bond rate of propagation
k_{pte}	0	L/mol/min	Terminal double bond rate of propagation
Δ	0.001	L/g	Reaction radius for segmental diffusion
V_{fc}	5.3277exp(-3059/RT)	L	Critical free volume

V_{fm}	0.025	L	Free volume of the monomer
α_m	0.001	L/K	Thermal expansion coeff. of the monomer
V_{fp}	0.025	L	Free volume of the polymer
α_p	0.0048	L/K	Thermal expansion coeff. of the polymer
B	0.5		Rate of decrease of k_p
m	0.5		Gel-effect model parameter
n	1.75		Gel-effect model parameter
A	0.95		Rate of decrease of k_t
K_3	0.8313exp(-7979.9/RT)		Onset pt. of translational diffusion-control
n_s	120		Avg. number of monomer units per chain
l_0	$6.2*10^{-8}$	cm	Length of monomer unit per chain
k_{th}	0	$L^2/mol^2/min$	Thermal (/self) initiation rate

Table A-8. Kinetic database for Butyl Acrylate

Parameter	Value	Unit	Description
Mw	128.17	g/mol	Molecular weight of the monomer
T_{gm}	185.15	K	Glass transition temp. of the monomer
T_{gp}	218	K	Glass transition temperature of the polymer
C_{pm}	430	cal/kg/K	Heat capacity of the monomer
C_{pp}	400	cal/kg/K	Heat capacity of the polymer
ΔH	$-1.84*10^4$	cal/mol	Heat of reaction
ρ_m	0.919-0.001012(T-273.15)	kg/L	Density of the monomer
ρ_p	1.212-0.000845(T-273.15)	kg/L	Density of the polymer
k_p	$1.326*10^9\exp(-4278.1/RT)$[1]	L/mol/min	Rate of propagation
k_t	$8.04*10^{10}\exp(-1338.4/RT)$[1]	L/mol/min	Rate of termination
$k_{td,ratio}$	0.1		Disproportionation to combination ratio
k_{fm}	$9.3436*10^5\exp(-7475/RT)$	L/mol/min	Transfer to monomer rate
k_{fp}	0	L/mol/min	Transfer to polymer rate
k_{pin}	0	L/mol/min	Internal double bond rate of propagation
k_{pte}	0	L/mol/min	Terminal double bond rate of propagation
Δ	0.001	L/g	Reaction radius for segmental diffusion
V_{fc}	$0.01\exp(-1443.6/RT)$	L	Critical free volume
V_{fm}	0.025	L	Free volume of the monomer

α_m	0.001	L/K	Thermal expansion coeff. of the monomer
V_{fp}	0.025	L	Free volume of the polymer
α_p	0.0048	L/K	Thermal expansion coeff. of the polymer
B	0.5		Rate of decrease of k_p
m	0.5		Gel-effect model parameter
n	1.75		Gel-effect model parameter
A	1.31		Rate of decrease of k_t
K_3	$0.02\exp(-1.2109*10^4/RT)$		Onset pt. of translational diffusion-control
n_s	200		Avg. number of monomer units per chain
l_0	$6.54*10^{-8}$	cm	Length of monomer unit per chain
k_{th}	$4.96*10^4\exp(-17483/RT)$[1]	$L^2/mol^2/min$	Thermal (/self) initiation rate
k_p^{tert}	$3594\exp(-127.6/RT)$[2]	L/mol/min	Rate of propagation of tertiary radicals
$k_t^{tert\text{-}ert}$	$8.04*10^{10}\exp(-1338.4/RT)$[3]	L/mol/min	Rate of termination of tertiary radicals
$k_t^{sec\text{-}tert}$	$8.04*10^{10}\exp(-1338.4/RT)$[3]	L/mol/min	Termination of tertiary and secondary rad.
k_{bb}	$2.32*10^8\exp(-4568/RT)$[2]	/min	Rate of backbiting
k_β	$1.73*10^{19}\exp(-34860/RT)$[2]	/min	Rate of beta-scission
k_{fm}^{tert}	$1.2*10^7\exp(-1.10*10^4/RT)$[1]	L/mol/min	Transfer to monomer for tertiary radicals

[1]Ref (154) [2]Ref (152) [3]Ref (146)

Table A-9. Kinetic database for Butyl Methacrylate

Parameter	Value	Unit	Description
Mw	142.191	g/mol	Molecular weight of the monomer
T_{gm}	224.2	K	Glass transition temp. of the monomer
T_{gp}	293	K	Glass transition temperature of the polymer
C_{pm}	420	cal/kg/K	Heat capacity of the monomer
C_{pp}	401.914	cal/kg/K	Heat capacity of the polymer
ΔH	-18.373	cal/mol	Heat of reaction
ρ_m	0.911-0.000886(T-273.15)	kg/L	Density of the monomer
ρ_p	1.19-0.000807(T-273.15)	kg/L	Density of the polymer
k_p	$2.064*10^8 exp(-5574.2/RT)$	L/mol/min	Rate of propagation
k_t	$2.352*10^9 exp(-701/RT)$	L/mol/min	Rate of termination
$k_{td,ratio}$	0.65		Disproportionation to combination ratio
k_{fm}	$3.0795*10^5 exp(-8322.5/RT)$	L/mol/min	Transfer to monomer rate
k_{fp}	0	L/mol/min	Transfer to polymer rate
k_{pin}	0	L/mol/min	Internal double bond rate of propagation
k_{pte}	0	L/mol/min	Terminal double bond rate of propagation
Δ	0.001	L/g	Reaction radius for segmental diffusion
V_{fc}	0.06	L	Critical free volume
V_{fm}	0.025	L	Free volume of the monomer

α_m	0.001	L/K	Thermal expansion coeff. of the monomer
V_{fp}	0.025	L	Free volume of the polymer
α_p	0.0048	L/K	Thermal expansion coeff. of the polymer
B	1		Rate of decrease of k_p
m	0.5		Gel-effect model parameter
n	1.75		Gel-effect model parameter
A	1.02		Rate of decrease of k_t
K_3	$5.8*10^6$		Onset pt. of translational diffusion-control
n_s	126		Avg. number of monomer units per chain
l_0	$6.2*10^{-8}$	cm	Length of monomer unit per chain
k_{th}	0	$L^2/mol^2/min$	Thermal (/self) initiation rate

Table A-10. Kinetic database for Ethyl Acrylate

Parameter	Value	Unit	Description
Mw	101.12	g/mol	Molecular weight of the monomer
T_{gm}	167.1	K	Glass transition temp. of the monomer
T_{gp}	249	K	Glass transition temperature of the polymer
C_{pm}	429.4	cal/kg/K	Heat capacity of the monomer
C_{pp}	437.5	cal/kg/K	Heat capacity of the polymer
ΔH	$-1.927*10^4$	cal/mol	Heat of reaction
ρ_m	0.949-0.00128(T-273.15)	kg/L	Density of the monomer
ρ_p	1.11	kg/L	Density of the polymer
k_p	$3*10^{10}\exp(-8002.9/RT)$	L/mol/min	Rate of propagation
k_t	$1.046*10^{10}\exp(-2950.4/RT)$	L/mol/min	Rate of termination
$k_{td,ratio}$	$191.6\exp(-3817.75/RT)$		Disproportionation to combination ratio
k_{fm}	$1.487*10^{12}\exp(-17543/RT)$	L/mol/min	Transfer to monomer rate
k_{fp}	0	L/mol/min	Transfer to polymer rate
k_{pin}	0	L/mol/min	Internal double bond rate of propagation
k_{pte}	0	L/mol/min	Terminal double bond rate of propagation
Δ	0.001	L/g	Reaction radius for segmental diffusion
V_{fc}	$0.2865\exp(-984.94/RT)$	L	Critical free volume
V_{fm}	0.025	L	Free volume of the monomer

α_m	0.001	L/K	Thermal expansion coeff. of the monomer
V_{fp}	0.025	L	Free volume of the polymer
α_p	0.0048	L/K	Thermal expansion coeff. of the polymer
B	1		Rate of decrease of k_p
m	0.5		Gel-effect model parameter
n	1.75		Gel-effect model parameter
A	1.552		Rate of decrease of k_t
K_3	43.68exp(-7921.83/RT)		Onset pt. of translational diffusion-control
n_s	100		Avg. number of monomer units per chain
l_0	$5.8*10^{-8}$	cm	Length of monomer unit per chain
k_{th}	0	$L^2/mol^2/min$	Thermal (/self) initiation rate

Table A-11. Kinetic database for Glycidyl Methacrylate

Parameter	Value	Unit	Description
Mw	142.16	g/mol	Molecular weight of the monomer
T_{gm}	185.15	K	Glass transition temp. of the monomer
T_{gp}	347	K	Glass transition temperature of the polymer
C_{pm}	429.397	cal/kg/K	Heat capacity of the monomer
C_{pp}	437.5	cal/kg/K	Heat capacity of the polymer
ΔH	-13.74	cal/mol	Heat of reaction
ρ_m	1.09-0.00104(T-273.15)	kg/L	Density of the monomer
ρ_p	$1.13-7.07*10^{-4}$(T-273.15)	kg/L	Density of the polymer
k_p	$3.0455*10^{8}\exp(-5473/RT)$[1]	L/mol/min	Rate of propagation
k_t	$6.6*10^{10}\exp(-2465.87/RT)$[2]	L/mol/min	Rate of termination
$k_{td,ratio}$	0.65		Disproportionation to combination ratio
k_{fm}	$9360\exp(-5207.9/RT)$[2]	L/mol/min	Transfer to monomer rate
k_{fp}	0	L/mol/min	Transfer to polymer rate
k_{pin}	0	L/mol/min	Internal double bond rate of propagation
k_{pte}	0	L/mol/min	Terminal double bond rate of propagation
Δ	0.001	L/g	Reaction radius for segmental diffusion
V_{fc}	0.07	L	Critical free volume
V_{fm}	0.025	L	Free volume of the monomer

α_m	0.001	L/K	Thermal expansion coeff. of the monomer
V_{fp}	0.025	L	Free volume of the polymer
α_p	0.0048	L/K	Thermal expansion coeff. of the polymer
B	1		Rate of decrease of k_p
m	0.5		Gel-effect model parameter
n	1.75		Gel-effect model parameter
A	1.02		Rate of decrease of k_t
K_3	$5.8*10^6$		Onset pt. of translational diffusion-control
n_s	126		Avg. number of monomer units per chain
l_0	$6.2*10^{-8}$	cm	Length of monomer unit per chain
k_{th}	0	$L^2/mol^2/min$	Thermal (/self) initiation rate

[1]Ref (110) [2]Ref (23)

Table A-12. Kinetic database for Hydroxyethyl Acrylate

Parameter	Value	Unit	Description
Mw	116.12	g/mol	Molecular weight of the monomer
T_{gm}	185.15	K	Glass transition temp. of the monomer
T_{gp}	258	K	Glass transition temperature of the polymer
C_{pm}	429.397	cal/kg/K	Heat capacity of the monomer
C_{pp}	437.5	cal/kg/K	Heat capacity of the polymer
ΔH	$-1.84*10^4$	cal/mol	Heat of reaction
ρ_m	1.011-0.001012(T-273.15)	kg/L	Density of the monomer
ρ_p	1.041-0.000845(T-273.15)	kg/L	Density of the polymer
k_p	$6.487*10^8\exp(-6706.2/RT)$[1]	L/mol/min	Rate of propagation
k_t	$2.63*10^{11}\exp(-6639.5/RT)$[1]	L/mol/min	Rate of termination
$k_{td,ratio}$	$191.61\exp(-3817.8/RT)$		Disproportionation to combination ratio
k_{fm}	$9.3436*10^5\exp(-7475.1/RT)$	L/mol/min	Transfer to monomer rate
k_{fp}	0	L/mol/min	Transfer to polymer rate
k_{pin}	0	L/mol/min	Internal double bond rate of propagation
k_{pte}	0	L/mol/min	Terminal double bond rate of propagation
Δ	0.001	L/g	Reaction radius for segmental diffusion
V_{fc}	$\exp(-2100/RT)$[1]	L	Critical free volume
V_{fm}	0.0275	L	Free volume of the monomer

α_m	0.0011	L/K	Thermal expansion coeff. of the monomer
V_{fp}	0.0275	L	Free volume of the polymer
α_p	0.000528	L/K	Thermal expansion coeff. of the polymer
B	1		Rate of decrease of k_p
m	0.5		Gel-effect model parameter
n	1.75		Gel-effect model parameter
A	3.5		Rate of decrease of k_t
K_3	$4*10^{-5}\exp(-1.447*10^4/RT)$[1]		Onset pt. of translational diffusion-control
n_s	126		Avg. number of monomer units per chain
l_0	$6.2*10^{-8}$	cm	Length of monomer unit per chain
k_{th}	0	$L^2/mol^2/min$	Thermal (/self) initiation rate

[1]Refined through sensitivity analysis based on the work by (77)

Table A-13. Kinetic database for Hydroxyethyl Methacrylate

Parameter	Value	Unit	Description
Mw	130.14	g/mol	Molecular weight of the monomer
T_{gm}	185.15	K	Glass transition temp. of the monomer
T_{gp}	381.15	K	Glass transition temperature of the polymer
C_{pm}	429.397	cal/kg/K	Heat capacity of the monomer
C_{pp}	437.5	cal/kg/K	Heat capacity of the polymer
ΔH	$-1.84*10^4$	cal/mol	Heat of reaction
ρ_m	$1.092-0.00098(T-273.15)^1$	kg/L	Density of the monomer
ρ_p	1.041-0.000845(T-273.15)	kg/L	Density of the polymer
k_p	$4.325*10^8 exp(-6706.2/RT)$	L/mol/min	Rate of propagation
k_t	$2.631*10^{11} exp(-6639.5/RT)$	L/mol/min	Rate of termination
$k_{td,ratio}$	191.61exp(-3817.8/RT)		Disproportionation to combination ratio
k_{fm}	$9.3436*10^5 exp(-7475.1/RT)$	L/mol/min	Transfer to monomer rate
k_{fp}	1500	L/mol/min	Transfer to polymer rate
k_{pin}	0	L/mol/min	Internal double bond rate of propagation
k_{pte}	0	L/mol/min	Terminal double bond rate of propagation
Δ	0.001	L/g	Reaction radius for segmental diffusion
V_{fc}	exp(-2100/RT)	L	Critical free volume
V_{fm}	0.0275	L	Free volume of the monomer

α_m	0.0011	L/K	Thermal expansion coeff. of the monomer
V_{fp}	0.0275	L	Free volume of the polymer
α_p	0.000528	L/K	Thermal expansion coeff. of the polymer
B	1		Rate of decrease of k_p
m	0.5		Gel-effect model parameter
n	1.75		Gel-effect model parameter
A	3.5		Rate of decrease of k_t
K_3	$4*10^{-5}\exp(-1.447*10^4/RT)$		Onset pt. of translational diffusion-control
n_s	126		Avg. number of monomer units per chain
l_0	$6.2*10^{-8}$	cm	Length of monomer unit per chain
k_{th}	0	$L^2/mol^2/min$	Thermal (/self) initiation rate

[1]Ref (139)

Table A-14. Kinetic database for Methacrylic Acid

Parameter	Value	Unit	Description
Mw	86.1	g/mol	Molecular weight of the monomer
T_{gm}	188.532	K	Glass transition temp. of the monomer
T_{gp}	501	K	Glass transition temperature of the polymer
C_{pm}	502.39	cal/kg/K	Heat capacity of the monomer
C_{pp}	432.69	cal/kg/K	Heat capacity of the polymer
ΔH	$-1.352*10^4$	cal/mol	Heat of reaction
ρ_m	1.019-0.0004(T-273.15)	kg/L	Density of the monomer
ρ_p	1.014-0.00078(T-273.15)	kg/L	Density of the polymer
k_p	$4.4979*10^8 exp(-4379.3/RT)$	L/mol/min	Rate of propagation
k_t	$2.78*10^9 exp(-430.57/RT)$	L/mol/min	Rate of termination
$k_{td,ratio}$	0.3		Disproportionation to combination ratio
k_{fm}	$1.717*10^9 exp(-11117/RT)$	L/mol/min	Transfer to monomer rate
k_{fp}	0	L/mol/min	Transfer to polymer rate
k_{pin}	0	L/mol/min	Internal double bond rate of propagation
k_{pte}	0	L/mol/min	Terminal double bond rate of propagation
Δ	0.001	L/g	Reaction radius for segmental diffusion
V_{fc}	3.095exp(-1683.2/RT)	L	Critical free volume
V_{fm}	0.025	L	Free volume of the monomer

α_m	0.001	L/K	Thermal expansion coeff. of the monomer
V_{fp}	0.025	L	Free volume of the polymer
α_p	0.00048	L/K	Thermal expansion coeff. of the polymer
B	1		Rate of decrease of k_p
m	0.5		Gel-effect model parameter
n	1.75		Gel-effect model parameter
A	1.65		Rate of decrease of k_t
K_3	$5*10^6$		Onset pt. of translational diffusion-control
n_s	126		Avg. number of monomer units per chain
l_0	$6.2*10^{-8}$	cm	Length of monomer unit per chain
k_{th}	$4.5*10^6\exp(-2.745*10^4/RT)$	$L^2/mol^2/min$	Thermal (/self) initiation rate

Table A-15. Kinetic database for Methyl Methacrylate

Parameter	Value	Unit	Description
Mw	100.12	g/mol	Molecular weight of the monomer
T_{gm}	167.1	K	Glass transition temp. of the monomer
T_{gp}	378	K	Glass transition temperature of the polymer
C_{pm}	411.1	cal/kg/K	Heat capacity of the monomer
C_{pp}	400	cal/kg/K	Heat capacity of the polymer
ΔH	$-1.381*10^4$	cal/mol	Heat of reaction
ρ_m	0.9665-0.001164(T-273.15)	kg/L	Density of the monomer
ρ_p	1.195-0.00033(T-273.15)	kg/L	Density of the polymer
k_p	$2.952*10^7\exp(-4353/RT)$	L/mol/min	Rate of propagation
k_t	$5.88*10^9\exp(-701/RT)$	L/mol/min	Rate of termination
$k_{td,ratio}$	$1.6093\exp(-440.12/RT)$		Disproportionation to combination ratio
k_{fm}	$9.3435*10^4\exp(-7475/RT)$	L/mol/min	Transfer to monomer rate
k_{fp}	0	L/mol/min	Transfer to polymer rate
k_{pin}	0	L/mol/min	Internal double bond rate of propagation
k_{pte}	0	L/mol/min	Terminal double bond rate of propagation
Δ	0.001	L/g	Reaction radius for segmental diffusion
V_{fc}	$0.7408\exp(-1589.6/RT)$	L	Critical free volume
V_{fm}	0.025	L	Free volume of the monomer

α_m	0.001	L/K	Thermal expansion coeff. of the monomer
V_{fp}	0.025	L	Free volume of the polymer
α_p	0.00048	L/K	Thermal expansion coeff. of the polymer
B	1		Rate of decrease of k_p
m	0.5		Gel-effect model parameter
n	1.75		Gel-effect model parameter
A	1.11		Rate of decrease of k_t
K_3	0.563exp(-8900/RT)		Onset pt. of translational diffusion-control
n_s	47		Avg. number of monomer units per chain
l_0	$6.9*10^{-8}$	cm	Length of monomer unit per chain
k_{th}	$2.26*10^{-6}$exp(-6578/RT)	$L^2/mol^2/min$	Thermal (/self) initiation rate

Table A-16. Kinetic database for α-methyl Styrene

Parameter	Value	Unit	Description
Mw	118.18	g/mol	Molecular weight of the monomer
T_{gm}	150.15	K	Glass transition temp. of the monomer
T_{gp}	449.15	K	Glass transition temperature of the polymer
C_{pm}	400	cal/kg/K	Heat capacity of the monomer
C_{pp}	400	cal/kg/K	Heat capacity of the polymer
ΔH	$-1.7*10^4$	cal/mol	Heat of reaction
ρ_m	0.875-0.000918(T-273.15)	kg/L	Density of the monomer
ρ_p	1.15-0.000918(T-273.15)	kg/L	Density of the polymer
k_p	$3.54*10^8\exp(-8870/RT)$[1]	L/mol/min	Rate of propagation
k_t	$1.38*10^{10}\exp(-2100/RT)$[1]	L/mol/min	Rate of termination
$k_{td,ratio}$	0.07		Disproportionation to combination ratio
k_{fm}	$3.3615*10^9\exp(-15177/RT)$	L/mol/min	Transfer to monomer rate
k_{fp}	0	L/mol/min	Transfer to polymer rate
k_{pin}	0	L/mol/min	Internal double bond rate of propagation
k_{pte}	0	L/mol/min	Terminal double bond rate of propagation
Δ	0.0001	L/g	Reaction radius for segmental diffusion
V_{fc}	1.2exp(-2220/RT)	L	Critical free volume
V_{fm}	0.025	L	Free volume of the monomer

α_m	0.001	L/K	Thermal expansion coeff. of the monomer
V_{fp}	0.025	L	Free volume of the polymer
α_p	0.00048	L/K	Thermal expansion coeff. of the polymer
B	0.5		Rate of decrease of k_p
m	0.5		Gel-effect model parameter
n	1.75		Gel-effect model parameter
A	0.55		Rate of decrease of k_t
K_3	10^{10}		Onset pt. of translational diffusion-control
n_s	120		Avg. number of monomer units per chain
l_0	$5*10^{-8}$	cm	Length of monomer unit per chain
k_{th}	0	$L^2/mol^2/min$	Thermal (/self) initiation rate

[1]Ref. (115)

Table A-17. Kinetic database for Styrene

Parameter	Value	Unit	Description
Mw	104.12	g/mol	Molecular weight of the monomer
T_{gm}	185	K	Glass transition temp. of the monomer
T_{gp}	378	K	Glass transition temperature of the polymer
C_{pm}	430	cal/kg/K	Heat capacity of the monomer
C_{pp}	400	cal/kg/K	Heat capacity of the polymer
ΔH	$-1.7*10^4$	cal/mol	Heat of reaction
ρ_m	0.924-0.000918(T-273.15)	kg/L	Density of the monomer
ρ_p	1.084-0.000605(T-273.15)	kg/L	Density of the polymer
k_p	$1.302*10^9 exp(-7759.2/RT)$[1]	L/mol/min	Rate of propagation
k_t	$4.92*10^{11} exp(-3471.3/RT)$[1]	L/mol/min	Rate of termination
$k_{td,ratio}$	0.01		Disproportionation to combination ratio
k_{fm}	$1.386*10^8 exp(-12670/RT)$[2]	L/mol/min	Transfer to monomer rate
k_{fp}	0	L/mol/min	Transfer to polymer rate
k_{pin}	0	L/mol/min	Internal double bond rate of propagation
k_{pte}	0	L/mol/min	Terminal double bond rate of propagation
Δ	0.001	L/g	Reaction radius for segmental diffusion
V_{fc}	0.31105exp(-1671.8/RT)	L	Critical free volume
V_{fm}	0.025	L	Free volume of the monomer

α_m	0.001	L/K	Thermal expansion coeff. of the monomer
V_{fp}	0.025	L	Free volume of the polymer
α_p	0.00048	L/K	Thermal expansion coeff. of the polymer
B	1		Rate of decrease of k_p
m	0.5		Gel-effect model parameter
n	1.75		Gel-effect model parameter
A	0.348		Rate of decrease of k_t
K_3	$9.44\exp(-3832.9/RT)^3$		Onset pt. of translational diffusion-control
n_s	173		Avg. number of monomer units per chain
l_0	$7.4*10^{-8}$	cm	Length of monomer unit per chain
k_{th}	$1.35*10^7\exp(-27450/RT)^2$	$L^2/mol^2/min$	Thermal (/self) initiation rate

[1]Ref. (168), [2]Ref. (118), [3]Ref. (123)

Table A-18. Kinetic database for Vinyl Acetate

Parameter	Value	Unit	Description
Mw	86.09	g/mol	Molecular weight of the monomer
T_{gm}	109.15	K	Glass transition temp. of the monomer
T_{gp}	303	K	Glass transition temperature of the polymer
C_{pm}	471.6	cal/kg/K	Heat capacity of the monomer
C_{pp}	318.1	cal/kg/K	Heat capacity of the polymer
ΔH	$-2.0895*10^4$	cal/mol	Heat of reaction
ρ_m	0.9574-0.00127(T-273.15)	kg/L	Density of the monomer
ρ_p	1.2145-0.000875(T-273.15)	kg/L	Density of the polymer
k_p	$7.8*10^{10}\exp(-8403.5/RT)$	L/mol/min	Rate of propagation
k_t	$9.84*10^{11}\exp(-3401.4/RT)$	L/mol/min	Rate of termination
$k_{td,ratio}$	0		Disproportionation to combination ratio
k_{fm}	$1.117*10^7\exp(-9895/RT)$	L/mol/min	Transfer to monomer rate
k_{fp}	$4.255*10^6\exp(-8947/RT)$	L/mol/min	Transfer to polymer rate
k_{pin}	0	L/mol/min	Internal double bond rate of propagation
k_{pte}	$2.7289*10^7\exp(-5509.9/RT)$	L/mol/min	Terminal double bond rate of propagation
Δ	0.0001	L/g	Reaction radius for segmental diffusion
V_{fc}	0.06	L	Critical free volume
V_{fm}	0.025	L	Free volume of the monomer

α_m	0.001	L/K	Thermal expansion coeff. of the monomer
V_{fp}	0.025	L	Free volume of the polymer
α_p	0.00048	L/K	Thermal expansion coeff. of the polymer
B	1		Rate of decrease of k_p
m	0.5		Gel-effect model parameter
n	1.75		Gel-effect model parameter
A	0.8		Rate of decrease of k_t
K_3	3.1866exp(-7065.6/RT)		Onset pt. of translational diffusion-control
n_s	100		Avg. number of monomer units per chain
l_0	$7.5*10^{-8}$	cm	Length of monomer unit per chain
k_{th}	$2*10^{-10}$	$L^2/mol^2/min$	Thermal (/self) initiation rate

Appendix III. Chain Transfer Agent and Solvent Databases

The remaining databases can be found here with all the kinetic parameters coming from WATPOLY (Gao and Penlidis (134, 83, 18)).

Table A-19. Kinetic database for Xylene

Parameter	Monomer	Value	Unit	Description
Mw	General	106.16	g/mol	Molecular weight of the solvent
T_g	General	187.4	K	Glass transition temperature
C_p	General	420	cal/kg/K	Heat capacity
ρ_s	General	0.868	kg/L	Density of the solvent
k_{fs}	Styrene	$0.0001*k_{pSty}$	L/mol/min	Chain transfer to solvent
	BA	$17.6\exp(-3870/T)*k_{pBA}$		
	BMA	$5.55\exp(-4590/T)*k_{pBMA}$		
	General	$1.373*10^5\exp(-4353/RT)$		
V_{fs}	General	0.025	L	Free volume of solvent
α_s	General	0.001	L/K	Thermal expansion coefficient

Table A-20. Kinetic database for Toluene

Parameter	Monomer	Value	Unit	Description
Mw	General	92.14	g/mol	Molecular weight of the solvent
T_g	General	113	K	Glass transition temperature
C_p	General	404.8	cal/kg/K	Heat capacity
ρ_s	General	$0.883-9.16*10^{-4}(T-273.15)$	kg/L	Density of the solvent
k_{fs}	General	$1.237*10^{7}\exp(-1.14*10^{4}/RT)$	L/mol/min	Chain transfer to solvent
V_{fs}	General	0.025	L	Free volume of solvent
α_s	General	0.001	L/K	Thermal expansion coefficient

Table A-21. Kinetic database for Benzene

Parameter	Monomer	Value	Unit	Description
Mw	General	78.12	g/mol	Molecular weight of the solvent
T_g	General	171	K	Glass transition temperature
C_p	General	414.7	cal/kg/K	Heat capacity
ρ_s	General	0.876	kg/L	Density of the solvent
k_{fs}	Styrene	$1.237*10^7 exp(-1.14*10^4/RT)$	L/mol/min	Chain transfer to solvent
	BMA	3261exp(-5574/RT)		
	General	$1.373*10^5 exp(-4353/RT)$		
V_{fs}	General	0.025	L	Free volume of solvent
α_s	General	0.001	L/K	Thermal expansion coefficient

Table A-22. Kinetic database for Ethyl Acetate

Parameter	Monomer	Value	Unit	Description
Mw	General	88.12	g/mol	Molecular weight of the solvent
T_g	General	181	K	Glass transition temperature
C_p	General	460.7	cal/kg/K	Heat capacity
ρ_s	General	0.928-0.00138*(T-273.15)	kg/L	Density of the solvent
k_{fs}	BA	$3.93*10^{16}\exp(-2.4*10^4/RT)$	L/mol/min	Chain transfer to solvent
	General	$1.373*10^5\exp(-4353/RT)$		
V_{fs}	General	0.025	L	Free volume of solvent
α_s	Styrene	0.00081	L/K	Thermal expansion coefficient
	General	0.001		

Table A-23. Kinetic database for Carbon Tetra-chloride

Parameter	Monomer	Value	Unit	Description
Mw	General	153.82	g/mol	Molecular weight of the CTA
k_{fCTA}	Styrene	$1.736*10^7\exp(-7759/RT)$	L/mol/min	Chain transfer to CTA
	AA	7085exp(-4353/RT)		
	General	1*105		

Table A-24. Kinetic database for Octanethiol

Parameter	Monomer	Value	Unit	Description
Mw	General	146.3	g/mol	Molecular weight of the CTA
k_{fCTA}	EA	$3*10^{11}exp(-7128/RT)$	L/mol/min	Chain transfer to CTA
	General	$7.124*10^{10}exp(-7128/RT)$		

Table A-25. Kinetic database for Dodecanethiol

Parameter	Monomer	Value	Unit	Description
Mw	General	202.2	g/mol	Molecular weight of the CTA
k_{fCTA}	EA	$1.167*10^{10}exp(-7759/RT)$	L/mol/min	Chain transfer to CTA
	General	$2.718*10^{12}exp(-1.3*10^{4}/RT)$		